January 2018

A Study Of Two-Phase Flow Through Static Mixers And Their Effects On Downstream Pressure Behavior

Adam A. Stoker

A STUDY OF TWO-PHASE FLOW THROUGH STATIC MIXERS AND THEIR EFFECTS ON DOWNSTREAM PRESSURE BEHAVIOR

by

Adam Alan Stoker

Bachelor of Science in Mechanical Engineering, University of North Dakota, 2016

A Thesis

Submitted to the Graduate Faculty

of the

University of North Dakota

in partial fulfillment of the requirements

for the degree of

Master of Science

Grand Forks, North Dakota

August

2018

This thesis, submitted by Adam Stoker in partial fulfillment of the requirements for the Degree of Master of Science from the University of North Dakota, has been read by the Faculty Advisory Committee under whom the work has been done and is hereby approved.

_____

Dr. Clement Tang

_____

Dr. Nanak Grewal

_____

Dr. Surojit Gupta

This thesis is being submitted by the appointed advisory committee as having met all of the requirements of the School of Graduate Studies at the University of North Dakota and is hereby approved.

_____

Grant McGimpsey
Dean of the School of Graduate Studies

_____

Date

PERMISSION

Title A STUDY OF TWO-PHASE FLOW THROUGH STATIC MIXERS AND THEIR EFFECTS ON ITS DOWNSTREAM PRESSURE BEHAVIOR

Department Mechanical Engineering

Degree Master of Science

In presenting this thesis in partial fulfillment of the requirements for a graduate degree from the University of North Dakota, I agree that the library of this University shall make it freely available for inspection. I further agree that permission for extensive copying for scholarly purposes may be granted by the professor who supervised my thesis work or, in his absence, by the Chairperson of the department or the dean of the School of Graduate Studies. It is understood that any copying or publication or other use of this thesis or part thereof for financial gain shall not be allowed without my written permission. It is also understood that due recognition shall be given to me and to the University of North Dakota in any scholarly use which may be made of any material in my thesis.

Adam Stoker

August 3rd, 2018

TABLE OF CONTENTS

LIST OF FIGURES

Page

LIST OF TABLES

Page

ACKNOWLEDGMENTS

I would like to give my most genuine appreciation to my advisor, Dr. Clement Tang, for his support, direction, and encouragement throughout this Master's program and thesis. I would also like to thank my committee members Dr. Nanak Grewal and Dr. Surojit Gupta for their help throughout this process. I would also like to thank The University of North Dakota Mechanical Engineering Department and many of its faculty that have taught and aided me throughout the years. Finally, I would like to thank my family who have supported me financially and emotionally during my schooling and entire life.

ABSTRACT

The following thesis entails the research relating to single and two-phase flow through various static mixer geometries and the measurement of fluid viscosity, viscous behavior, and density. Previous studies on the effects of static mixers on flow behavior, and the determination of fluid properties have been examined and summarized. Fluid viscosity and viscous behavior was measured using a rheometer that determined the shear stress on the fluid with a range of spindle shear rates from 0 to 250 1/s and a temperature range of 5 to 35 degrees Celsius. The results validated the fluid viscosities and the viscous behavior as Newtonian. A closed flow loop was used to test a variety of single and two-phase flow fluids through a static mixer and a static pressure transducer test section. Gas and liquid Reynolds numbers ranged from 0 to 1336 and 328 to 1452, respectively. Reynolds mixture numbers were generated based on the homogeneous flow model and ranged from 328 to 2374, which demonstrated a range of laminar and turbulent flow through the 3.175 mm diameter test section. Ten pressure transducers downstream of the static mixer were used to measure local static pressures. Differential pressures across the entire test section including the static mixer and the test section were also measured. Analysis showed the static pressure profile, downstream differential pressure, average downstream static pressure in the pipe, overall system differential pressure, and the comparison of the usage of helical, double plate, and triple plate static mixer geometries to an empty pipe over the range of mixture Reynolds numbers.

NOMENCLATURE

a	Interfacial area [m^2/m^3]
CCD	Charge couple device
CFD	Computational Fluid Dynamics
cm	centimeter
cP	Centipoise
D	Diameter [mm]
DP	Differential Pressure [kPa]
DPmix	Differential pressure with static mixer
DPnomix	Differential pressure without static mixer
dv/dx	Velocity gradient
g	Gravitational constant
g/s	Grams per second
ID	Inner diameter [mm]
kl	Mass transfer coefficient [s^{-1}]
L/D	Length to diameter ratio
LPM	Liters per minute
m	Mass [g]
$\dot{m}$	Mass Flow Rate [g/s]
$\dot{m}l$	Liquid mass flow rate [g/s]
$\dot{m}v$	Gas mass flow rate [g/s]
ml	Milliliter
mm	Millimeter
Ne	Newton number

P	Pressure [kPa] [psi] [psia] [psig]
Patm	Atmospheric pressure [kPa]
Pmix	Pressure with static mixer
Pnomix	Pressure without static mixer
ReD	Reynolds number
ReDl	Reynolds number for liquid
ReDmix	Reynolds number for mixture
ReDv	Reynolds number for vapor
RPM	Revolutions per minute
RTD	Residence time distribution
SLA	Stereolithography
SLPM	Standard liters per minute
T	Temperature [K] or [Celsius]
Tatm	Atmospheric temperature [Celsius]
t	Time [s] [min] [hr]
t_m	Mean residence time
UV	Ultraviolet
X	Martinelli number

Greek Symbols

ρ	Density [g/cm^3]
μ	Viscosity [cP]
τ	Shear Stress [N/m^2]
γ	Shear rate [1/s]

CHAPTER 1

INTRODUCTION

Static mixer performance has been studied previously regarding the differential pressure across the mixer, static pressure inside the mixer, residence time distribution, the flow pattern downstream of the static mixer, and the various fluid properties of the experimental fluid used in flow applications. Most studies were done on single-phase flow systems, with little information on what happens in the two-phase flow regime. Two-phase flow mixing applications are important in the heat transfer, polymerization, chemical reaction, and many other industries. Utilizing static mixers allows for enhanced mixing, to improve the performance of these applications, but does generally increase the differential pressure and static pressure downstream of the mixer. Static mixer behavior correlations that were created in the two-phase flow regime, were based on the specific geometry and flow parameters of the individual experiments, and not for a broad spectrum of variables. This limits the understanding of how static mixers behave and their applicability in industry and as well as CFD analysis. The performance downstream of a static mixer regarding pressure drop, static pressure profile, and overall average static pressure has been studied minimally in the past. Using an experimental set up that includes: a gas and liquid flow pump, a differential pressure sensor, ten downstream pressure transducers, a 3D printed static mixer model, and a data acquisition unit, differential pressure and the pressure profile downstream of the static mixer can be analyzed. Knowing how the differential pressure changes with the addition of a static mixer aids in understanding the possible increased power

requirement. The static pressure profile provides experimental data that can be used in CFD analysis and show the effects a static mixer plays on the change in static pressure based on given flow rates and geometries.

1.1 Objectives

This research was conducted to investigate concepts of determining fluid properties and understanding static mixers and their downstream pressure effects, which until now has been insufficiently studied in previous literature. The first goal was to study the fluid properties of a specific fluid called Hydromx, which is an ethylene glycol blended fluid. The fluid properties under investigation were density, viscosity, and the viscous behavior of the fluid. Viscosity was measured using a rheometer to measure the shear stress of the fluid as a spindle rotated at various shear rates ranging from 10 to 250 1/s. The viscous behavior will then be analyzed as a function of shear stress versus shear rate to determine if the fluid behaves as a Newtonian fluid. The second goal inspected what happens to the differential pressure across the entire test section, like methods which have been done previously in literature. The third goal of this thesis was to better understand various static mixer models and their effect of downstream differential pressure and pressure profile. The differential pressure and pressure profile were monitored during two-phase flow experiments based on their independent gas and liquid flow rates, which ranged from laminar to turbulent. Mixture Reynolds number was then calculated off the independent flow rates utilizing the homogeneous flow model to give insight into characterizing the flow with a static mixer versus an empty pipe. The data obtained from these studies can help better understand what happens downstream of a static mixer while two-phase flow passes by and help fill voids left in literature and aid in giving experimental data to validate CFD analysis.

1.2 Scope of Study

Gas and liquid mass flow rates ranged from 0-.06 and 4.75-21 g/s, respectively. These mass flow rates converted to gas and liquid Reynolds numbers ranging from 0 to 1336 and 328 to 1452, respectively. Reynolds mixture numbers are based off the gas and liquid mass flow rates and range from 328 to 2374, which ranges from laminar to turbulent flow through the test section. Viscosity of the liquid is measured from a range of 0 to 250 1/s shear rates. The temperature range that viscosity is measured is from 5 to 30 degrees Celsius. This temperature range covers the operating temperature of the working fluid for the single- and two-phase flow measurements.

CHAPTER 2

LITERATURE REVIEW

2.1 Observations of Two-phase Flow Patterns in a Horizontal Circular Channel

Ewing et al. conducted a study on observing flow patterns in a transparent circular channel [1]. The purpose of the study was to show different flow regimes using a photographic set up and compare them to a flow regime map that was developed by Breber et al. based on experiments conducted by Taitel and Dukler [2, 3]. Figure 1 shows the flow regime map that was created based on those experiments.

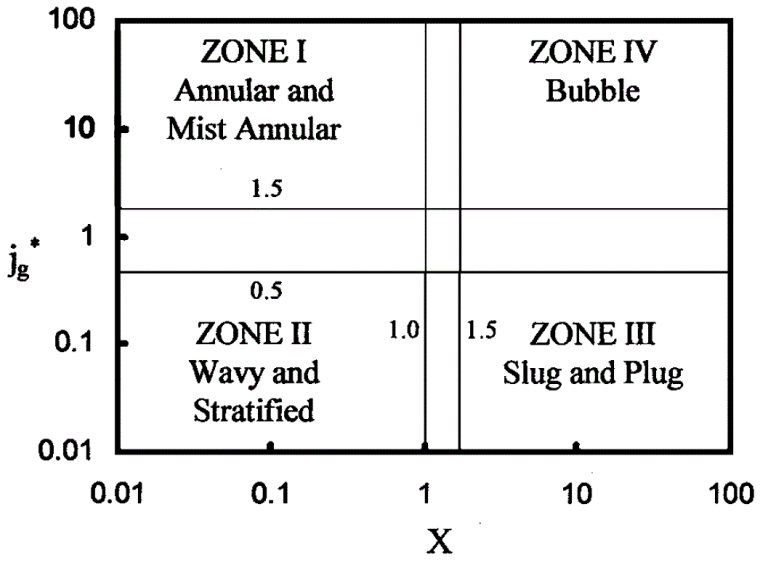

Figure 1. Flow Regime Map of Breber et al. [3]

The map shows four zones: Annular and Mist Annular, Wavy and Stratified, Bubble, and Slug and Plug Flow [3]. The map is plotted based on the Martinelli number, X, which is defined in Equation 2.1.1 and by the Wallis factor, j_g*, given by Equation 2.1.2.

$$X = \left(\frac{1-x}{x}\right)^{.9} \left(\frac{\rho_v}{\rho_l}\right)^{.5} \left(\frac{\mu_l}{\mu_v}\right)^{.1} \quad 2.1.1$$

$$j_g^* = \frac{G_t x}{\sqrt{D g \rho_v (\rho_l - \rho_v)}} \quad 2.1.2$$

The map utilizes horizontal and vertical lines and easily classifies the flow into four different zones based on the criteria of X and j_g*. Ewing et al. compared his experimental data to the map created by Breber due to the map being easier to classify flow regimes than other flow regime maps created, which helps the design in two-phase applications [1, 3].

Ewing conducted adiabatic two-phase flow tests using air and water supplies that were measured with a series of rotameters. The static mixer used was a perforated copper tube inserted into the liquid stream by a compression fitting. After the flow mixed it entered a flow observation section, which utilized a transparent acrylic tube of 1.9cm ID. The observation region was located at a position of 240 cm downstream (L/D = 126) to allow for flow development downstream of the mixer where the visualization of the flow pattern would begin, and static pressure was monitored [1].

Ewing kept a fixed located flow rate, while varying the air flow rates and observed the flow pattern downstream. The flow regimes were identified using visual observation and photographic data. High-speed flows needed to be observed using a strobe light that was flashed at a frequency that held the flow in place to allow for observation of the flow regime [1]. Figure 2 shows the

photographs of a variety of flow patterns that were observed during testing. It shows the corresponding X and j_g* values along with the flow regime type.

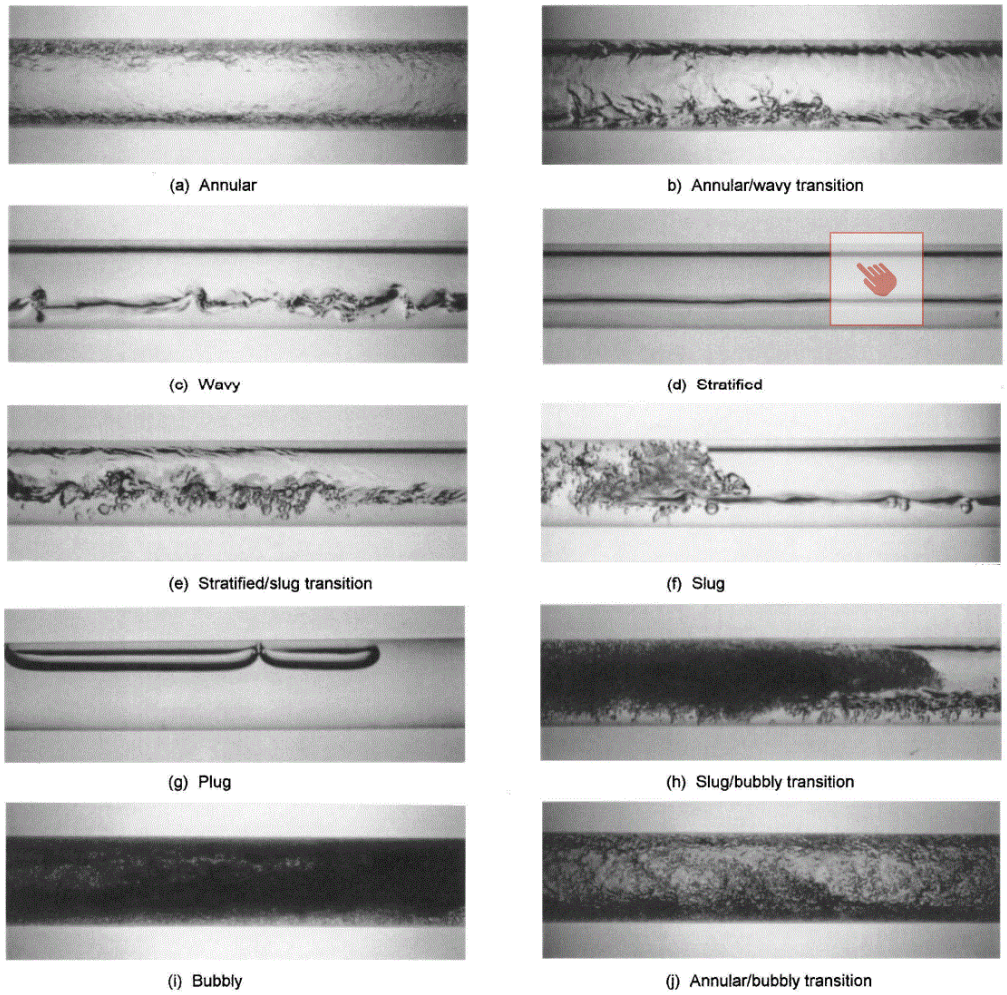

Figure 2. Photographs of representative flow patterns: (a) X = .21, jg* = 2.02; (b) X = .25, jg* = 1.10; (c) X = .23, jg* = .49; (d) X = .11, jg* = .28; (e) X =1.49, jg* = .22; (f) X = 2.1, jg* = .11; (g) X = 5.8, jg* = .05; (h) X = 5.6, jg* = .32; (i) X = 1.61, jg* = 1.72; (j) X = 1.35, jg* = 1.73 [1]

The results of these photographs along with the X and j_g* values were plotted in a similar fashion to the flow regime map by Breber [3]. The results of the experiment showed favorable results to that of the flow regime map. The predictions in zones 1 and 2 (Annular and Stratified Flow), along with the associated transitions matched well. Zones 3 and 4 showed similar results but

didn't match up as well due to the testing facility limitations [1]. Overall, this experiment helped show the consistency between Breber's flow regime map and two-phase experimental data to determine flow patterns.

2.2 Influence of Gas Injection on Bubble Diameters and Void Fraction

Kurtulus et al. studied the characteristics of bubble size and void fraction due to the influence of gas injection in a horizontal circular channel [4]. Void fraction and bubble size lead to pressure drops in systems and can have important roles in the development of models of multiphase flow. These parameters have been studied experimentally to help obtain correlations between the mass, momentum, and energy equations on theoretical models. The effects of void fraction and bubble size on the two-phase flow were determined using a dual optical probe [4].

Water was pumped into a system, while compressed air was injected into the water flow by an immersed injector. After the air was injected, the flow was measured at three locations equal distance from the injector by a dual optical probe along the radial direction of the pipe. The dual optical probe took measurements at four locations around the pipe: 90°, 45°, 0°, and -45°. The measurements were taken at radial intervals throughout the experiment to show the data throughout the diameter of the pipe. The results of the experiment showed that local void fraction increased with increasing value of volumetric void fraction, and bubble size also showed an increase with local void fraction distribution. Kurtulus et al., determined that bubbles gather toward the upper part of the pipe due to the buoyancy force applied on them. This conclusion also pointed to the finding that bubble size profile and local void fraction increase in specified tendency downstream of the injector [4].

2.3 Void Fraction Measurement in Two-phase Flow by Capacitance Sensor

Jaworek and Krupa investigated methods to experimentally determine the void fraction of two-phase flow using a radio-frequency capacitance sensor [5, 6, 7]. Understanding void fraction calculation helps provide insight to fully understand two-phase flow in various applications [8, 9]. The capacitance sensor utilized in this experiment used two electrodes that were placed on the outer wall of the pipe through where a two-phase system is flowing [5]. As the flow moved through the pipe and past the location of measurement of the sensor, the changing gas and liquid percentages caused a change in the capacitance read by the sensor [8]. The sensor used in this study was connected to a resonant circuit of an electronic oscillator that was tuned to a high frequency to increase the sensitivity of the measurement [5]. The researchers found that capacitance between the electrodes depends on the effective permittivity of the dielectric between them. The researchers then determined to use two half-cylinder electrodes due to the high sensitivity when compared to other electrode configurations shown in Figure 3 [5, 8].

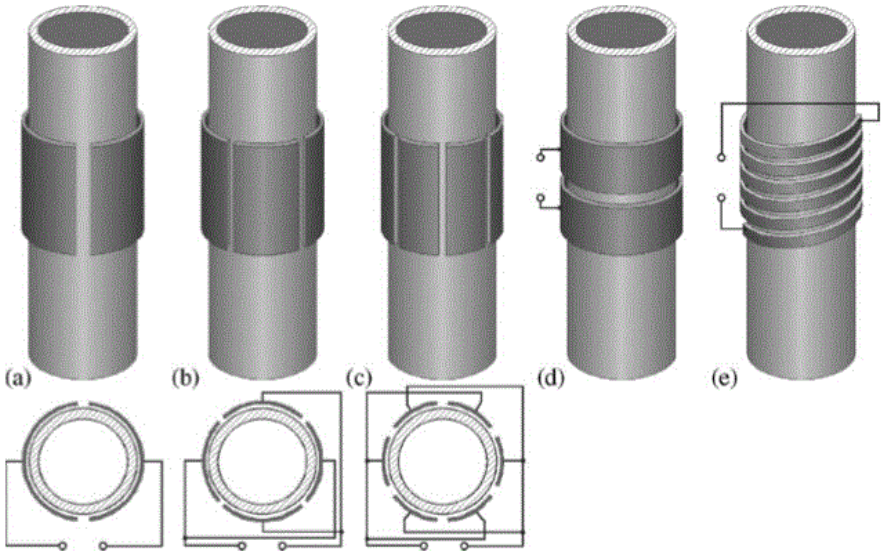

Figure 3. Configurations of capacitance sensors [5]

The results of the study were that a theoretical model could be verified by the experimental tests for the given capacitance sensor to measure gas percentage in the flow. The capacitance sensor could be used in other gas/liquid experiments but would need to be calibrated for the specific liquid and gas used, depending on their dielectric constants [5].

2.4 Pressure Drop in Motionless Mixers

Yang and Park conducted a study on the pressure drop in various motionless mixers [10]. Motionless mixers or static mixers involve a pipe containing several "mixing elements" that allow two-phase flow to be mixed and react in a system. Static mixers also can be designed by changing their size, geometry, and orientation, depending on the application. Figure 4 shows an example of a Kenics static mixer with four spiral mixing elements [10]. Static mixers are used to allow for homogeneity in the flow characteristics after mixing. Static mixers are more widely used when compared to dynamics mixers due to their reduction in cost, ability to be placed into existing pipelines, and lower shear forces that are placed on the mixer during the process [10].

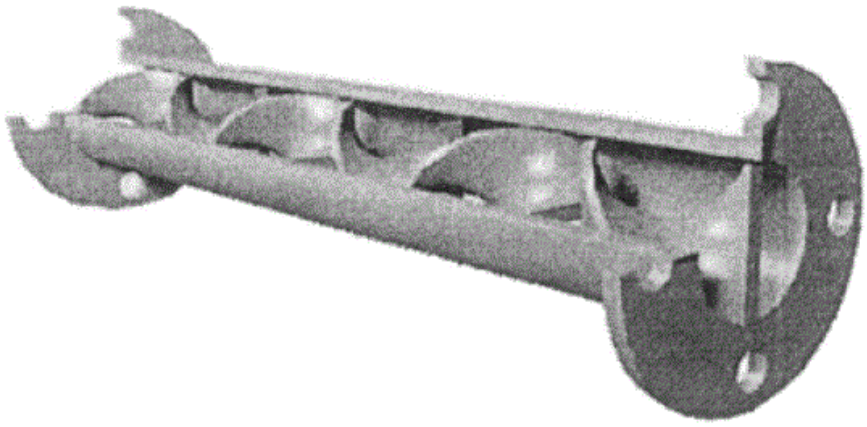

Figure 4. Kenics static mixer [10]

In this study, Yang and Park chose to study the effects of three different mixers: SSC, YNU, and Sulzer SMX and can be seen in Figure 5 [10]. These static mixers are typically used in viscous and applications with low Reynolds numbers. This experiment consisted of these mixers inside of a 40mm diameter acrylic tube, with eight mixing elements. The SSC and YNU models were created to give and update to the Sulzer SMX model by lowering the pressure drop seen, and by limiting the reduction mixing efficiency when compared to the Sulzer SMX [10]. The Sulzer SMX model had been previously studied by other researchers in different applications. Shah and Kale, Li et al., Cybulski and Wener, and Kalbitz all investigated the Sulzer SMX model previously and developed their own results for the friction factor at similar conditions to the present experiment [11, 12, 13, 14]. These elements were placed in a flow loop that utilized a hydraulic manometer to measure the differential pressure on either side of the mixer. The experiment was then ran with single-phase glycerin at low Reynolds numbers (ReD < 20).

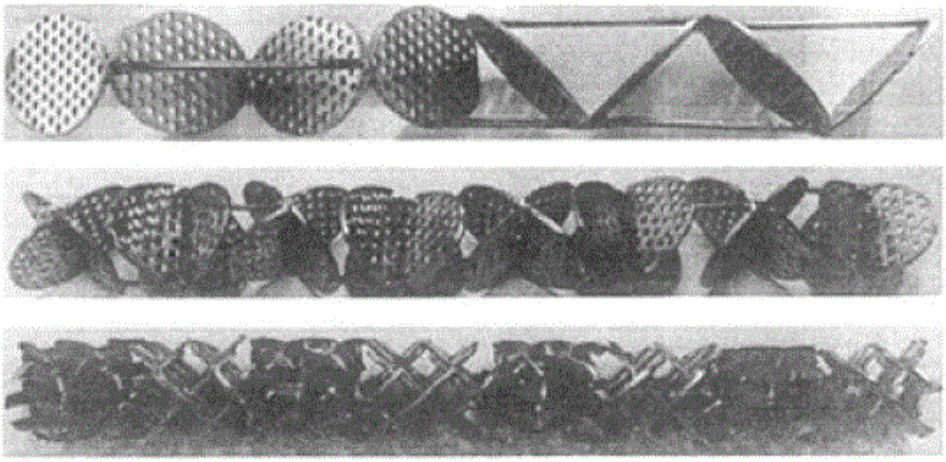

Figure 5. SSC, YNU, and Sulzer SMX static mixing elements [10]

Yang and Park found that the friction factor, derived from differential pressure measurements, from the SSC model was 36% lower than the Sulzer SMX. The YNU model was found to have a

6% higher friction factor when compared to the Sulzer SMX. Friction factor of the Sulzer SMX found in this experiment were also compared to the previous studies mentioned and show that the data is in good agreement. Another key takeaway from their experiment was with an increase in mixing elements, friction factor and differential pressure was also increased. This experiment showed methods to measure differential pressure and compare different static mixing models and their friction coefficient. However, Yang and Park suggest that more investigations should be conducted to show how mixing efficiency, and other parameters are influenced with the addition of elements and modification of geometries [10].

2.5 Experimental Study on Two-Phase Flow in Millimeter-Size Channels

Pehlivan et al. conducted a study on two-phase gas-liquid flow and its effects on frictional pressure drop and flow pattern in small horizontal channels with sizes of 3mm, 1mm, and .8mm diameters and changing flow rates [15]. The purpose of this study was to generate data and compare it to previous correlations regarding friction pressure drop, and to compare flow regime findings to previous flow regime maps [15]. Friedel and Chisholm generated their own correlations alongside the general homogeneous model to help predict the pressure drop in horizontal channels [16, 17]. These correlated models work well when compared to macro-channel flow applications but seem to differ when a micro-channel is used. Kawahara et al., Triplett et al., and Damianides and Westwater conducted previous studies with equivalent diameters to that of the current study to create flow regime maps with transition lines at a range of flow rates in small horizontal tubes [18, 19, 20].

The test set-up consisted of an air and water supply attached to a flow loop. The two flows would meet inside a mixing chamber and be released into a test section where differential pressure

measurements would be measured. During the time the flow passed through the test section a CCD camera would take pictures of the flow to help determine the flow regime for the given flow parameters such as flow rate, temperature, and inlet pressure [15]. The pressure drop measurement data was then compared to the Friedel, Chisholm, and homogeneous pressure drop models alongside data by Ekberg that was generated using a similar test set-up and for a 1mm hydraulic diameter channel [16, 17, 21]. **Error! Reference source not found.**Figure 6 and Figure 7 shows the comparison of Friedel's, Chisholm's, and the homogeneous models for the experimental data found from Pehlivan and Ekberg [15, 16, 17, 21].

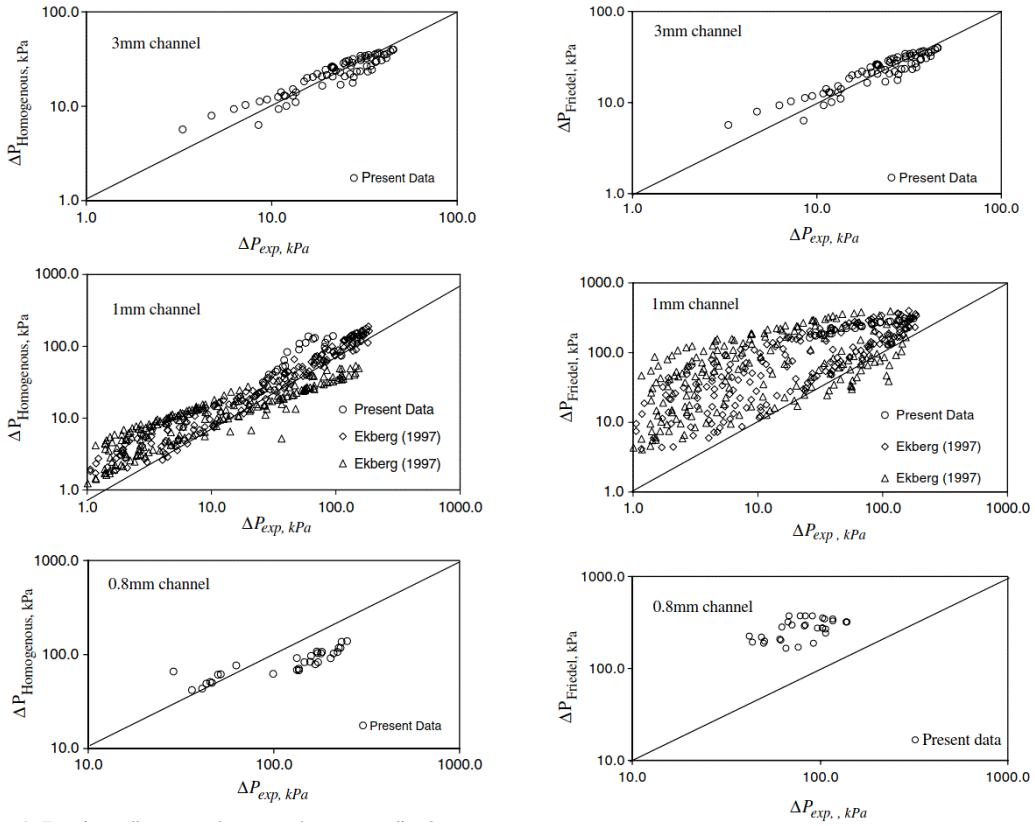

Figure 6 . The comparison of experimental data of Ekberg and Pehlivan for the homogeneous and Friedel flow model [15, 16, 17, 21]

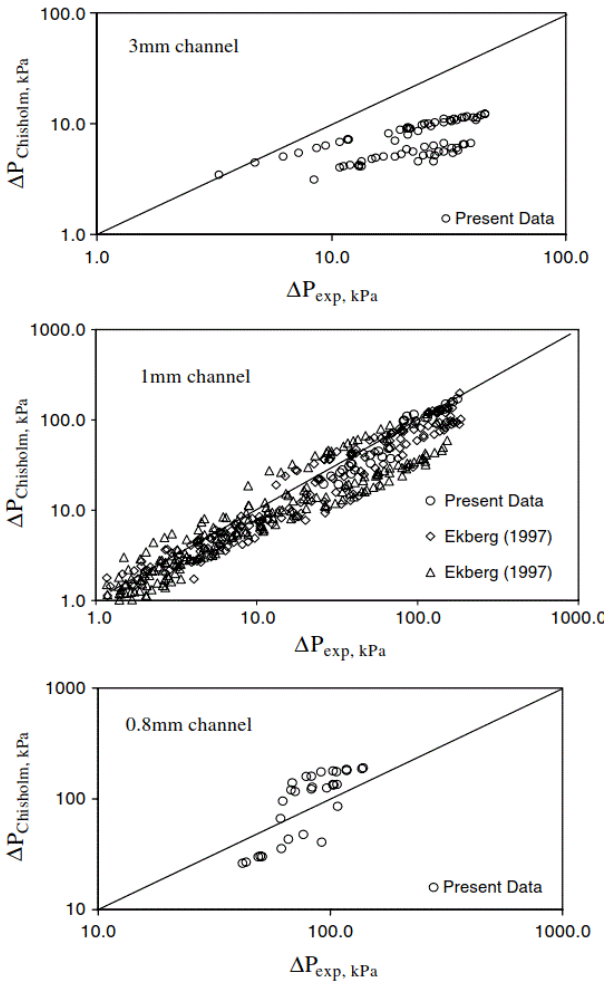

Figure 7 . The comparison of experimental data of Ekberg and Pehlivan for the Chisolm flow model [15, 16, 17, 21]

The findings of the pressure drop comparisons were that the homogeneous model showed the most similarities between the expected and experimental data, but still had discrepancies as the hydraulic diameter was reduced [15]. The Friedel Model generally over-estimated the pressure drop for the given test sections, while the Chisholm Model predicted the experimental data for the 1mm and .8mm diameter tubes [16, 17]. The large takeaway from these comparisons is that the standard deviation tends to increase as the hydraulic diameter of the test section is reduced

[15]. This finding helps back the idea that more experimental data is needed to be able to generate a general, or diameter specific correlation [15].

Previous flow regime maps were compared to that found in the current experiment [18, 19]. The most common discrepancies between the flow regime maps are at points of transition between the different flow regimes. Pehlivan used the previous flow regime maps to create a map that was derived from the current and previous experiments [18, 19, 20, 22]. Figure 8 shows the derived flow regime map applied to the current experimental data.

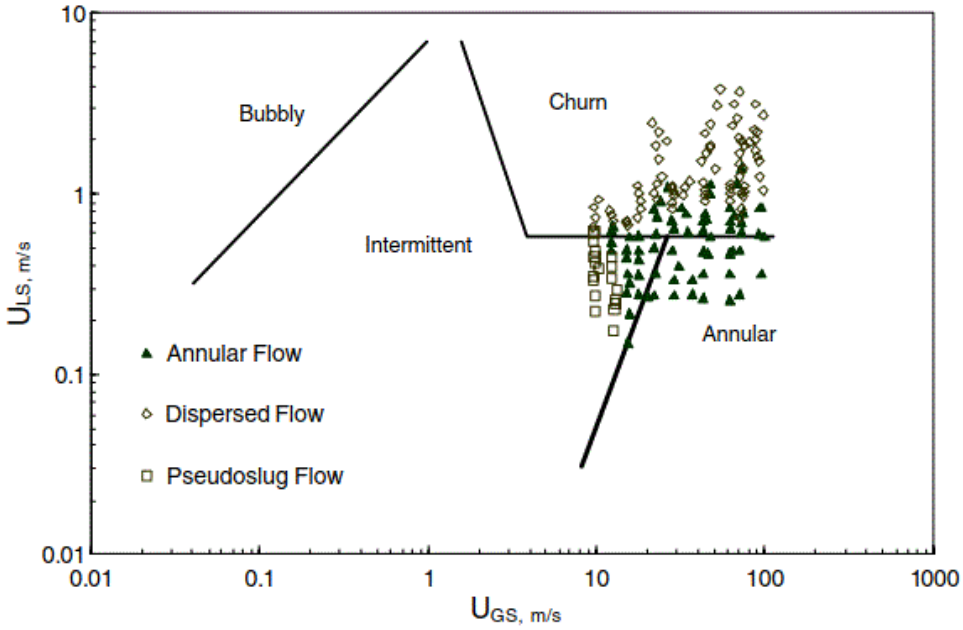

Figure 8. Pehlivan flow regime map compared to present experimental data [15]

The graph shows that the flow patterns determined in this experiment match well with the flow regime map created. Pehlivan's flow regime map was also compared with the results from previous studies and showed good correlation between expected flow regime and what was occurring [15]. Most discrepancies occurred where transition between regimes were occurring,

which leads to the assumption that more experimental data is needed to create a better correlated flow regime map.

2.6 Hydrodynamics and Mass Transfer

Heyouni et al. looked into studying ways to characterize hydrodynamic behavior and mass transfer in a static mixer in a horizontal pipe [23]. Static mixers were studied due to their mixing ability, high interfacial area, high mass transfer coefficient, and other positive impacts in two-phase flow applications. Previous studies were conducted to show the use of static mixers in industrial applications as well as their mass transfer capabilities and dispersion between immiscible phases [24, 25, 26]. The current study looked at static mixer's ability to transfer O_2 and O_3 in a liquid-gas flow system. The parameters found were pressure drop, bubble diameters, interfacial area, and mass transfer coefficient with varying liquid and gas flow rates [23]. The system contained a typical flow loop attached to a gas and water supply, with a pressure sensor and oxygen probe on either side of the static mixer [23]. Pressure drop was measured using a manometer attached to either side of the static mixer. A video camera recorded the flow as it exited the mixer and utilized a software that measured the average diameter of the bubbles [23]. The mass transfer coefficient was measured by feeding nitrogen into the oxygen saturated water. As the water moved through the static mixer, nitrogen transferred from the gas bubbles into the liquid, and the oxygen moved from the liquid to the gas bubbles. Oxygen probes then took measurements before and after the static mixer to measure the mass transfer coefficient of the static mixer [23]. Correlations for pressure drop, bubble diameter, and mass transfer coefficient were generated and produced good results to the data and previous studies [23]. The results of the study showed that pressure drop changed with different geometries of static mixers, and the

pressure drop increased faster with an increase of liquid velocity than when compared to an increase in gas velocity. Bubble diameters were affected by different geometries of static mixers and grew in size with an increase in gas velocity, while decreased with an increase in liquid velocity. Increases in liquid and gas flow rates led to an increase in mass transfer coefficient [23]. Figure 9 shows a comparison of mass transfer coefficient and interfacial area versus the dissipated power for static mixers, stirred vessels, and bubble columns. It can be shown that static mixers provide a higher mass transfer coefficient than their counterparts given the same power dissipation [23].

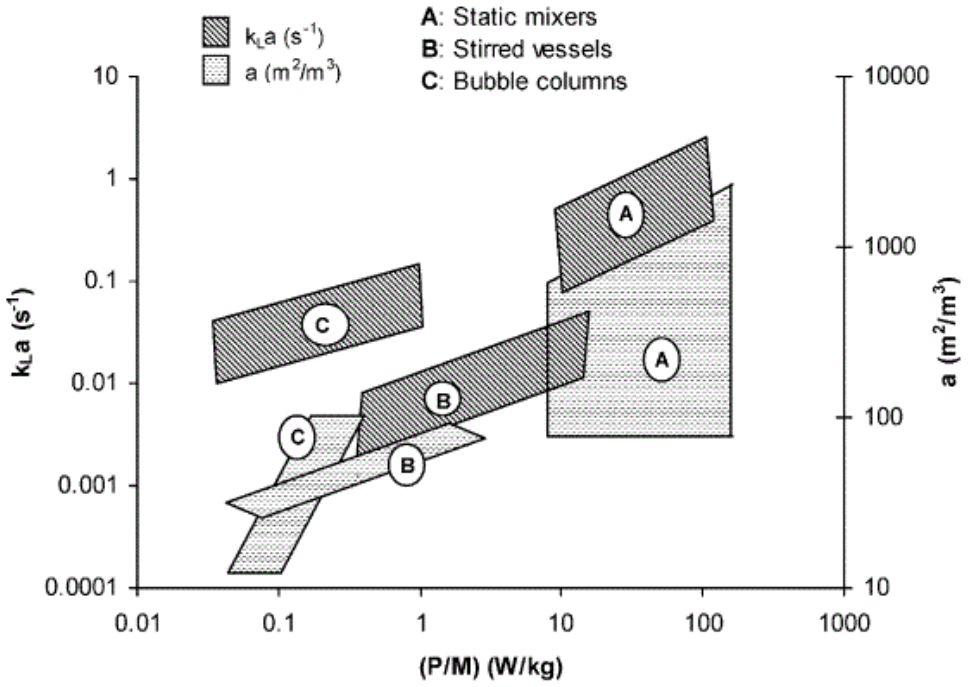

Figure 9. Mass transfer coefficient and interfacial area versus power dissipation [23]

2.7 Study of Fluid Dynamics Conditions in Selected Static Mixers - Pressure Drop

Stec and Synowiec conducted a study looking at fluid dynamic conditions in industrial static mixers, mainly pressure drop due to the mixer [27]. The two static mixers that were looked at were the Kenics and Koflo static mixers. The Kenics is a widely used helical static mixer in many different applications, thus had more previous studies conducted on it. The researchers also looked at the Koflo semicircular bladed static to compare its flow conditions to that of the Kenics static mixer and to a pipe with no mixing element present. A typical single-phase flow loop experiment with pressure drop measurements before and after the static mixer were conducted [27]. The experiments were then ran at Reynolds numbers ranging from 200 to over 10,000. Correlations were formed from the experimental data and were presented as differential pressure and Newton number with respect to Reynolds number in the system. Computational Fluid Dynamic (CFD) simulations were also conducted over the same range of Reynolds numbers and static mixer geometries. The experimental data found was also compared to the manufacturers correlation for their static mixers. Stec and Synowiec found that it is difficult to compare differential pressure data of static mixers to empty tubes based on Reynolds number. This is due to the static mixers already working in the turbulent regime, while the empty pipe might still be acting in the laminar regime. This has been previously shown through studies and manufacturer investigations that the onset of turbulence in a static mixer could occur at Reynolds numbers of 1000 [28, 29]. The results of the experiments were compared to the correlations generated and showed that the average error between the experimental results and correlations were 2.3% for the Kenics mixer, 4.9% for the Koflo mixer, and 7.6% for the empty pipe [27]. Manufacturer pressure drop equations for their static mixer showed a slightly higher expected value than that

of the experimental data, which could be due to the manufacturers wanting to provide a better margin of error in the expected outcome. The comparison between CFD models and experimental correlations showed good comparability in the turbulent regime, but found large discrepancies when data from the laminar regime was compared due to the difficulty of modeling flow through a static mixer at lower Reynolds numbers [27]. Another result of this study was to show how Koflo static mixers compare to other industrial static mixers, as there hasn't been a lot of investigation on its performance. Figure 10 shows the Newton number versus Reynolds number comparison between Kenics, Koflo, and other widely used static mixers. The performance of the Koflo static mixer shows good contrast between the other static mixers and could be a viable option for use in flow systems [27, 30].

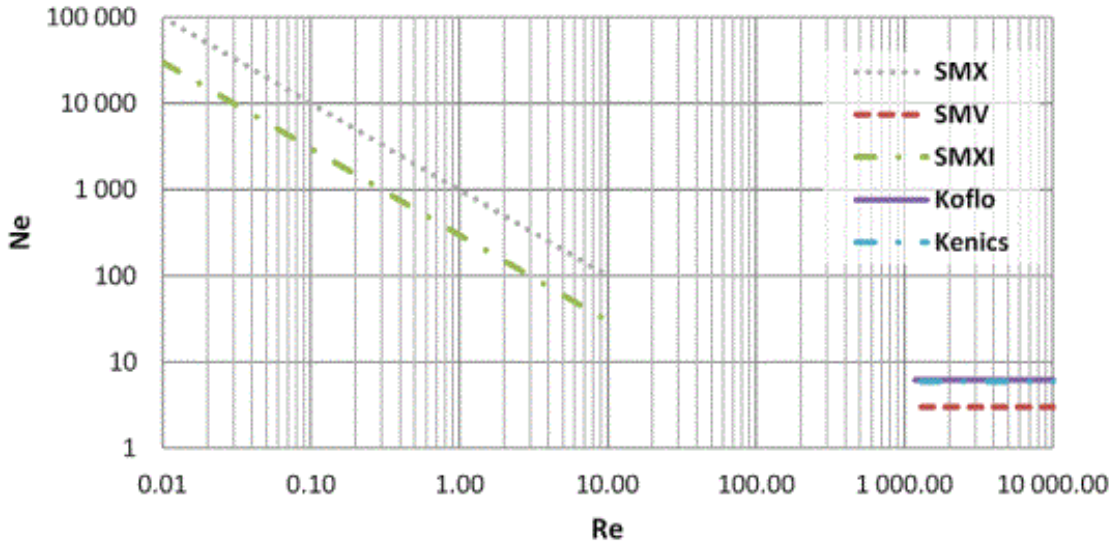

Figure 10. Newton number versus Reynolds number comparison for different static mixer designs [27, 30]

2.8 Study of Fluid Dynamics Conditions - Residence Time

Stec and Synowiec conducted another experiment as an addition to the pressure drop experiments of static mixers relating to the residence time distribution in Kenics and Koflo static mixers [31]. The residence time distribution (RTD) was looked at over a range of Reynolds numbers in both the laminar and turbulent regimes. The study investigates the RTD function E(t), cumulative distribution function F(t), mean residence time t_m, and the variance σ^2 [31]. CFD models were then generated to see how well the models compared to the experimental data generated. Residence time distribution is an important parameter to know during chemical reaction process, mixing, and heat and mass transfer and leads to knowing the mean residence time [31]. It allows the user to know how long elements in a two-phase flow will stay inside the static mixer, or downstream from the mixer, which determines if the contact between the phases is sufficient for mixing or reacting and its reaction rate [31]. The RTD will also give insight to the flow regime occurring inside the system. A water flow loop with a static mixer was previously used in pressure drop experiments by the authors and would be used again, except with an added tracer input valve into the stream [27]. The RTD measurements were taken by injecting a chemical tracer into the reactor by use of a pulse input experiment [31]. Pulse inputs occurred when the tracers were injected into the stream abruptly into the stream following previous studies using pulse inputs [32]. The previous study found that the injection must be injected at time interval smaller than that of the residence times with low rates of dispersion when entering the stream [32]. Following the pulse input of tracers, the outlet concentration of tracers was measured as a function of time to be able to generate the parameters and distributions needed.

The results of the study yielded interesting results when comparing the static mixing elements to an empty pipe regarding RTD and mean residence time. The RTD narrowed when the Reynolds number of the system was increased from a range of 1000 to around 5000, but the flow behavior remained in between ideal mixing and plug flow [31]. The RTD remained relatively the same during turbulent flow in the mixers and the empty pipe as shown in Figure 11. This could lead to the assumption that in turbulent flow, mixing geometry or existence might not play a role changing the RTD in a system [31]. Figure 12 shows the RTD comparison between the devices at laminar flow conditions. The RTD of the Kenics mixer is much narrower than that of the Koflo mixer and even more so of the empty pipe. This explains that the Kenics static mixer has a larger fraction of fluid elements inside that mixer at the same time [31]. This finding could be due to the shape of the mixer, allowing the flow to be more streamlined as it is mixer due to the helical mixing elements.

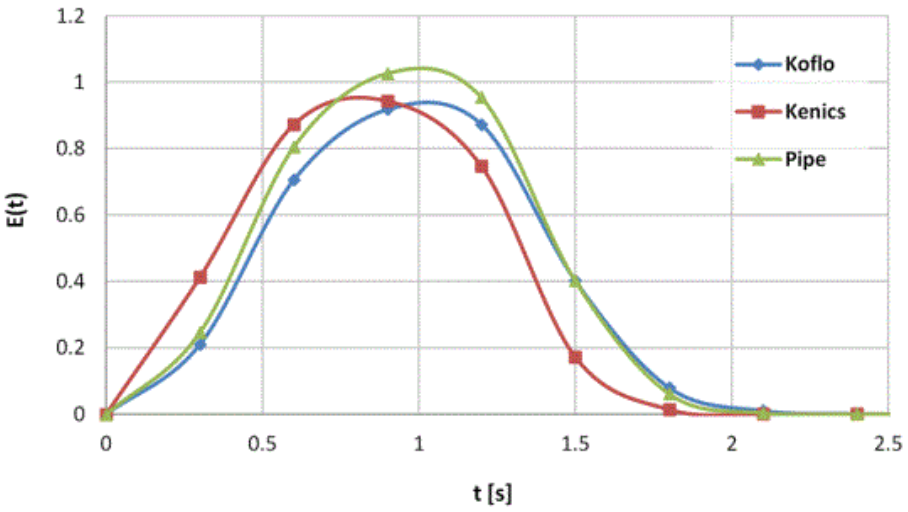

Figure 11 RTD comparisons between the tested devices for turbulent flow (Re = 5186) [31]

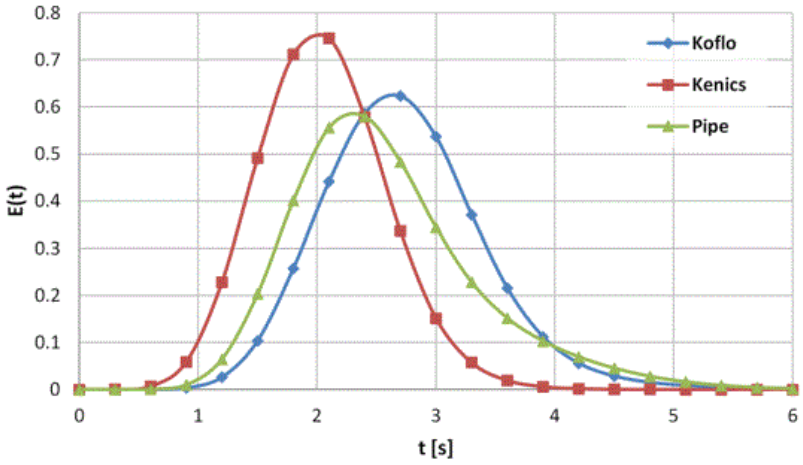

Figure 12 RTD comparisons between the tested devices for laminar flow (Re = 1037) [31]

Over the range of Reynolds numbers, both static mixers showed mean residence time values much higher than theoretical values. The researchers believed this was due to the presence of bypassing and channeling occurring in the device. This allows for a fraction of tracers to exit the mixer immediately, leaving the system to have a smaller effective flow rate and therefore allow for the tracers to have more time in the device [33]. The mean residence time in the empty pipe had data very close to that of the theoretical values during laminar flow. When the Reynolds number increased towards turbulent flow, the values started to deviate due to mixing and disruption [31].

2.9 Improvements to the SMX Static Mixer

Many studies have been conducted in the past on the performance of the Sulzer static mixer and its benefits and uses in two-phase flow applications [14, 29, 34, 35, 36]. The Sulzer SMX static mixer thrives in laminar mixing of high viscous fluids and in many turbulent applications like dispersion of a gas in a liquid stream [37]. Hirschberg et al. conducted a study looking into the

improvements of the new Sulzer SMX plus static mixer versus the previous model [37]. CFD simulations were generated based on both models and compared to laboratory experiments to show measurements of turbulent dispersion and pressure drop across the mixer improved with the new model. Figure 13 shows the two models in the study, the left picture shows the previous version Sulzer SMX static mixer, and the right shows the new Sulzer SMX plus static mixer [37].

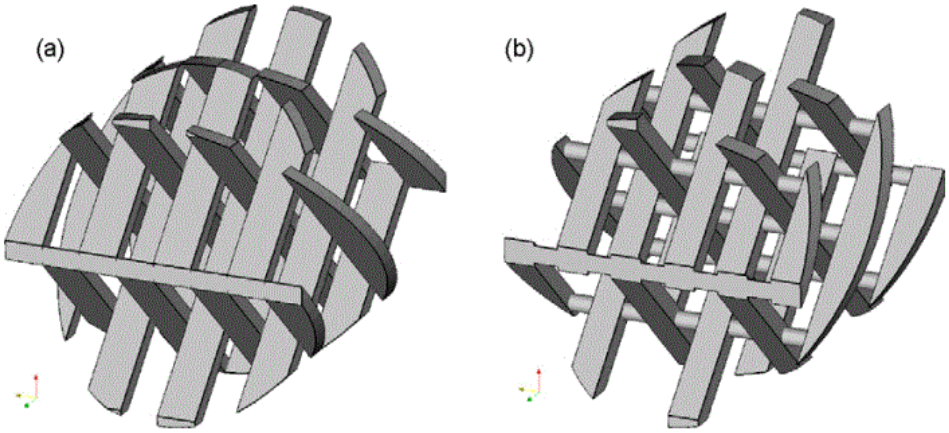

Figure 13 (a) Original Sulzer SMX mixer; (b) SMX plus mixer [37]

The models are similar in the fact that the bars intersect each other at a 45-degree angle to the tube axis and that their mixing elements have a length to diameter ratio equal to 1. Gaps are present in the new model in between the bars, as well as a reduced number of bars, yielding 6 bars compared to 8 bars in the previous model. The experimental approach involved utilizing a laser-induced fluorescence (LIF) test rig to compare to the CFD results generated that the author had previously used in other studies on mixing performance [38]. Decolorization tests were also performed on the mixer to determine mixing of strongly different viscosities. The results of this study were that CFD analysis predicted well with the experimental data. There was a similar

mixing effect between the new model and the old model, but the pressure drop in the new SMX plus mixer had a pressure drop of 50% less when compared to the previous SMX static mixer [37]. The results of the decolorization tests in the SMX plus mixer yielded similar results to that of the prior SMX static mixer dispersion properties. This study showed that the Sulzer SMX plus static mixer performs as well as the old SMX model, but with a lower pressure drop, which leads to a better alternative in two-phase flow applications.

2.10 Optimizing the SMX Static Mixer

Singh et al., investigated further optimizing the Sulzer SMX static mixer with the use of CFD simulations [39]. Different designs were created by changing the three different parameters of the SMX static mixer: The number of cross-bars over the width of the channel, N_x, the number of parallel cross-bars per element, N_p, and the angle between the cross bars [39]. Typical parameters for the current Sulzer SMX static mixer model is $N_x = 8$, $N_p = 3$, and the bars cross at a 45-degree angle. The elements rotate 90 degrees downstream from each individual element [40]. Changing these parameters from the typical SMX model lead the researchers to find an optimum series to be able to achieve similar mixing characteristics between models. The mapping method was utilized in this study to generate CFD simulations for all static mixer designs. Simulations were ran keeping N_x and N_p constant to see the effects of each parameter on each other. The results of the simulation led the researchers to find an optimized series when designing a static mixer for different purposes. The optimized SMX(n) series was found to be: $(n, N_p, N_x) = (n, 2n-1, 3n)$ when compared to SMX^n type series, which could be utilized when designing new SMX style mixers [39]. The SMX^n and SMX(n) series were then plotted as a function of dimensionless pressure drop to determine the performance of each model and can be

seen in Figure 14 [39]. It can be seen that the simplest design (n=1, N_p=1,N_x=3, where n is the number of spaces created by the parallel bar) led to the best mixing for lowest energy consumption, or the differential pressure [39]. However, Singh et al. believed that this design shouldn't be compared to that of the more complex designs, but some of the other simpler static mixer designs, due its long dimensionless length L/D [39]. Also, it can be seen for better mixing applications, or lower log(I) (where log(I) is the discrete, cross-section averaged, flux weighted intensity of segregation), the SMX(n) series would be best, even though the SMX^n initially provides better mixing quality with a short length [39].

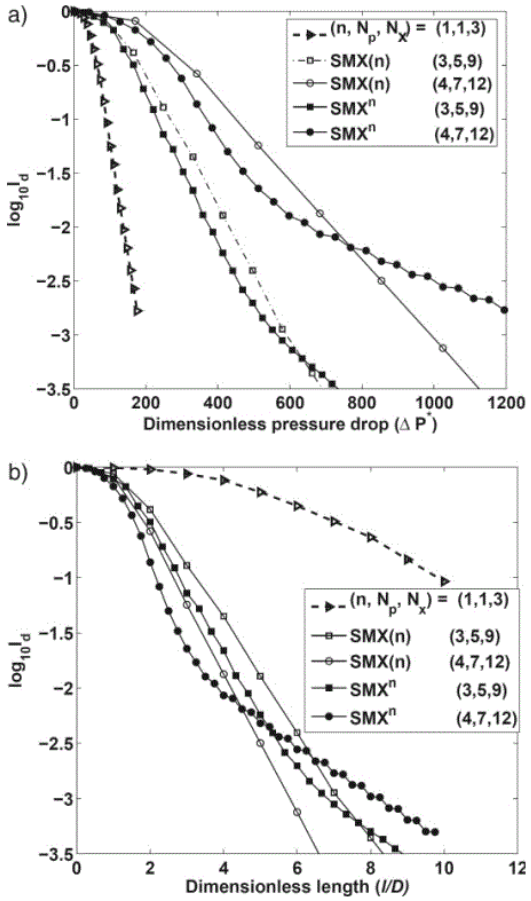

Figure 14 (a) Differential pressure, (b) L/D comparison of SMX^n and SMX(n) series [39]

2.11 Single-Phase Mechanistic Model for Pressure Drops in Static Mixers

Paglianti and Montante conducted experimental data to generate a mechanistic model for pressure drops of single phase flow through corrugated static mixers [41]. The effects of static mixer element length and position between elements and their effect on pressure drop were also investigated [41]. Corrugated static mixers have been found to perform better in the turbulent regime when compared to SMX and helical style mixers, while being limited when in the laminar regime [42]. In a typical turbulent mixing flow in an empty pipe, it has been experimentally shown that the mixing length necessary for achieving homogenous flow was around 100 pipe diameters, while 3-8 diameters has been shown to provide adequate mixing for static mixers [43]. Previous studies have investigated the analysis and modeling of pressure drop of static mixers, but found difficulty creating a universal model [29, 30, 43]. Single-phase flow pressure drop correlations have been used in previous studies and are in terms of Newton number, Ne, as a function of the pipeline Reynolds number, Re [29, 41, 42, 44]. The current study utilizes a typical single-phase flow loop, with a static mixer in the flow path and pressure sensors on either side of the mixer. Figure 15 shows the corrugated static mixers that were investigated at typical L/D =1 and unconventional L/D =.31, to see the effects of "by-pass" on a unit [41]. Paglianti and Motante based their model off of, "the assumption that the overall frictional pressure drops are dependent on the distributed pressure drop between the fluid and mixer walls, and the concentrated pressure drop at the inlet, outlet, and at the surface between consecutive elements [41]." The theoretical mechanistic model derived by the researchers was then compared to prior experiments and their own experimental data. The finding was that the

model worked well with prior data and could be manipulated to be used in estimating other static mixer configurations [41].

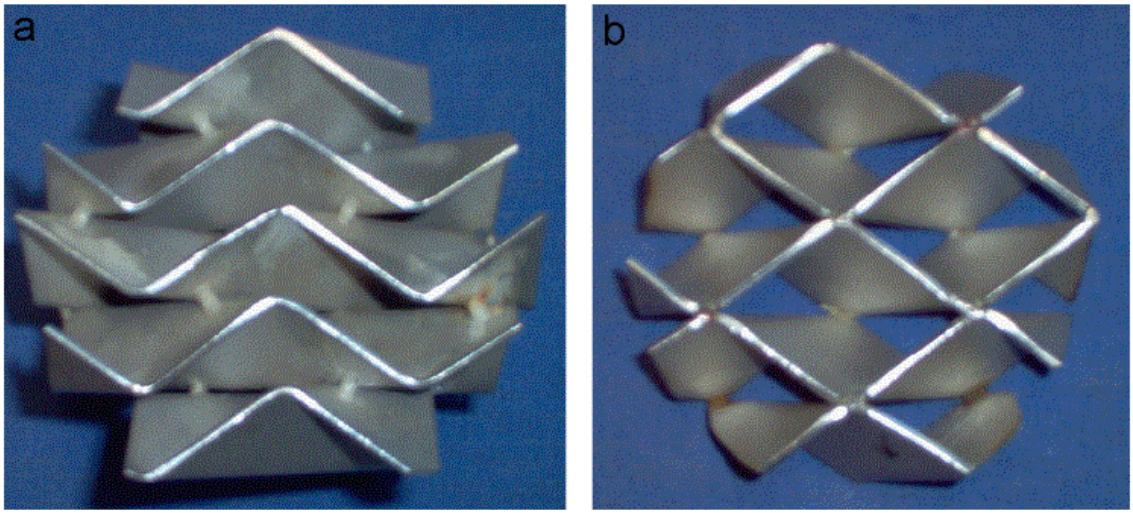

Figure 15 Front view of (a) standard length element and (b) unconventional length element [41]

2.12 The Rheology of Suspensions of Solid Particles

Pak and Nasser investigated the experimental effects on rheology of polymer solutions, solid suspensions, the addition of polymers to solid suspensions, and temperature. The researchers also obtained models to best fit the experimental data and compared them to typical flow models [45]. Rheology relates to the flow and deformation of materials, and for this study the dynamic viscosity of fluids. Polymer solutions typically exhibit non-Newtonian behavior, which means the viscosity changes with respect to shear rate, due to the entanglement of the polymer chains at rest [46]. An increase in concentration of polymer in a solution, the behavior of the solution tends to change from fluid-like to more elastic-like behavior, where a decrease in polymer concentration will cause the solution to depend only on the dynamics of the individual chains in

the fluid [47]. Bentonite, graphite and Corn starch were suspended in distilled water for the experiments. Four polymers (XC, HEC, CMC, and PVA) of different concentrations of 2, 5, 7, and 10 g/L were placed into the solid suspensions slurries at concentrations of 40g/L [45]. The rheological properties were measured using a Fann VG-Viscometer Model 35 A and ran at a rotation rate of 3, 5, 100, 200, 300, and 600 rpm for roughly 3 minutes. The results of the 10g/L and 2g/L of PVA in the 40g/L bentonite suspension is shown in Figure 16 and Figure 17 respectively, and the experimental data is plotted against the typical flow models [45]. These plots show that an increase in PVA will cause the suspension to go from a shear thickening behavior to a shear thinning behavior [45]. Pak and Nasser stated, "It was found that as the polymer and solid suspension concentrations increased, the flow behavior index decreased and increased respectively [45]." The researchers found that the utilization of the Bigham flow model produced the best results when compared to the PVA/Bentonite experimental data [45].

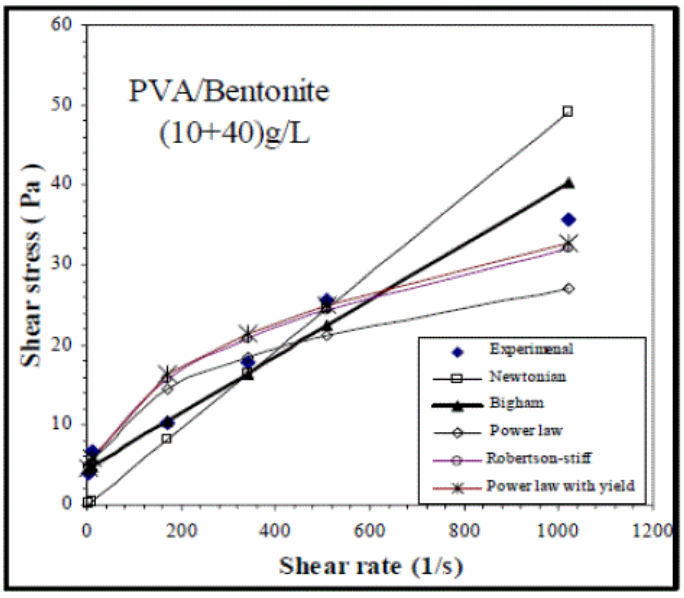

Figure 16 Experimental results and flow models for 10g/L PVA and Bentonite Suspensions at 35˚[45]

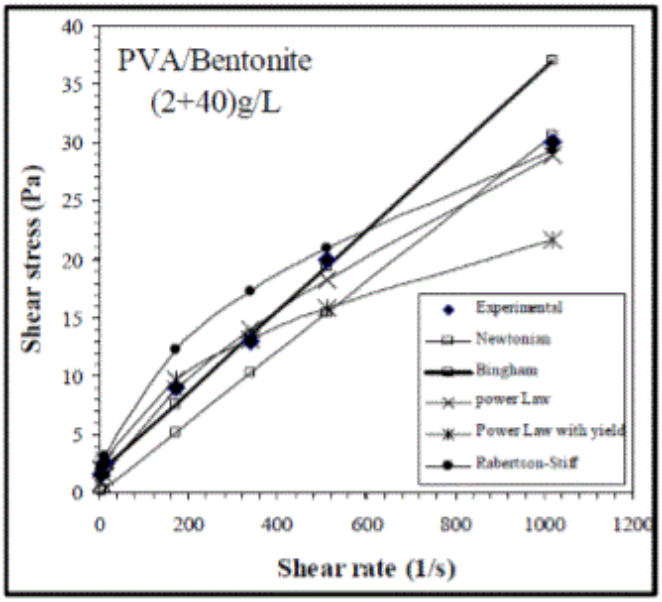

Figure 17 Experimental results and flow models for 2g/L PVA and Bentonite Suspensions at 35˚ [45]

CHAPTER 3

EXPERIMENTAL SETUP AND METHODOLOGY

3.1 Overview

The experimental set up needed to measure the differential pressure across the static mixer, the static pressure downstream of the static mixer, static temperature, and liquid and gas flow rates supplied to the system are explained below. The use of a rheometer will be explained to show how the values of liquid viscosity were determined. The findings from this data will help in analyzing the power input from the liquid pump, pressure profile downstream, Reynolds mixture number, and static mixer behavior. The three static mixer geometries used in the following experiments will also be further explained in this chapter. Figure 18 shows the experimental schematic containing the liquid storage tank, gear pump, mass flow meter, thermocouples, differential pressure transmitters, static pressure transducers, static mixer, and the data acquisition system.

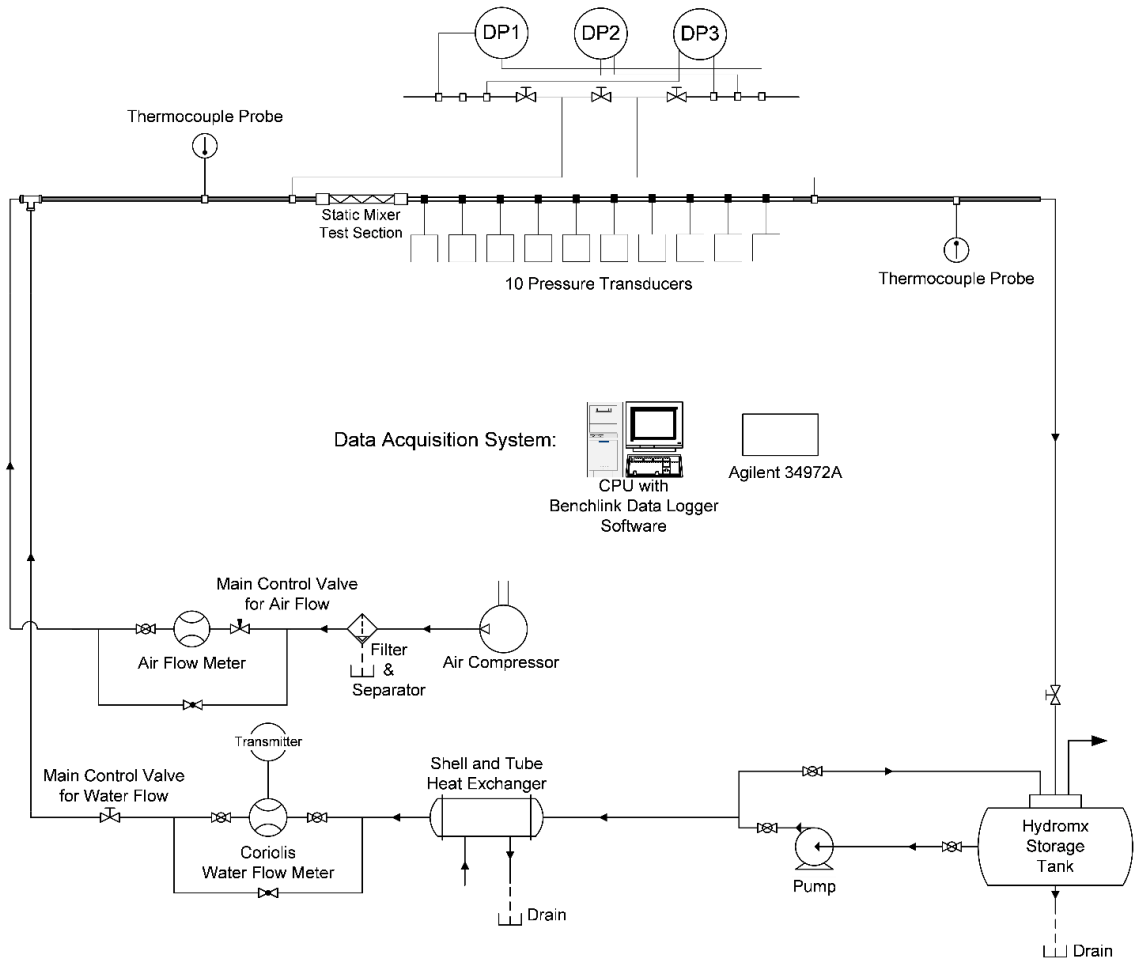

Figure 18 Schematic of the experimental set-up

A PVC cylindrical tank with a diameter of 0.25 m, and a tank volume capacity of 15 liters was used to hold the experimental fluid Hydromx that will be explained later. The testing fluid moved into the storage tank downstream of the test section, while the tank was covered. The tank was placed above the liquid gear pump to allow for a decrease in power needed to pump the liquid into the test section. The Hydromx storage tank and its plastic tubing connected to the flow loop can be seen in Figure 19.

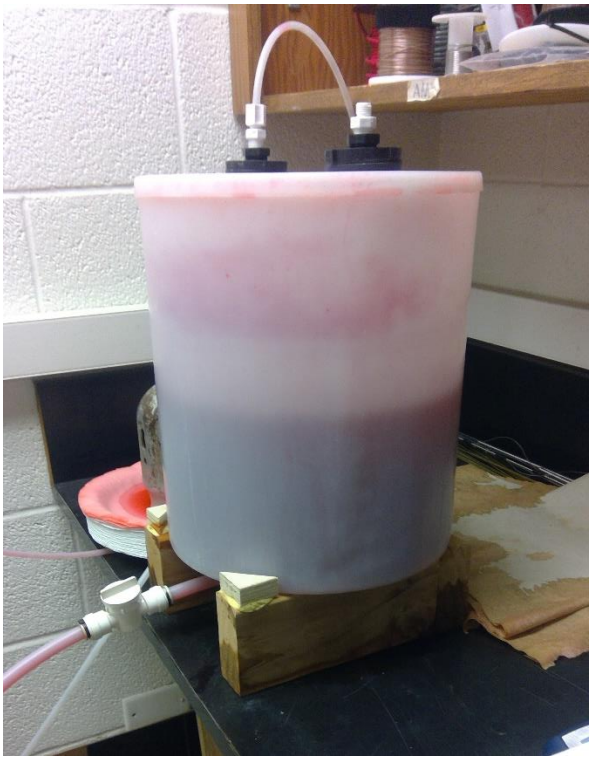

Figure 19 Hydromx storage tank

The liquid gear pump used in the experiment was the Liquiflo 35F shown in Figure 20 [48]. The design limits of the pump are 13 liters per minute (LPM) volumetric flow rate and a maximum pressure drop of 6.9 bars or roughly 100 psi [48]. Hydromx is fed from the storage tank into the pump and moves from the pump into the rest of the 3.175 mm ID pipe flow system. During the pumping process, a counter flow double-pipe heat exchanger is used to cool the working fluid and ultimately to keep the pump from overheating.

Figure 20 Liquiflo gear pump

The liquid flow rate from the gear pump was monitored by a CMFS010M Micromotion Coriolis mass flow meter and can be seen in Figure 21. The mass flow meter was used to measure and help the user in controlling the flow rate through the system. The maximum flow rate that can be measured by the mass flow meter is 30.5 grams per second and the liquid flow rate accuracy of this meter is ±0.05% [49]. The flow meter works on the principle of the Coriolis effect. Two measuring tubes are placed inside the sensor and allow liquid flow rate to move through the tube allowing a change in vibration between the flow tubes. The time difference between vibration waves is measured and can be correlated to mass flow rate [50]. The flow meter is then connected to the data acquisition system explained later, to measure the mass flow rate of the tests.

Figure 21 CMFS010M Mass Flow Meter

The gas supply that came from an air compressor and entered the system was monitored and controlled by an Alicat mass flow controller shown in Figure 22. Air was passed from the compressor through the controller at a volumetric flow rate ranging from 0.25 to 3 standard liters per minute (SLPM). The volumetric flow rate readings were taken using the display on the controller itself and were not monitored with the use of a data acquisition device. These values could then be converted to mass flow rate values with an uncertainty of ± (0.8% of Reading + 0.2% of Full Scale) for use in later calculations.

Figure 22 Alicat MC5 mass flow controller for air supply

Temperature of the bulk fluid system before and after the test section was measured by two Type T TMQSS-020U-6 thermocouples shown in Figure 23. The tips of the thermocouples were placed into the center of the pipe to allow for a bulk temperature reading. The accuracy of the temperature readings is ±0.4% [51]. The thermocouples were attached to the data acquisition unit and measured throughout each test. The temperature data allowed for the calculation of density and viscosity of the working fluid.

Figure 23 TMQSS-020U-6 Thermocouple

Emerson Rosemount differential pressure (DP) transmitters are shown in Figure 24. Three different units were used to allow for a greater range in pressure drop when static mixers were used, and flow rates increased. The limits of the DP transmitters used were 300, 36, and 9 psi with an accuracy of ±0.65%. The three transmitters were connected through a manifold that was also attached upstream and downstream of the test section. The transmitters were then attached to the data acquisition unit to allow for a continuous pressure drop readings across the test section. DP measurements are important to know to be able to quantify the power requirements of the system with different static mixer geometries implemented.

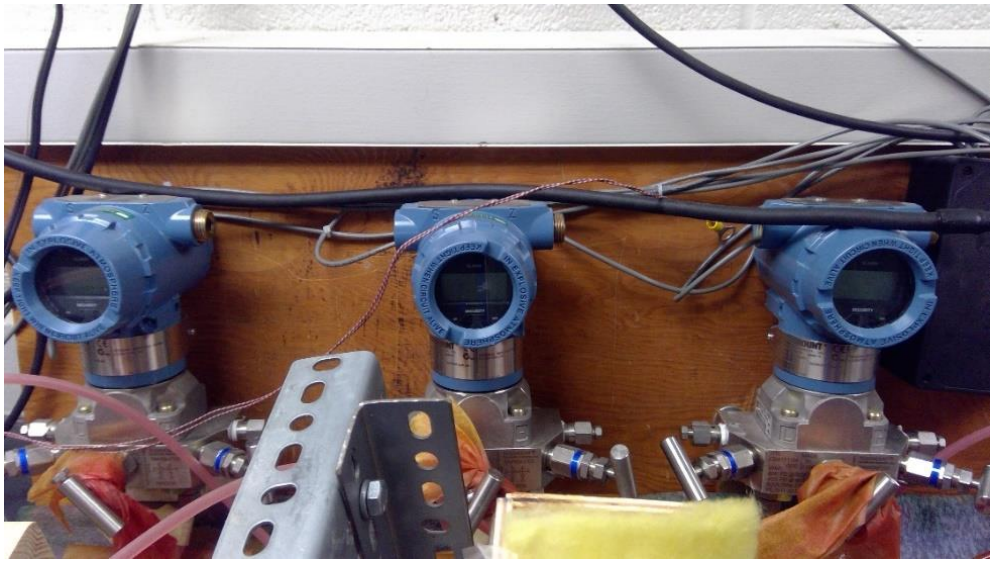

Figure 24 Rosemount differential pressure transmitters

3.2 Static Pressure Transducers

The static pressure downstream of the static mixer was measured by Honeywell heavy duty PX2 pressure transducers and is shown in Figure 25. The Honeywell PX2 heavy duty pressure transducers utilize a piezo resistive sensing technology to measure pressure [52]. The Honeywell

heavy duty pressure transducers were chosen because the static pressure measurements are critical to the findings of this study. The PX2 transducers have a life space of around 10 million cycles and with a six-sigma design standard, will give enough reliability to conduct the research. The accuracy of the pressure transducer is ±0.25% of the full-scale span (FSS) with the FSS being 50 psia [52].

Figure 25 Honeywell 50 PSIA PX2 heavy duty pressure transducer

Ten PX2 transducers will be used in the experiment downstream of the static mixer to allow for the measurement of the pressure profile as shown in Figure 26. Plastic tubing of equal lengths connected the pressure transducers to the pressure taps along the test section. The pressure taps were arranged with ten diameters (1.25” or 31.75 mm) between consecutive taps. The distance between these taps allows for an easier way to scale the test up for different diameter pipe systems. Ten diameters were also spaced between the exit of the static mixer to the first pressure tap, to allow for fully developed flow assuming turbulence. The pressure transducers were then attached to a 5-volt power supply and into the data acquisition unit to obtain voltage values from a pressure calibration device that were then converted to gage pressure values to be utilized in static pressure measurement tests.

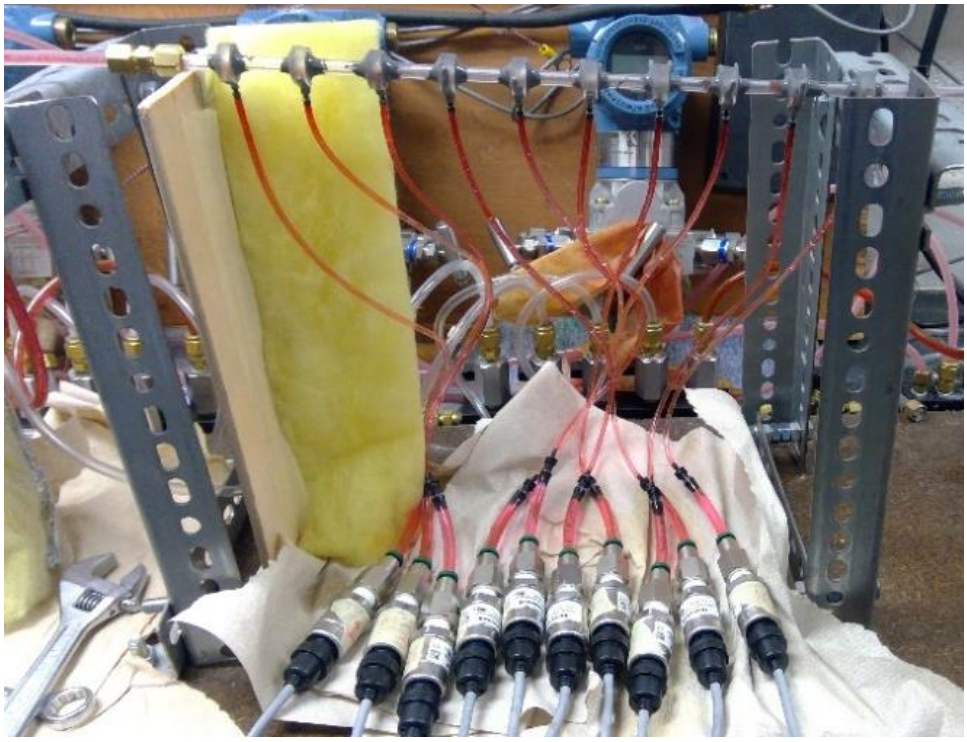

Figure 26 10 pressure taps downstream of static mixer

3.1 Static Pressure Transducer Calibration

The Honeywell PX2 pressure transducers were calibrated using a Fluke 3130 pressure calibrator shown in Figure 27. This was done by connecting the ten pressure transducers in line to the pressure calibrator. The transducers would output a voltage when a pressure signal was applied and be sent to the data acquisition unit. The pressure applied by the pressure calibrator would range from 0 to 35 psig, which is roughly the full range of the pressure transducer.

Figure 27 Fluke 3130 pressure calibrator

The voltage data from the data acquisition unit could be used to generate a linear regression curve fit equation for each pressure transducer shown in Figure 28. The linear fit line was generated based on an average of the 240 data points collected. The closeness of the data points to each other show that the pressure transducers are repeatable throughout experiments. The linear fit line was found based on the y = mx + b form, where y is the pressure reading, and x is the voltage output from the transducer into the data acquisition unit. The equation for the line was found to be:

$$y = 12.48897x - 20.22490 \quad (3.1.1)$$

The range of m and b values from the individual transducers were found to be 12.39453 to 12.52262, and -20.04518 to -20.33989 respectively. The percent error of the pressure values based on the calibration data was found to be ±0.75%.

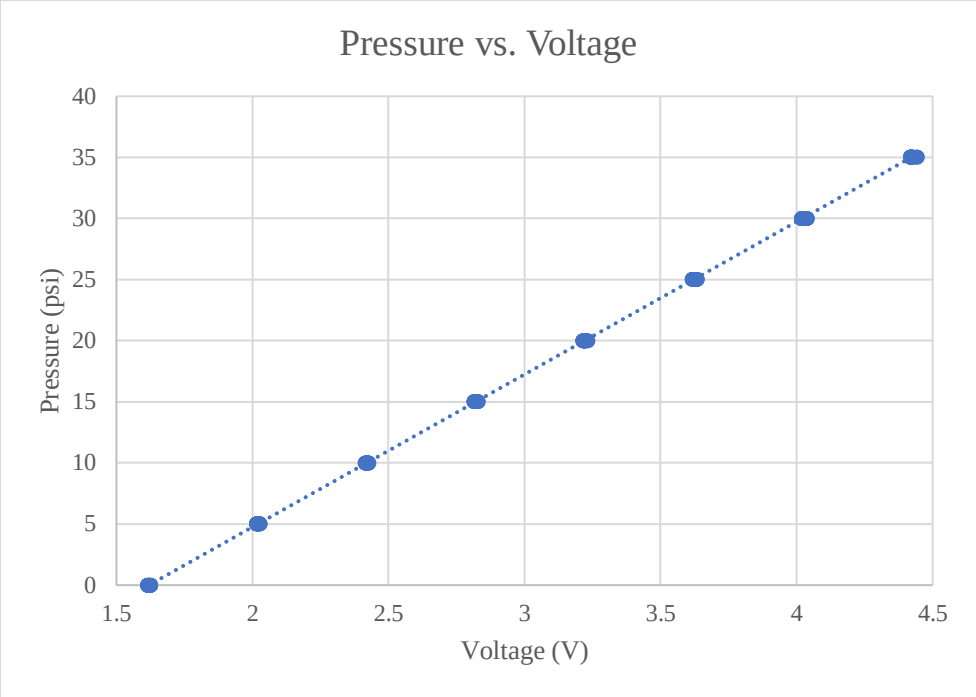

Figure 28 Average calibration curve for all transducer data points

3.3 Data Acquisition

The Agilent 34972A was used as the data acquisition unit for the entire study and is shown in Figure 29. The sample rate of the unit was roughly 0.7 seconds per sample when measuring three differential pressure transmitters, a mass flow unit, two thermocouples, and ten static pressure transducers. This sample rate was found to be sufficient for the study, but might need to be adjusted for future pressure fluctuation investigations. The Agilent unit would be connected to a computer and the data would be obtained using the BenchLink Data Logger Software.

Figure 29 Agilent 34972A data acquisition unit

3.4 Static Mixer Test Section

There was a total of four test sections that were studied. The first section that was studied was an empty pipe, which would give baseline data to how the flow interacts in the system. The three other test sections were three static mixers with geometrical differences. The test section was 10.16mm long and had an inner diameter and outer diameter of 3.125 mm and 6.25 mm, respectively. The test section can be seen in Figure 30, and was attached to the flow loop using quick attaching compression fittings for easy removal. The test section was between the inlet of the differential pressure sensor and roughly ten diameters away from the first static pressure transducers to allow for fully developed flow to be measured by the transducers.

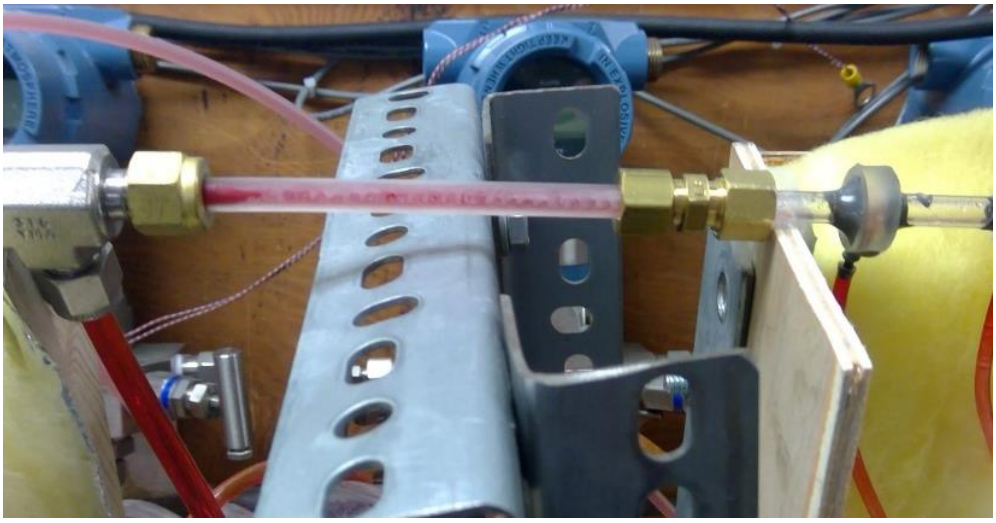

Figure 30 Static mixer test section

3.5 Static Mixer Creation

The three static mixer designs will be described by their geometries: the helical style, the double plate, and the triple plate static mixers. These element styles were created based off previous studies and common industrial static mixers. The studied static mixers were derived from the Kenics static mixer, Koflo static mixer, and a simplified Sulzer SMX static mixer previously mentioned [10, 27, 28, 39]. These designs were modeled in Creo Parametric and printed using a FormLabs Form2 3D printer shown in Figure 31. The Form2 printer is a stereolithography (SLA) type 3D printer. It prints prototypes utilizing an inverted SLA method, where liquid resin is emptied into a tank and a build platform is lowered into the liquid resin. The build platform is lowered into the resin a UV laser points at two mirror galvanometers, which direct light toward the build platform and curing a layer of photopolymer resin to the surface [53].

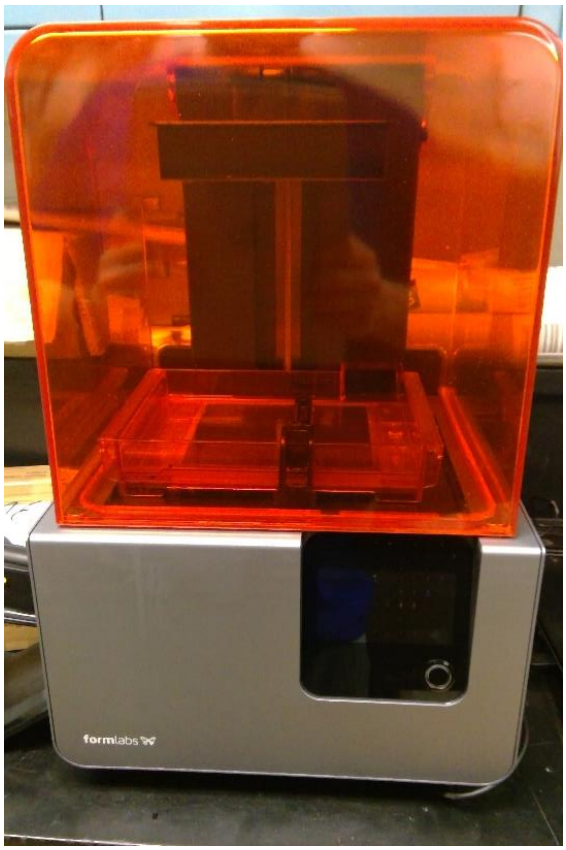

Figure 31 FormLabs Form2 3D printer

The curing of the photopolymer resin is done by a polymerization process. Short chains of polymers generally yield a viscous resin that is utilized in this set up. As the UV light interacts with the resin on the surface, the short chains of polymers in the resins join and cross-link to create longer chains [53]. The result of this process leaves a solid material on the surface. The Form2 printer can print at resolutions that other 3D printer types are not capable of, which result in a smooth surface in the printed static mixer test section. The 50-micron layer thickness was chosen in this study for the surface resolution of the printed parts. This resolution was chosen because it allowed for high quality prints but shortened the print time of the prototypes.

3.6 Static Mixer Design

The helical static mixer design can be seen in Figure 32 (a-c). Figure 32(a) shows the individual element, which consists of a 180-degree helical rotation of a flat plate of thickness (t = 0.0635 mm) and a length to diameter ration of (L/D = 1). Figure 32(b) shows a chain of four elements, which is the typical number of elements for this small diameter static mixer type [54]. Each consecutive element is rotated 90 degrees about the cylinder axis. Figure 32(c) shows the static mixer element chain inside the 3.175 mm ID and 10.16 mm long test section that would be used in the experiments. This design was chosen because it is a typical static mixer design type that has provided good differential pressure drop and mixing behavior in previous studies [10, 27, 31].

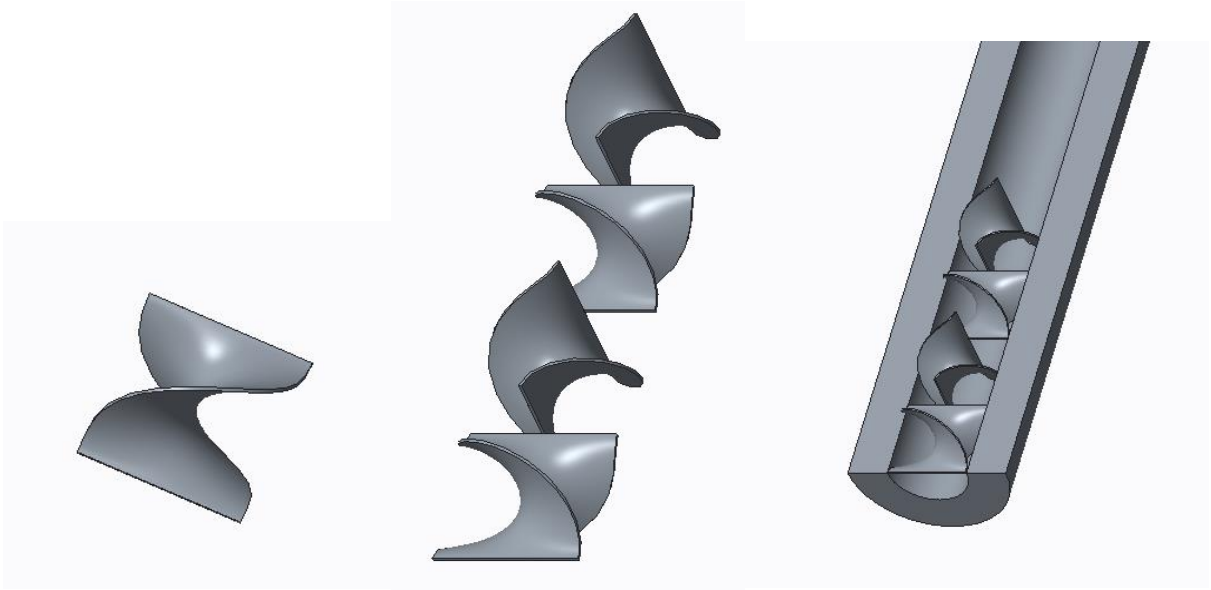

Figure 32 Helical (a) single element (b) element chain (c) static mixer

The double plate static mixer element, element chain, and static mixer is shown in Figure 33 (a-c). The element is comprised of two perpendicular plates opposite one another and oriented at an angle of 30 degrees to the pipe. The plates have of thickness (t = 0.0635 mm) and are consecutively rotated 180 degrees about the cylinder axis with an element length to diameter ratio of (L/D = 1.73). This design was similar to those used in previous studies that showed good behavior when compared to other industrial static mixers [27, 28, 31].

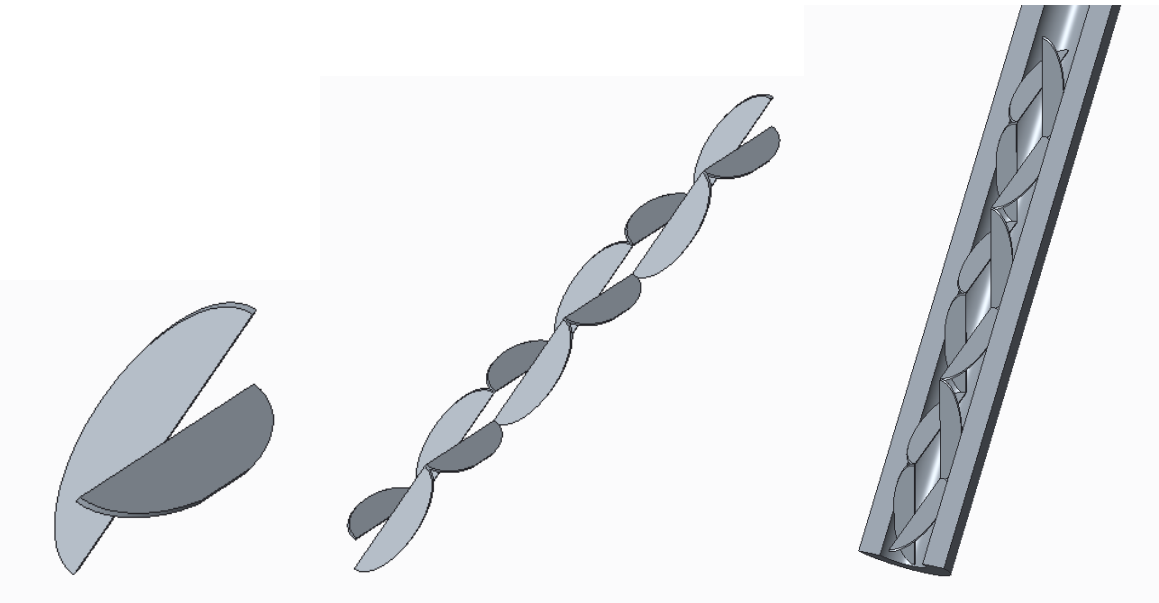

Figure 33 Double plate (a) single element (b) element chain (c) static mixer

The triple plate static mixer element, element chain, and static mixer is shown in Figure 34 (a-c). The element is comprised of two parallel plates that are perpendicular to a central plate. The plates are oriented at 45 degrees to the pipe. The plates have of thickness (t = 0.127 mm) and are consecutively rotated 90 degrees about the cylinder axis with an element length to diameter ratio of (L/D = 1). The width of the parallel plates is 0.0455” or 1.16 mm and the central plate has a

width of 0.86 mm. The design is a simplified model of the Sulzer SMX model, which is an industry proven static mixer, and was computationally shown to have similar mixing characteristics and a lower pressure drop to the original SMX model [34, 39, 40]. Table 1 shows the length, surface area, and volume of the completed static mixers. It is important to note that the triple plate static mixer has roughly the same volume as the double plate, while having a smaller overall length. This could affect certain parameters such as pressure drop across the static mixer as the volume/length measurement could be related to a cross sectional area of the mixer. A larger cross-sectional area should cause the differential pressure to rise across the static mixer test section.

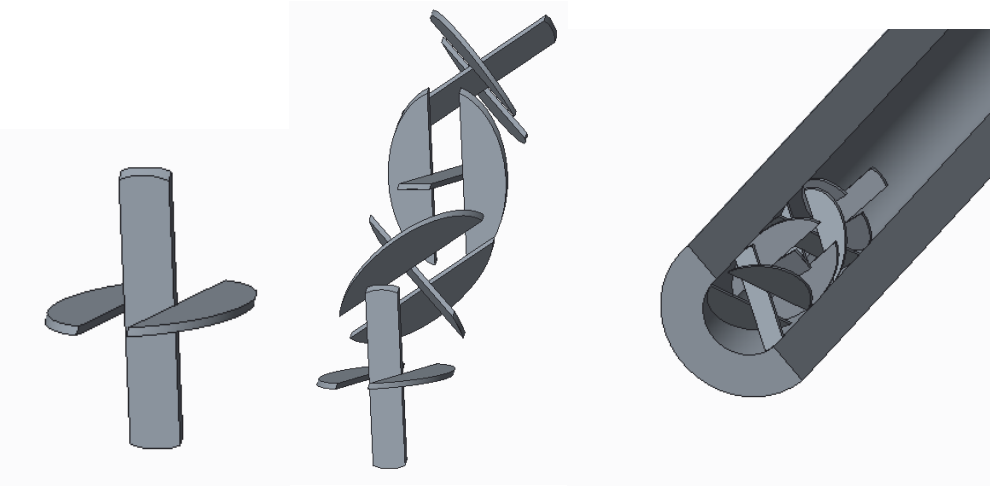

Figure 34 Triple Plate (a) single element (b) element chain (c) static mixer

Table 1 Volume, surface area, and length measurements of the corresponding static mixers

	Helical	Double Plate	Triple Plate
Number of Elements	4	6	4
Length (mm)	12.7	33.1	13.12
Surface Area (mm^2)	110.8	395.3	98.0
Volume (mm^3)	3.5	6.0	5.7
Volume to Length (mm^3)	.28	.18	.43

3.7 Single-Phase Experimental Procedure

The investigation of static mixers and their effects on the downstream profile began with generating baseline data for a single-phase experiment with an empty pipe. Hydromx was pumped through our flow system and the flow was manually controlled using a mass flow meter and our data acquisition software to monitor that data. As the flow traveled through the test section, differential pressure, temperature, and the pressure profile data was tracked at various mass flow rates measured in grams per second (g/s): 4.75, 7, 9.25, 11.5, 13.75, 16, 18.25, 20, 22.5, 25, 30, and 35. After the baseline data was measured using an empty pipe, the three static mixers were placed into the flow system and their data was recorded over the same range of mass flow rates as the empty pipe. Three cycles of varying the gas flow rate were conducted.

3.8 Two-phase Experimental Procedure

After the baseline single-phase flow data through a static mixer was obtained, two-phase flow tests were conducted. Gas flow entered the flow loop by a 100-psi gas supply from an air compressor. A method like the single-phase flow experiments was conducted in the two-phase flow tests. An empty pipe and the three static mixers were placed into the flow loop while liquid and gas mass flow rates were varied over a range of flow rates over a series of three cycles. The liquid flow rates used in the two-phase tests were: 4.75, 7, 10, 12, 15, 18, 21, and 24 g/s. The gas

flow rates that were used consisted of: 0.01, 0.02, 0.03, 0.04, 0.05, and 0.06 g/s. As the liquid flow rate was increased to around 18 g/s, the gas flow rate that could be used was limited, due to exceeding the limits of the static pressure transducers. The highest mass flow rates that could be evaluated were a mass and gas flow rate were 24 g/s and 0.02 g/s, respectively.

3.9 Viscosity Measurement

Viscosity behavior of the testing fluid Hydromx was measured using a Brookfield DV3T Rheometer which has an accuracy of ± 1% of full scale range and is shown in Figure 35. Viscosity is an important parameter to know when conducting flow experiments because it gives an insight into the flow behavior of the liquid. Viscosity is the measure of internal friction of a fluid [55]. Viscosity is found based on knowing the shear force on layers of liquid moving past each other and the velocity gradient and can be found utilizing the equation below:

$$\tau = \mu \frac{dv}{dx} \tag{3.9.1}$$

Figure 35 Brookfield DV3T Rheometer

Different flow behaviors of materials can be found when looking at shear stress vs. shear rate, and viscosity vs. shear rate experiments. The purpose of understanding the flow behavior will give insight to whether the material is Newtonian or non-Newtonian. The knowledge of understanding the flow behavior help when conducting flow experiments, and data manipulation. Figure 36 shows the behavior of a Newtonian fluid, where shear stress vs shear rate provides a linear line, and the slope is the viscosity of the fluid in graph A, while graph B shows that viscosity is constant with a change in shear rate [55].

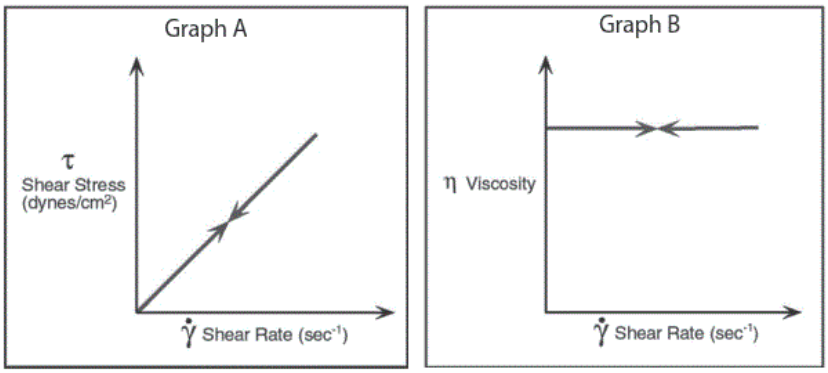

Figure 36 Newtonian behavior plot [55]

Non-Newtonian fluid behavior occurs when shear stress versus shear rate is not a constant linear slope [55]. The different behaviors can be classified as pseudo plastic, dilatant, plastic, thixotropic, and rheopectic [55]. Factors that will be investigated in the viscosity study are effects from temperature, shear rate, and time.

A cylindrical spindle was attached to the Brookfield DV3T rheometer to conduct the viscosity experiments and is shown in Figure 37. A sample of 8ml of Hydromx will be placed into a cylinder where the spindle will be inserted to begin measurements. Hydromx will be measured

with a 100%, 60:40, and a 50:50 ratio composition of Hydromx and distilled water, where the 50:50 ratio is the composition that is utilized in industrial applications. Measuring the three different compositions will provide insight to the viscosity of the fluid and what happens if there is any evaporation during the static mixer flow tests. The rheometer will provide a constant shear rate determined by the user and the rheometer will track the shear stress data. The rheometer also measures the experimental fluid temperature throughout the experiment, while a Brookfield TC-650 temperature bath is used to control the temperature of the fluid and is shown in Figure 38. The temperature range that the experiments were conducted at ranged from 5 to 30 degrees C. The shear rate or spindle speed in the fluid was conducted from 10-100% of the instruments torque scale, which varied with temperature [55]. The spindle would begin to spin at the set rpm value for 5 minutes, and then change spindle speed to the next increment, and would complete three cycles. The results of the tests were measured and evaluated using the RheocalcT software, which then could manipulate the data to provide information regarding the viscosity of the fluid.

Figure 37 Brookfield cylindrical LV spindle

Figure 38 Brookfield TC-650 temperature bath

3.10 Density Measurement

The density of the liquid that is in our flow system was measured at atmospheric conditions to help have a better understanding of the liquid properties. This was done using a Scout pro SP402 digital mass scale shown in Figure 39, which has an accuracy of ±0.01g. A 50 ml graduated cylinder with an accuracy of ±1 ml was used to hold different volumes of the Hydromx liquid. The beaker was weighed at 10 ml intervals ranging from 10 to 50 ml at three separate times. The data was then converted from g/ml to g/cm^3.

Figure 39 Scout Pro Scale

3.11 Hydromx

Hydromx will be the experimental fluid used in the current study. Hydromx is an ethylene glycol blended nanofluid, which consists of nanoparticles suspended into a working fluid. The nanoparticles are supposed to enhance heat transfer properties of the fluid and provide less energy requirements than water in heat transfer applications [56].

CHAPTER 4

RESULTS AND DISCUSSION

4.1 Overview

Fluid density and viscosity properties were measured, and the data is given below. Calibration fluid viscosity will also be determined to show the performance of the rheometer. Following the single and two-phase flow static mixer tests, differential pressure will be measured and plotted against each of the different test sections. Then static pressure measurements downstream of the static mixer test section will be displayed to show the pressure profile downstream. Then a comparison between the static mixers and an empty pipe downstream differential pressure and average static pressure in the pressure transducer test section will be shown with respect to the gas Reynolds numbers calculated.

4.2 Density Measurement

Mass and volume values were measured at atmospheric conditions for three cycles and the data is shown in Figure 40. The atmospheric conditions present at the time of measurement were Tatm = 21.8 °C and Patm = 97.9 kPa. The graph shows the mass versus volume of liquid measured and is modeled by a linear trend line with a high r squared value, which shows good relation to the data. The slope of the line indicates density of the liquid at atmospheric conditions is roughly 1.07 g/cm^3. Hydromx density in this case is assumed to be a constant throughout the experiments and when used in calculations.

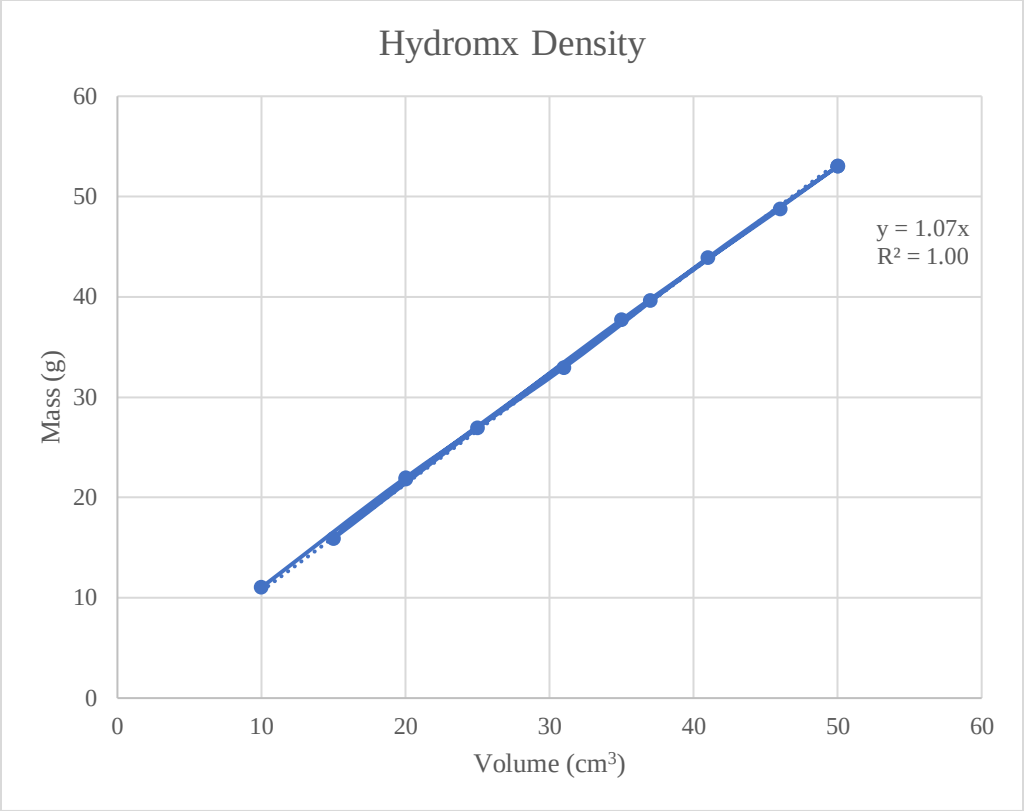

Figure 40 Hydromx density measurements at room temperature (21.8°C)

4.3 Viscosity Measurement

The Brookfield Engineering Rheometer was used in collaboration with the calibration fluid provided by Cannon Instrument Company. The calibration fluid was inserted into the rheometer to begin viscosity testing. Three different shear rates at the different calibrated temperatures were exerted onto the fluid over a series of three cycles. Figure 41 shows the average viscosity measurement plotted against the published calibration fluid viscosity. The plot shows that similar behavior can be seen from both experimental and published data, with a relatively small error in the temperature range that the Hydromx will be utilized (5-30 degrees Celsius). Table 2 shows the percent error value from the calibrated viscosity for each of the measured viscosity data. In the operating range of the two-phase flow tests the percent error is reliable.

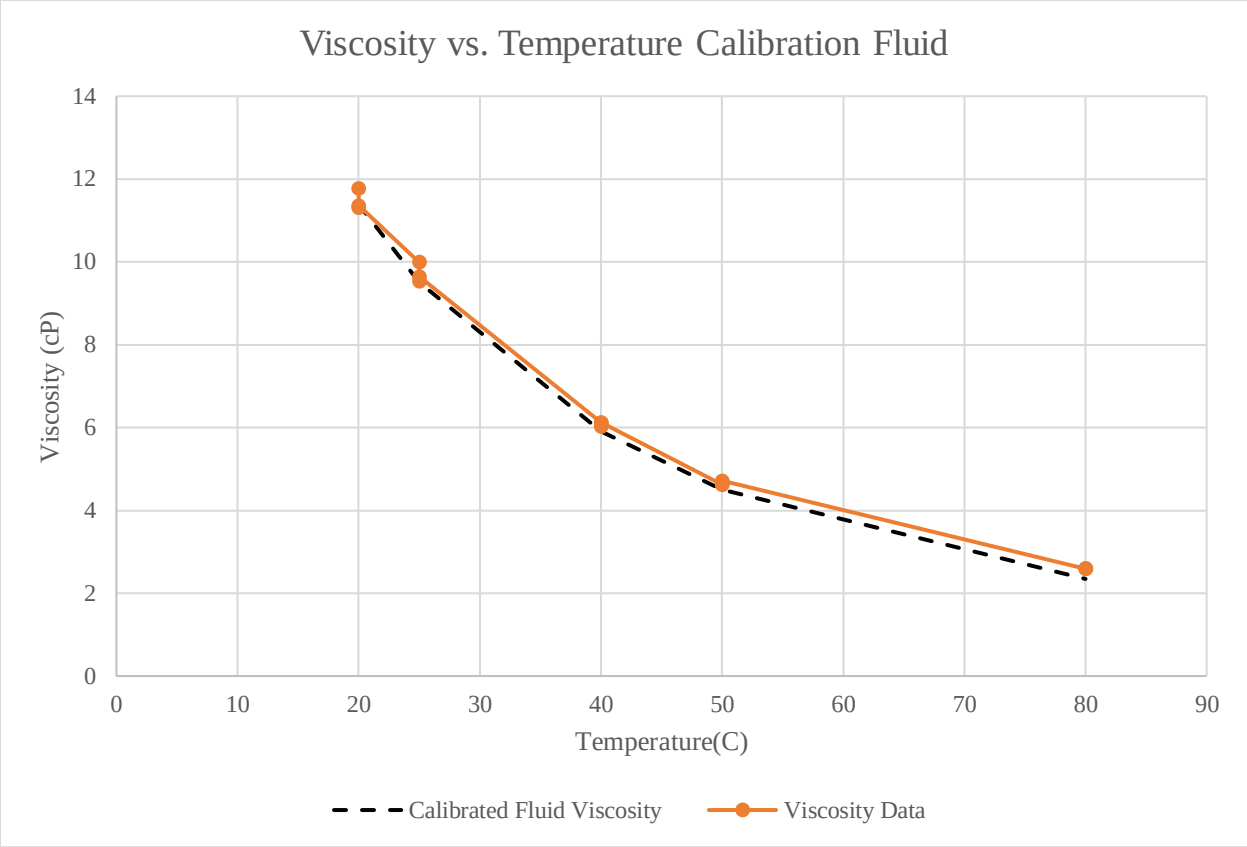

Figure 41 Calibrated fluid viscosity properties versus measured properties

Table 2 Measured viscosity data values and corresponding percent error to calibration fluid

Temperature	Viscosity Data	%error
20	11.483	0.819
25	9.725	2.315
40	6.090	3.115
50	4.670	3.847
80	2.590	10.445

Shear stress versus shear rate was obtained for the 100% Hydromx at a range of temperatures and shear rates from 5 to 30°C, and 13.2 to 211.2 1/s. The data for this experiment can be seen in Figure 42. The figure shows that all the experiments across the range of temperatures and shear rates can be modeled using a linear fit. This indicates that the fluid behaves as a Newtonian fluid

and we can expect Newtonian behavior when conduction flow experiments with the fluid. Another finding from the plot is the viscosity at the various temperatures, which can be shown from the slopes of the individual tests in units of Poise.

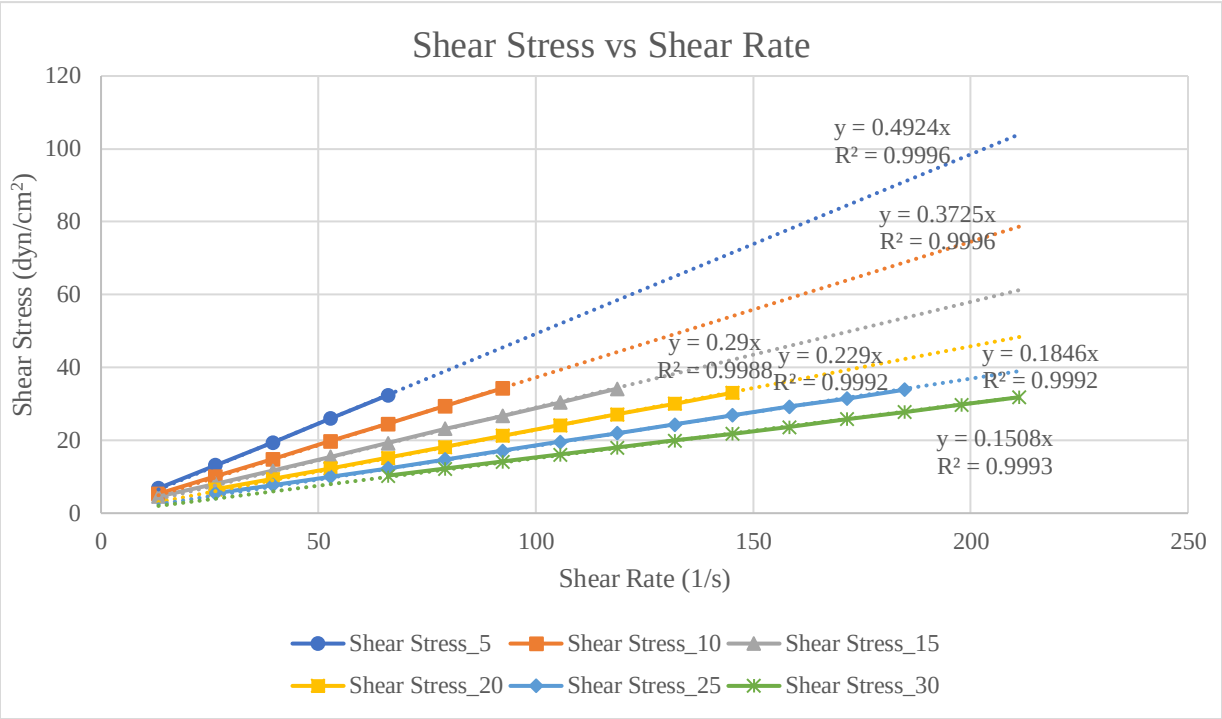

Figure 42 100% Hydromx shear stress versus shear rate plot

A similar experiment was done on the 50:50 mixture and the shear stress versus shear rate data can be seen in Figure 43. The linearity of the data from the experiments at a range of shear rate values indicate that the 50:50 mixture of Hydromx and water also demonstrate Newtonian behavior. The viscosity values are the slopes of the fitted lines for their respective experimental data trend line.

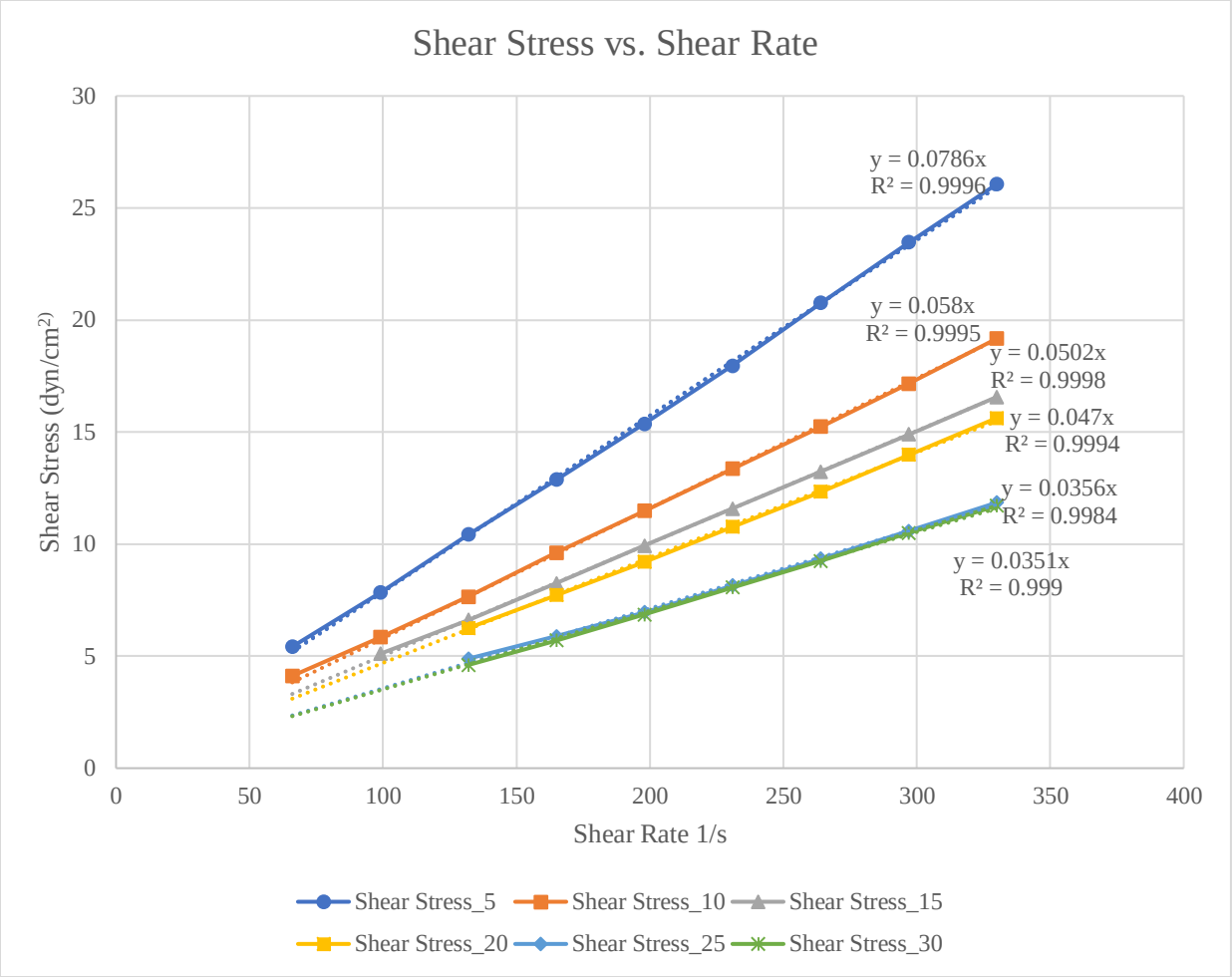

Figure 43 50:50 Hydromx and water shear stress versus shear rate plot

Figure 44 shows the extrapolated viscosity data from the 100% and 50:50 viscosity experiments. The averaged viscosity comes from the trendline data for each test. As shown, the viscosity of the 100% and 50:50 mixture range from 15 to 49.24 cP and 3.5 to 7.86 cP, respectively. The information of viscosity due to shear rate and temperature can be utilized when analyzing the two-phase flow data through the different static mixers and for calculating the respective liquid Reynolds number.

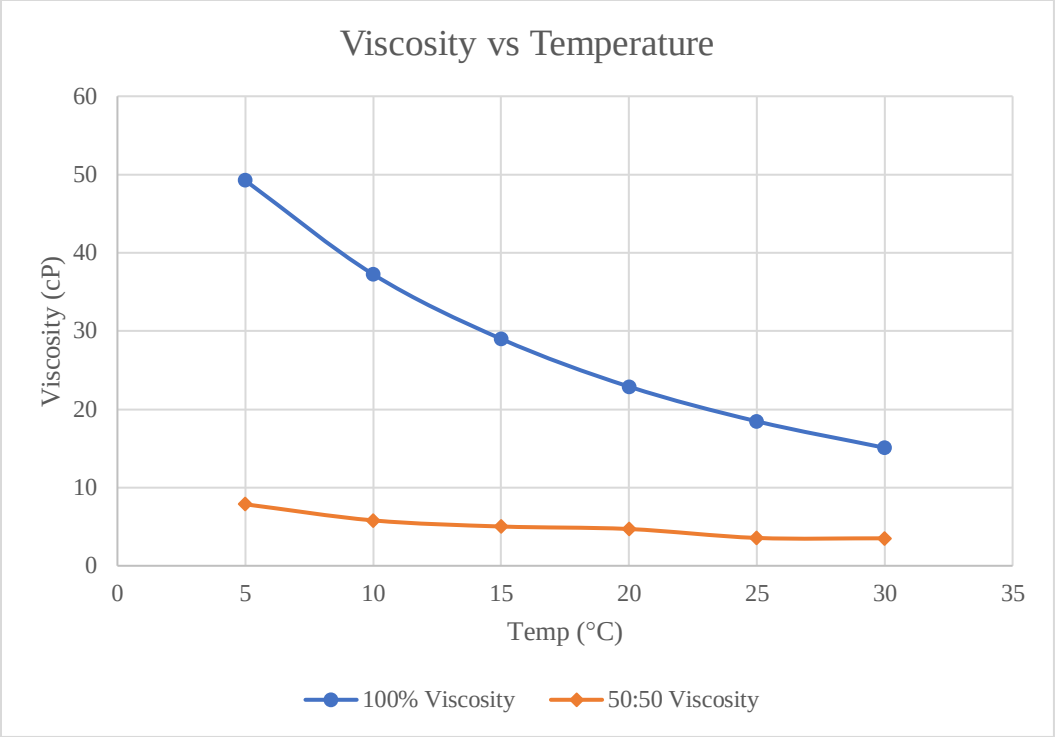

Figure 44 Viscosity vs Temperature plot

After the completion of the two-phase flow static mixing tests, the viscosity of the experimental fluid was measured to see if there was any viscosity change throughout the experiments and can be seen in Table 3. The typical temperature during the two-phase flow tests ranged between 8 and 10°C. Thus, the viscosity measurements after the experiments were conducted at 10°C to be able to recreate the environment the fluid is in during the test. The average viscosity found after the two-phase flow tests was higher than what was measured prior to testing. After the viscosity of the 50:50 Hydromx fluid was measured and a difference in viscosity was found, a 60:40 viscosity experiment was conducted to determine if there was an effect of evaporation of the water when the two-phase flow experiments were conducted. Though there is an increase in

viscosity post two-phase experiments, evaporation of water was less than 10 percent in the fluid throughout the experiments.

Table 3 Comparison of viscosity measurements

Liquid Composition	Average Viscosity (cP)
50:50 prior to two-phase experiments	5.8
50:50 post two-phase experiments	6.38
60:40 Hydromx and water fluid	8.05

4.4 Single-phase Flow Measurements

Single-phase flow tests were conducted to determine the differential pressure across the entire test section including the static mixer and the ten static pressure transducers. Figure 45 shows the differential pressure measurements across the entire test section for various liquid mass flow rates ranging from 4.75 to 24 g/s. It can be seen for the single-phase flow experiments that the triple plate static mixer has the largest differential pressure (DP) drop across the test section at higher liquid mass flow rates followed by the double plate, helical, and then the empty pipe. As expected, the empty pipe should have the smallest DP drop across the test section, due to having no obstructions in the pipe as in the static mixer test sections. Another observation from the data is that at liquid mass flow rates of 4.75 to roughly 10 g/s, the DP across the test section for the three different static mixers are shown to be very similar. This could mean at lower flow rate tests in the future, the selection of static mixer could be determined off other characteristics, such as static mixer length and mixing efficiency, due to the DP across the test section being roughly

the same throughout. It is noteworthy to point out that the DP trend of static mixer models could be related to the overall volume per length of the static mixer models themselves.

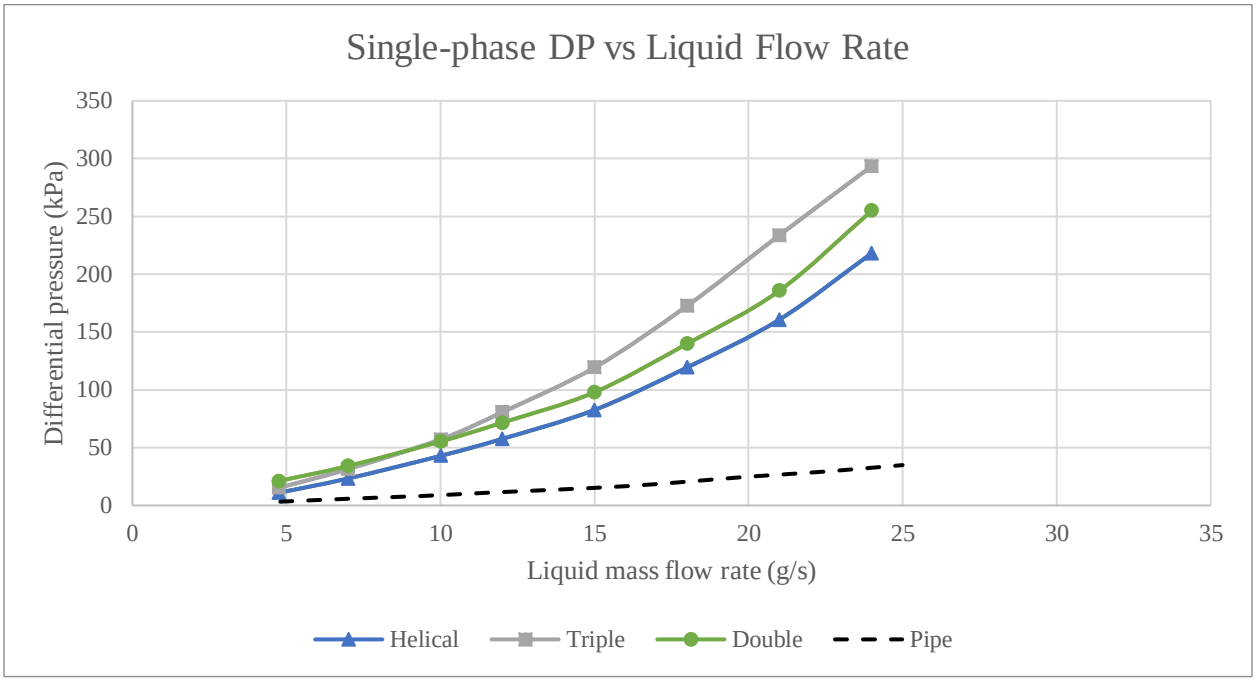

Figure 45 Single-phase flow differential pressure versus liquid mass flow rate across the entire test section

Figure 46, Figure 47, Figure 48, and Figure 49 show the single-phase static pressure measurements downstream of the static mixer test section for the ten calibrated pressure transducers at liquid mass flow rates ranging from 7 to 21 g/s. These measurements were used to compare the differences between an empty pipe and the three static mixers. As the liquid mass flow rate is increased, the static pressure downstream of the static mixer test section is also increased at different rates, which shows that the static mixer plays a role in the static pressure downstream. The helical style static mixer also demonstrates the highest average static pressure

downstream of the mixer followed by the double plate, triple plate, and the empty pipe. The data also shows a typical decrease in static pressure as the flow moves farther downstream.

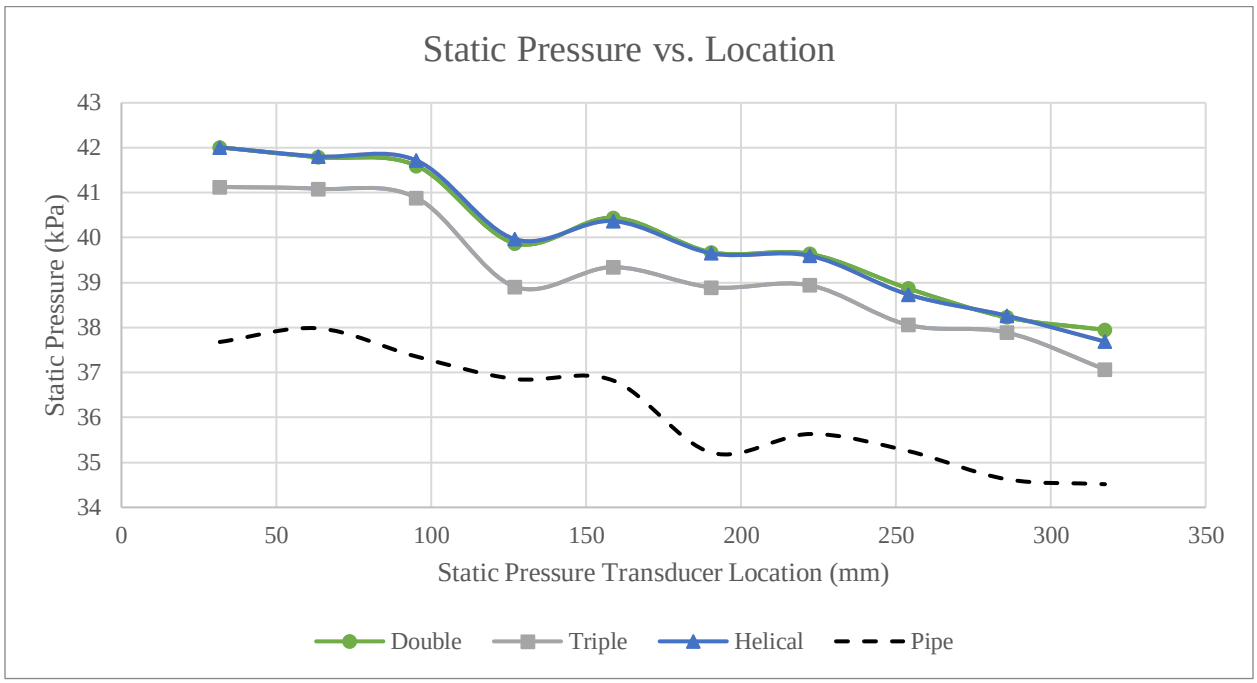

Figure 46 Static pressure versus static pressure transducers location downstream of static mixer at liquid mass flow rate of 7 g/s

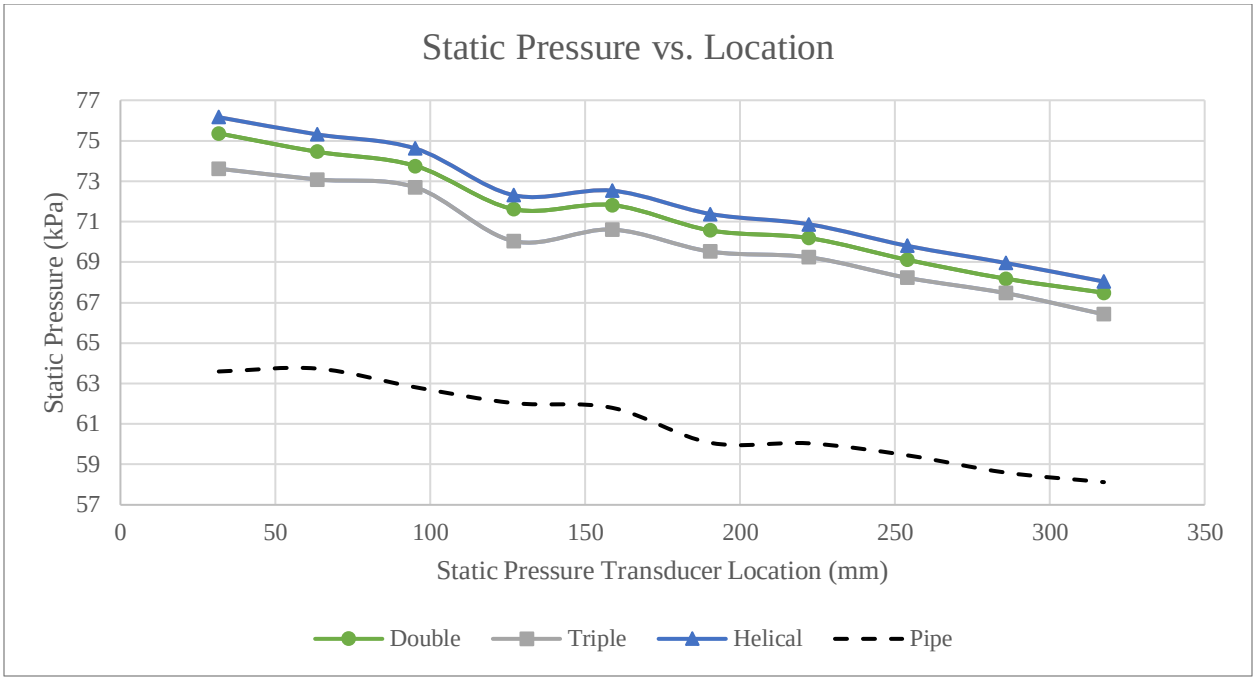

Figure 47 Static pressure versus static pressure transducers location downstream of static mixer at liquid mass flow rate of 12 g/s

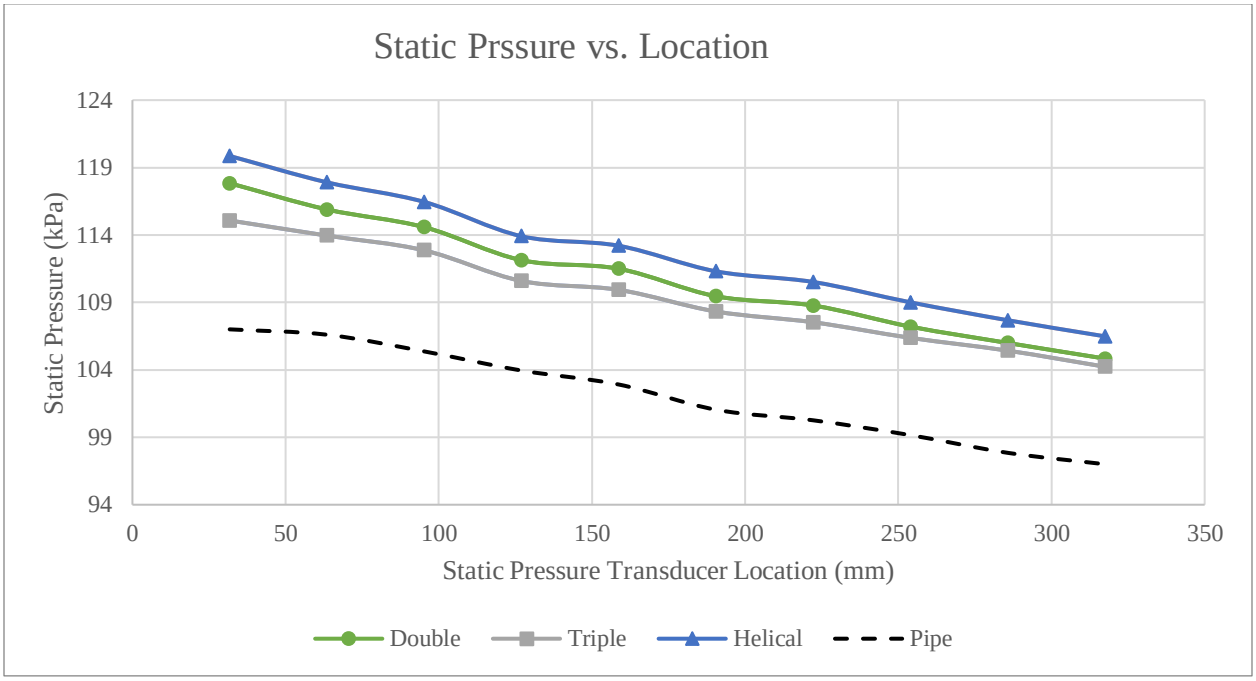

Figure 48 Static pressure versus static pressure transducers location downstream of static mixer at liquid mass flow rate of 18 g/s

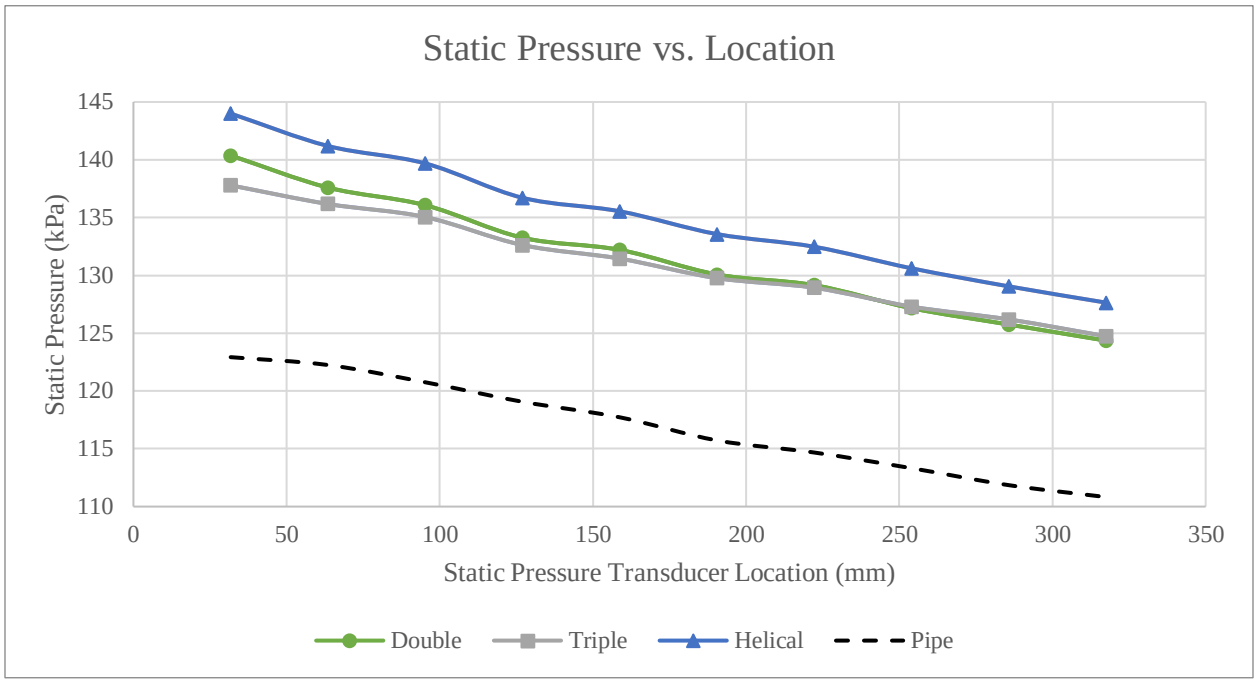

Figure 49 Static pressure versus static pressure transducers location downstream of static mixer at liquid mass flow rate of 21g/s

4.5 Two-phase Flow Measurements

Figure 50, Figure 51, Figure 52, and Figure 53 show the differential pressure measurements across the entire test section for the two-phase flow experiments. The liquid mass flow rate and gas mass flow rate range from 7 to 21g/s and 0.01 to 0.06 g/s, respectively. The differential pressure data shows information regarding pressure loss over the entire system including static mixer and the pressure transducer test section. This differential pressure data can be useful when finding the power input needed to use the various static mixers at different liquid and gas flow rates. Figure 50 shows the differential pressure loss at a constant liquid mass flow rate of 7 g/s. It shows that at this lower flow rate experiment that the double plate and triple plate static mixer behaves relatively the same with regards to pressure loss across the system. As the liquid flow

rate increases, the differential pressure across the system also increases, which is expected. The difference between the three static mixer pressure drops also increase as a function of the liquid mass flow rate. The triple plate static mixer has the largest pressure drop throughout the various flow rates, which could be due to the largest volume per length measurement of the static mixer compared to the other styles. The double plate style static mixer has the second highest pressure drop associated with it, followed by the helical style and empty pipe scenario. These experiments were conducted three times with over 100 test measurements at each of the various combinations of liquid and gas flow rates to ensure repeatability.

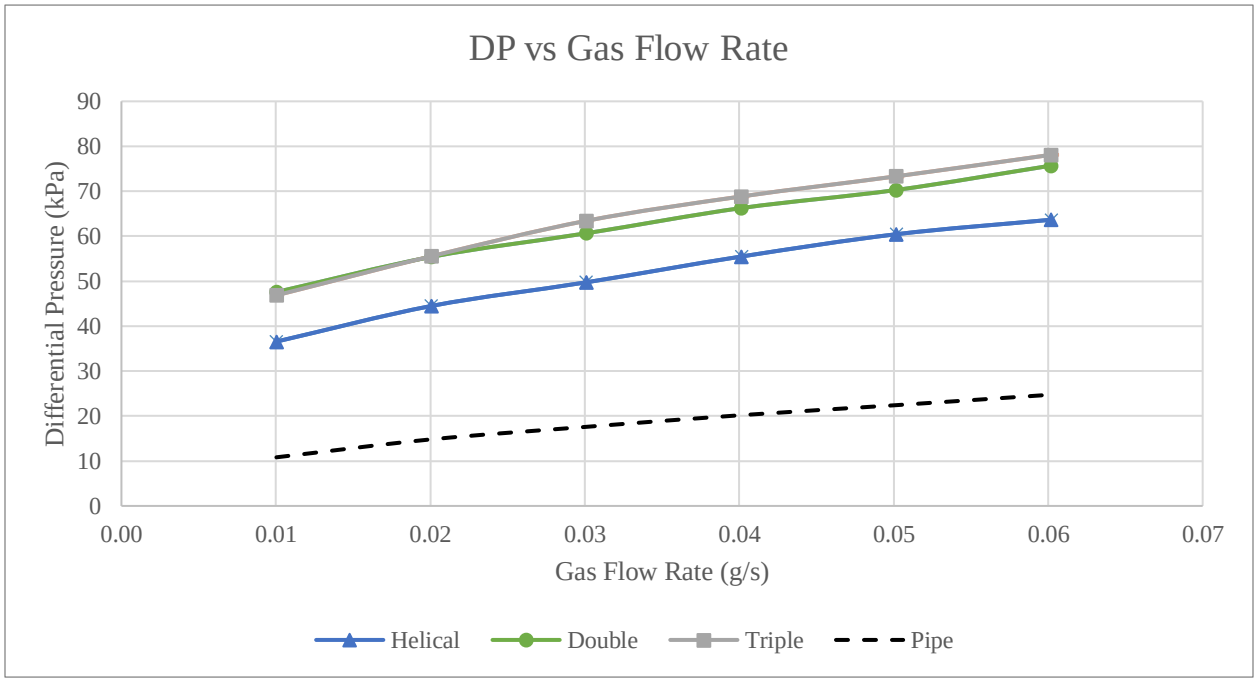

Figure 50 Differential pressure versus gas mass flow rate for different static mixer geometries at a liquid mass flow rate of 7 g/s

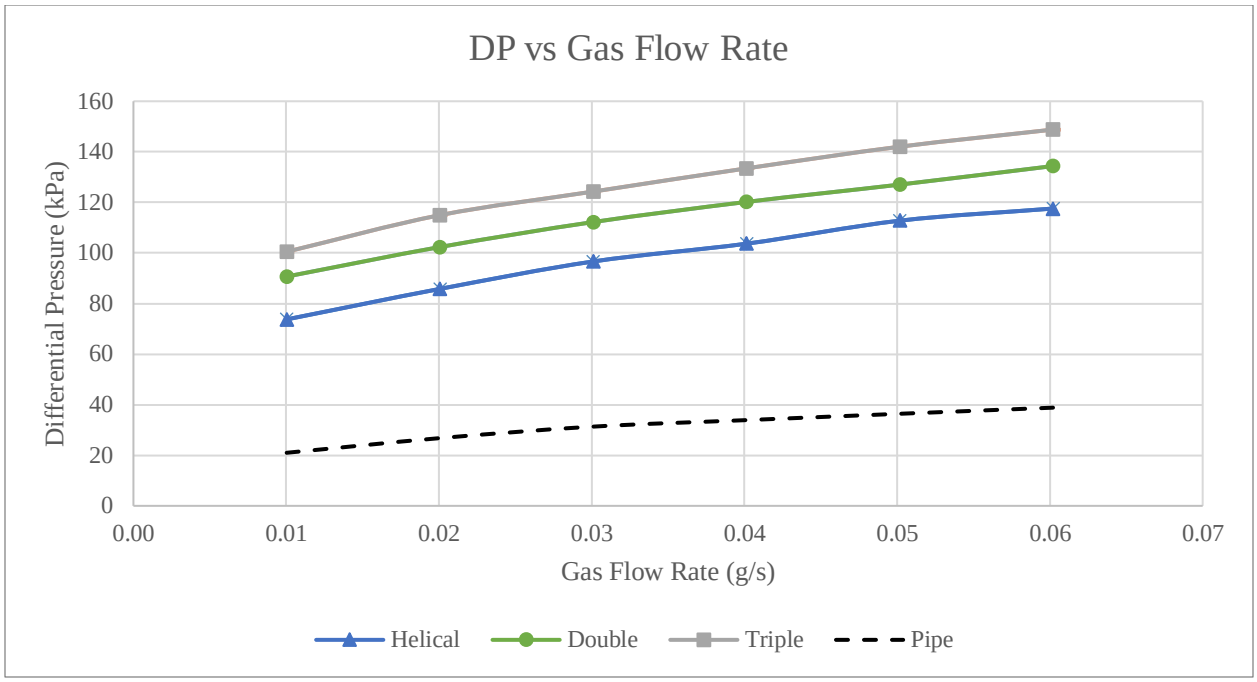

Figure 51 Differential pressure versus gas mass flow rate for different static mixer geometries at a liquid mass flow rate of 12 g/s

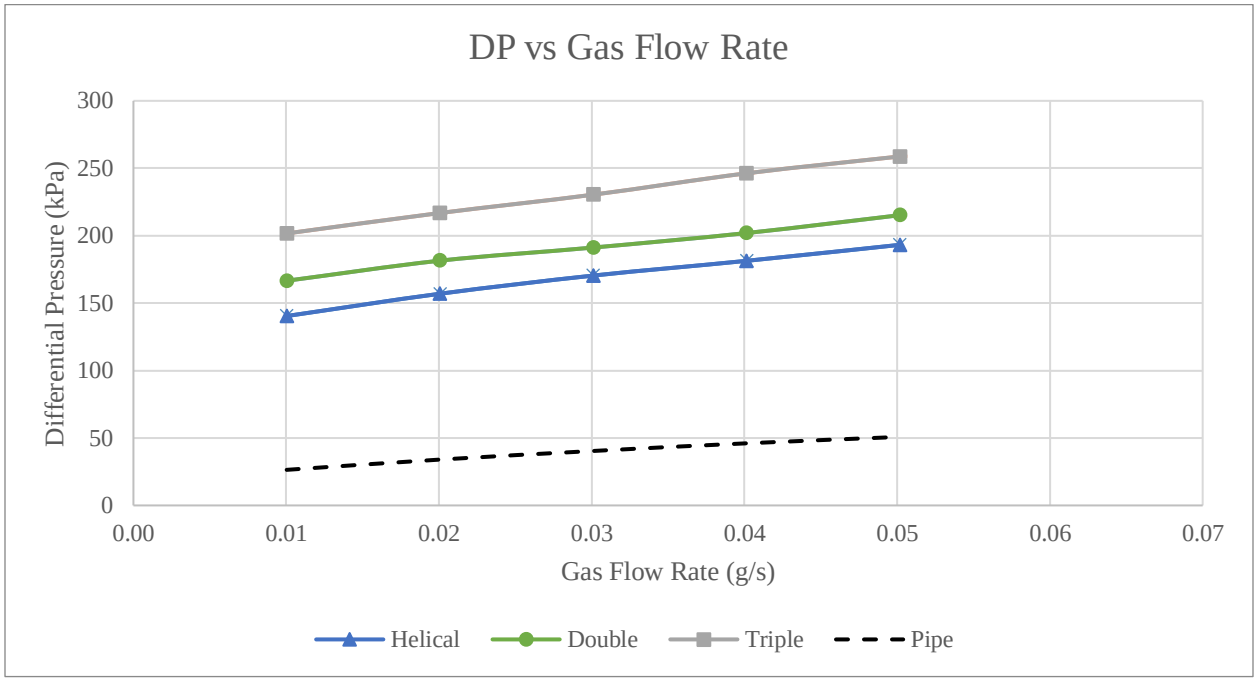

Figure 52 Differential pressure versus gas mass flow rate for different static mixer geometries at a liquid mass flow rate of 18 g/s

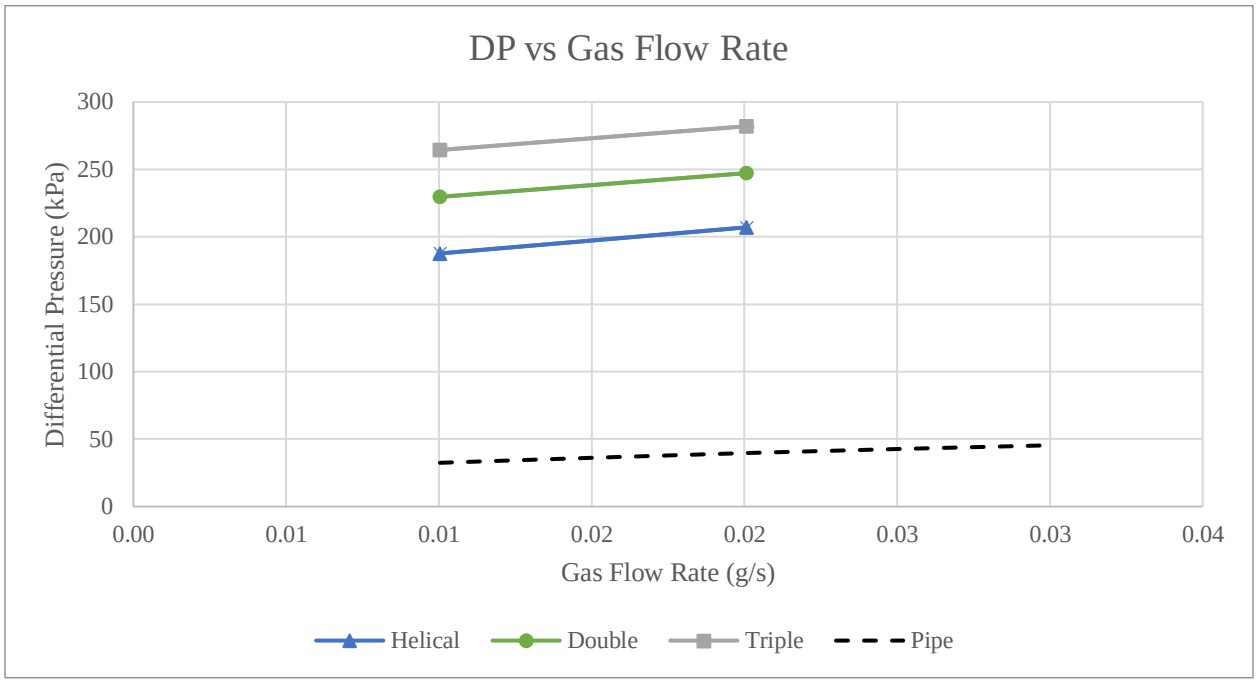

Figure 53 Differential pressure versus gas mass flow rate for different static mixer geometries at a liquid mass flow rate of 21 g/s. The two data points for the static mixer data are due to pressure transducer limitations.

Figure 54 through Figure 61 show the two-phase flow static pressure profile downstream of the static mixer test section. Overall, there is a general increase in static pressure as liquid and gas mass flow rate are increased. When comparing the three static mixers, the triple plate style generally has the lowest static pressure associated with it, especially when flow rate is increased. The empty pipe seems to change its static pressure sporadically and could be due to changing flow patterns with respect to a change in its respective mass flow rates.

Figure 54 and Figure 55 show the static pressure when the liquid flow rate is kept at a constant value of 7 g/s with a changing gas mass flow rate from 0.01 to 0.06 g/s. As the gas mass flow

rate is increased, the empty pipe sees a larger rise in static pressure when compared to the rise in static pressure with the static mixers.

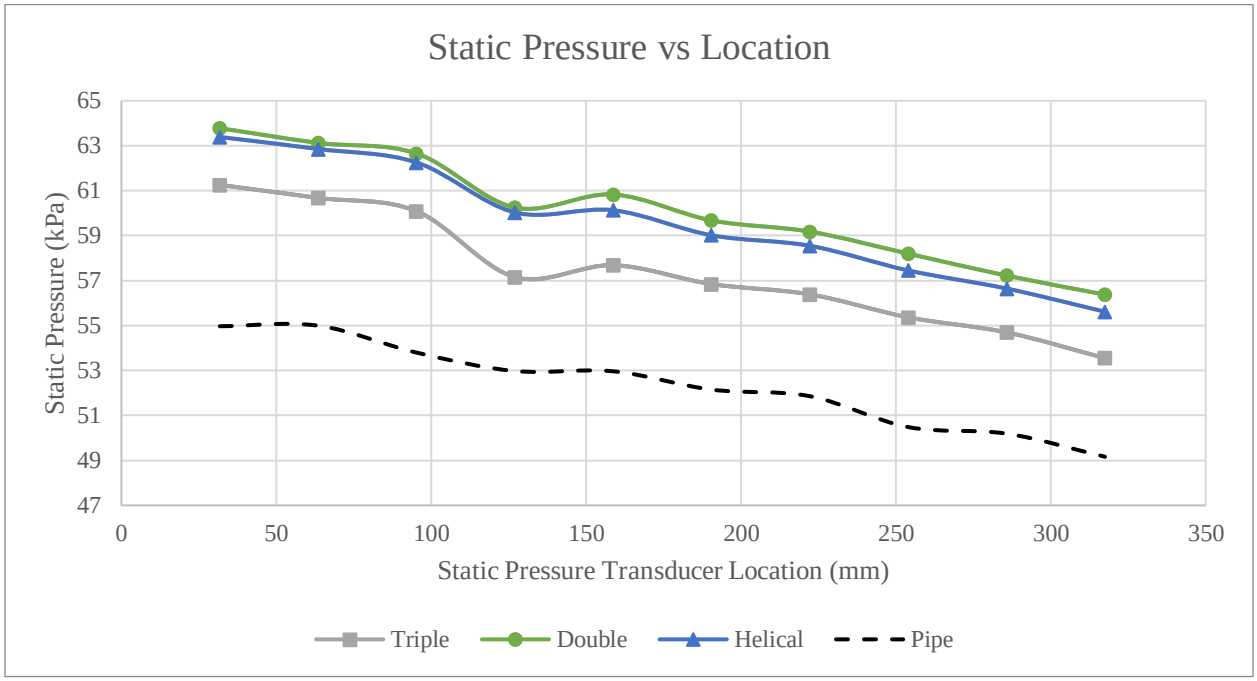

Figure 54 Static pressure versus pressure transducer location downstream of static mixer at liquid mass flow rate of 7 g/s and gas mass flow rate of 0.01 g/s

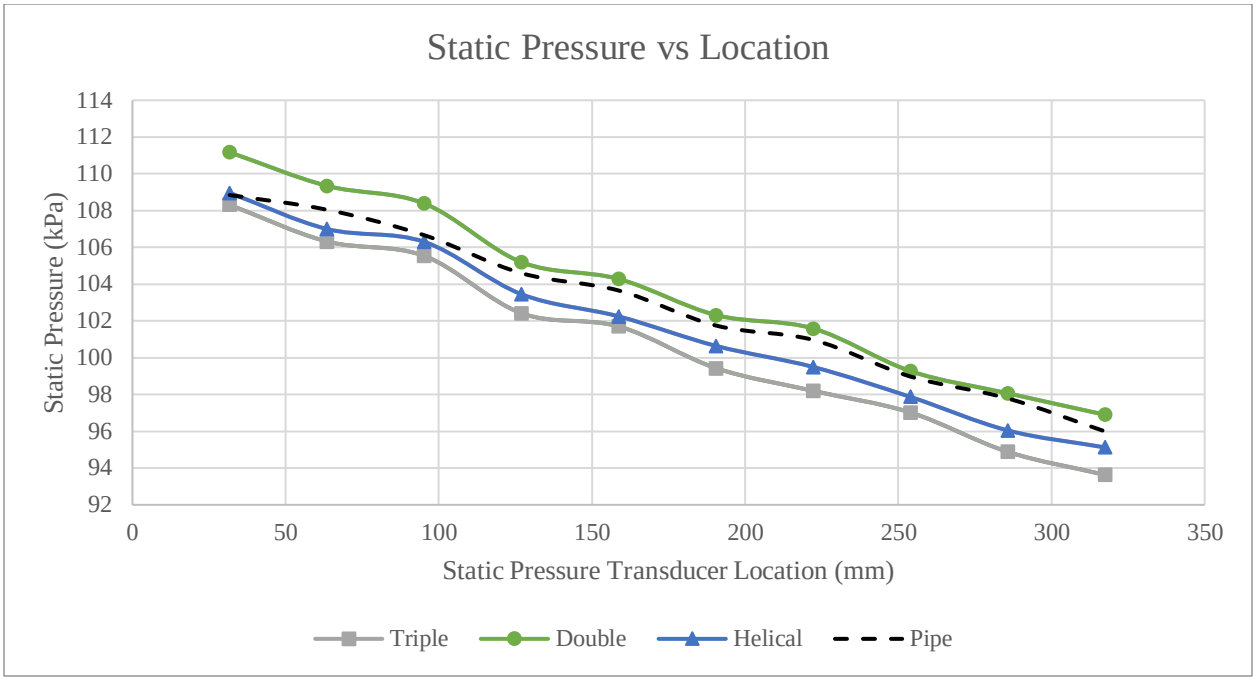

Figure 55 Static pressure versus pressure transducer location downstream of static mixer at liquid mass flow rate of 7 g/s and gas mass flow rate of 0.06 g/s

Figure 56 and Figure 57 show the static pressure profile at 12 g/s liquid mass flow rate and a gas mass flow rate from 0.01 to 0.06 g/s. Comparing the static mixers, it is shown that the triple plate static mixer has the lowest overall static pressure downstream of the static mixer test section, with an increase in gas flow rate. However, comparing the double plate and helical style static mixers, they have very similar static pressure profiles at low gas mass flow rates. As the gas flow rate is increased the double plate style static mixer has a larger increase in its static pressure profile. Another key finding from this test is that the empty pipe tends to have a larger overall static pressure when compared to the lower flow rates shown in Figure 54 and Figure 55.

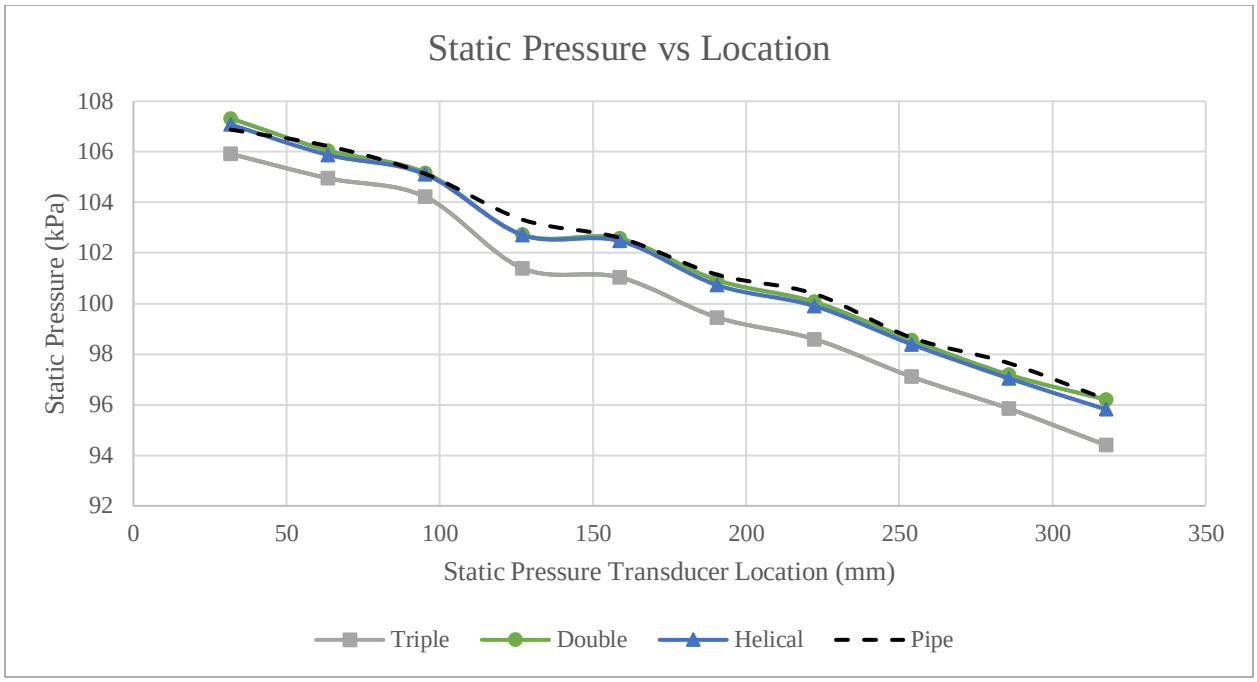

Figure 56 Static pressure versus pressure transducer location downstream of static mixer at liquid mass flow rate of 12 g/s and gas mass flow rate of 0.01 g/s

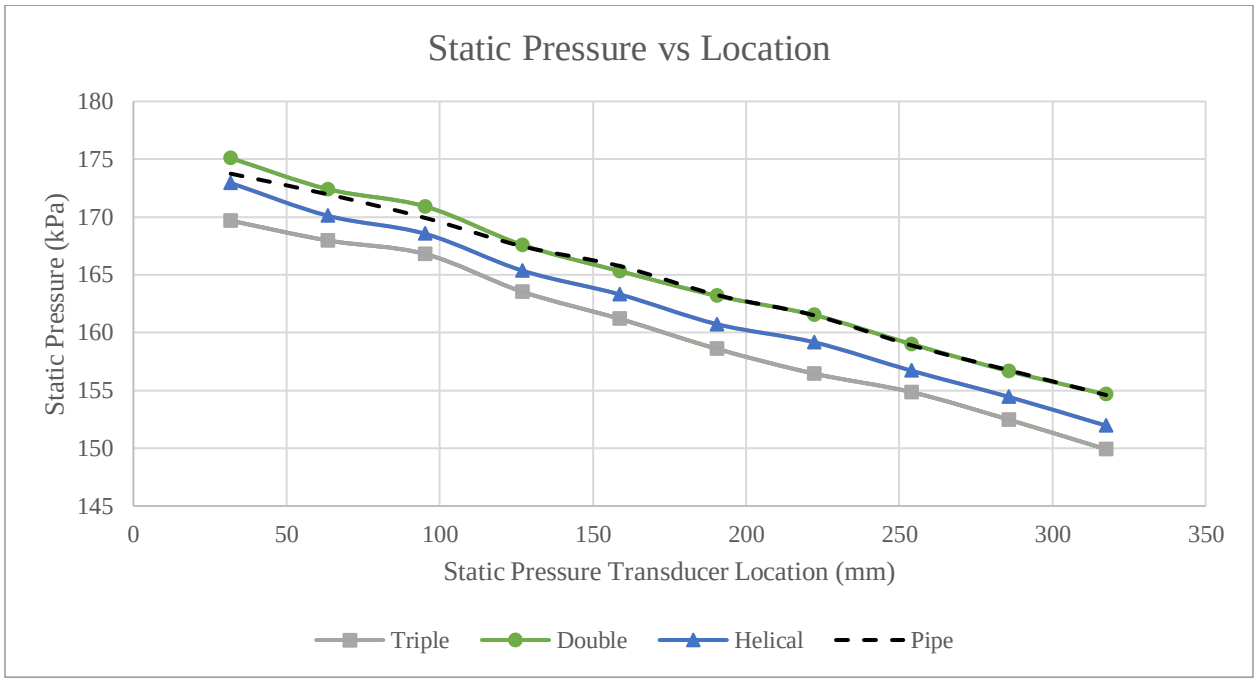

Figure 57 Static pressure versus pressure transducer location downstream of static mixer at liquid mass flow rate of 12 g/s and gas mass flow rate of 0.06 g/s

Figure 58 and Figure 59 show the static pressure downstream of the static mixer at the ten different pressure transducers at a liquid mass flow rate of 18 g/s and varying the gas mass flow rate of 0.01 g/s to 0.05 g/s. The empty pipe scenario yields a low static pressure at lower gas flow rates but increases to a static pressure profile higher than the triple plate and helical style, while being roughly the same to that of the double style static mixer, which indicates mixing could be inherently occurring at higher gas flow rates, which could eliminate the need for a static mixer. When comparing the static pressure profile with the use of the static mixers at low gas mass flow rates the static pressure is comparable with the three different static mixers. However, at higher gas mass flow rates, there is an increase in the overall static pressure profile, but the triple plate and helical style static mixers have significantly lower static pressure compared to the double plate and empty pipe, with the triple plate style having the lowest.

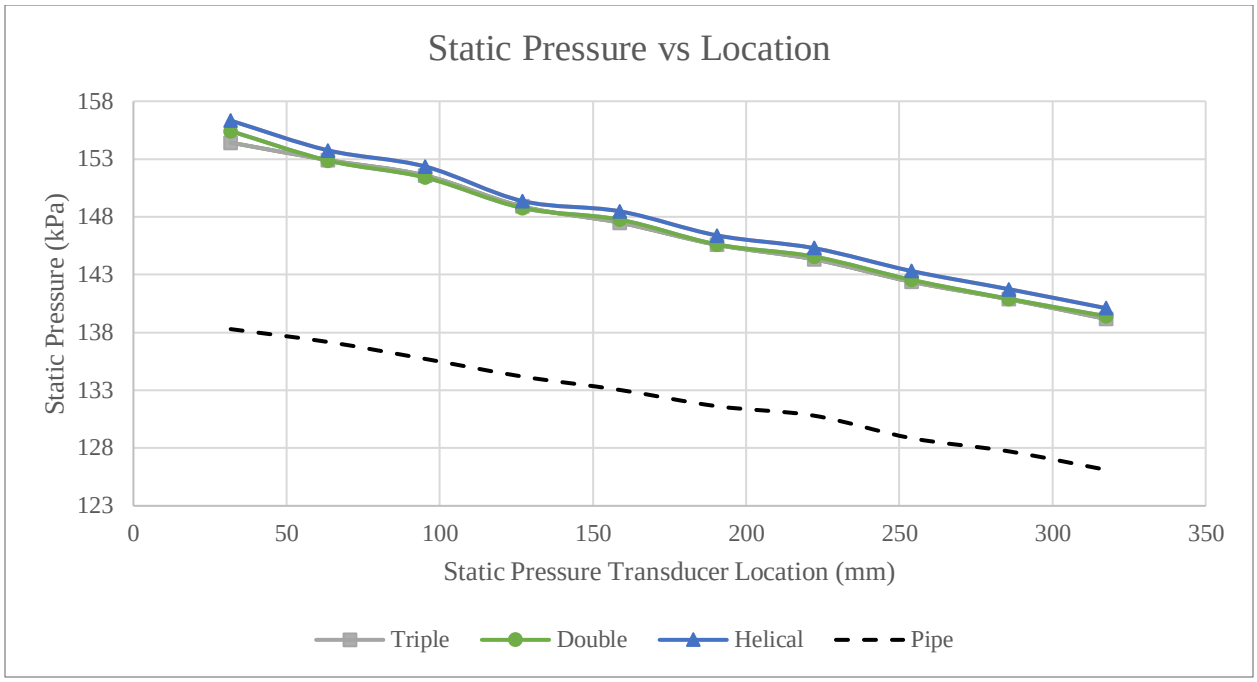

Figure 58 Static pressure versus pressure transducer location downstream of static mixer at liquid mass flow rate of 18 g/s and gas mass flow rate of 0.01 g/s

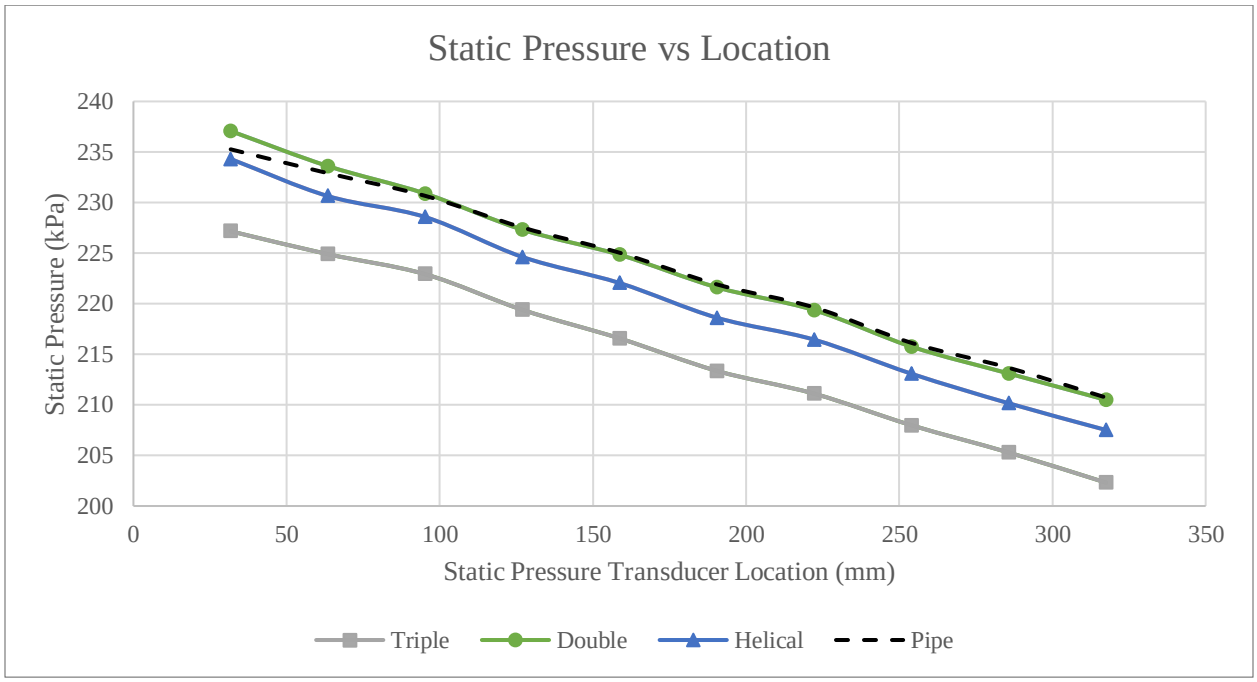

Figure 59 Static pressure versus pressure transducer location downstream of static mixer at liquid mass flow rate of 18 g/s and gas mass flow rate of 0.5 g/s

Figure 60 and Figure 61 show the static pressure profile at a liquid mass flow rate of 21 g/s and a gas mass flow rate of 0.01 and 0.02 g/s. There is a more spread out range of static pressure profiles for each of the static mixers and empty pipe scenarios. At the lower gas mass flow rate, the double plate and helical style static mixers have the highest overall static pressure and are roughly the same. The triple plate style has a slightly lower overall static pressure followed by the empty pipe scenario. As the gas mass flow rate is increased to 0.02 g/s the helical and double plate style static mixers still have roughly the same overall static pressure. The static pressure in the empty pipe has a higher overall increase in static pressure and is very similar to that of the triple plate style static mixer. If the gas flow rate could be increased more, the empty pipe scenario would probably start to reach the static pressure of the Helical and double style plate.

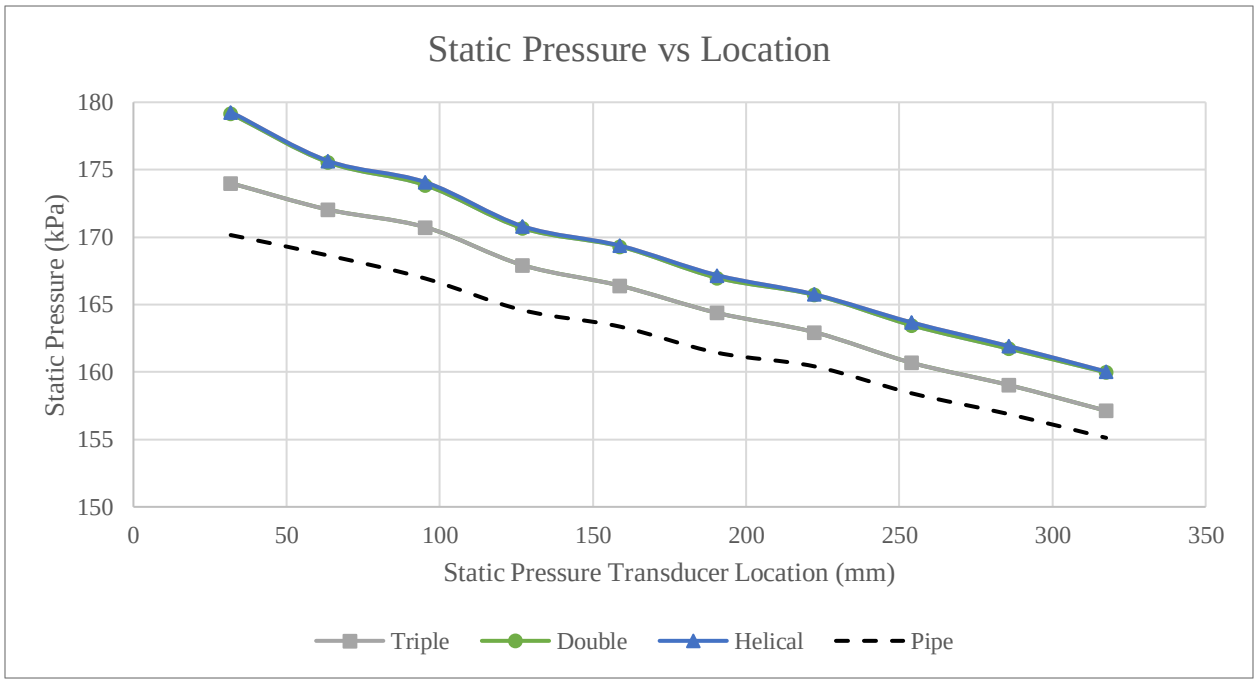

Figure 60 Static pressure versus pressure transducer location downstream of static mixer at liquid mass flow rate of 21 g/s and gas mass flow rate of 0.01 g/s

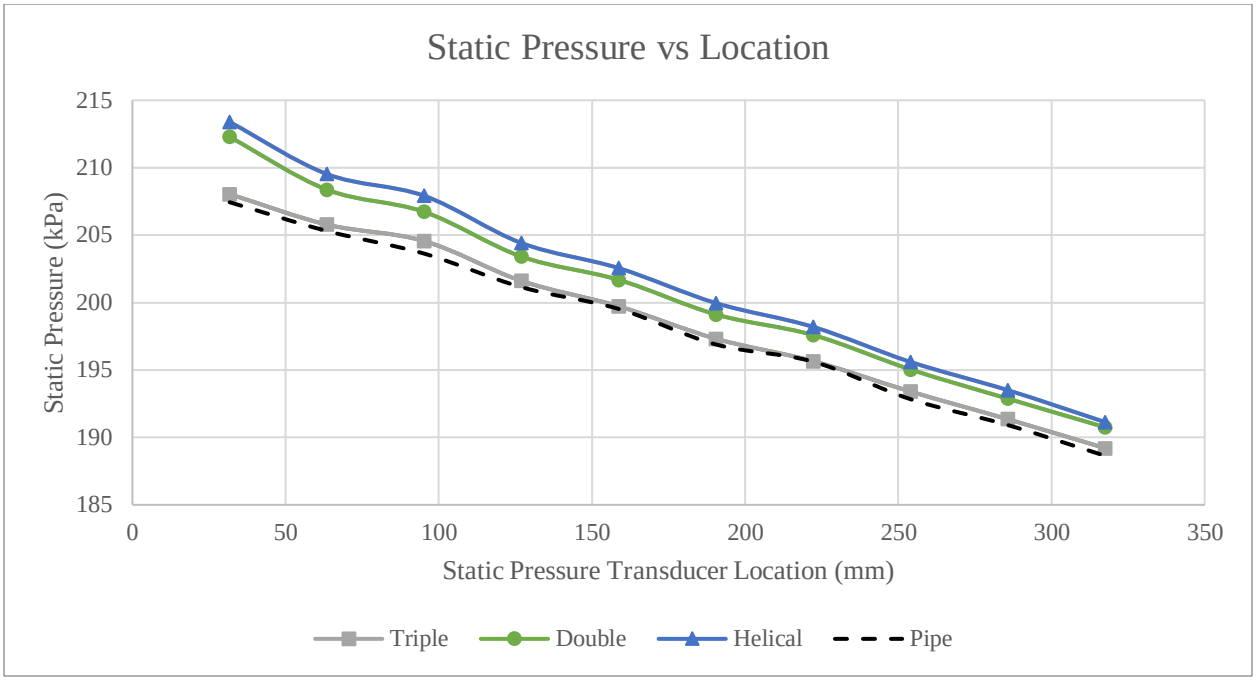

Figure 61 Static pressure versus pressure transducer location downstream of static mixer at liquid mass flow rate of 21 g/s and gas mass flow rate of 0.02 g/s

Figure 62 through Figure 66 show the comparison between the average static pressure in the downstream pressure transducer test section with a mixer to the experiments without the mixer. The average static pressure in the downstream test section was done by integrating the ten static pressure transducer values using the trapezoidal method. Utilizing this method, the average static pressure downstream can be found when the static mixer or empty pipe is used. The comparison between the two values was done at all experimental flow rates from 4.75 g/s to 21 g/s liquid mass flow rates over the full range of gas mass flow rates. The plots are graphed using the comparison value versus the gas Reynolds number to show what happens to the compared values as flow rates increase. The comparison was done downstream of the static mixer to show how the increase or decrease in static pressure happens with the various static mixer designs. The

knowledge of the static pressure in the downstream pressure profile can help with knowing the static pressure limits of a system as well as helping with CFD simulations.

Figure 62 shows the pressure comparison at a liquid mass flow rate of 4.75 g/s. As the gas phase is increased there is a small change in overall static pressure throughout the entire gas Reynolds number range. In most cases in this flow parameter set up, the average static pressure with a static mixer is lower than with an empty pipe. Figure 63 shows the comparison at a liquid mass flow rate at 7 g/s. At lower gas Reynolds numbers there is a higher static pressure with the mixer. As gas Reynolds number increases, the ratio starts to decrease to roughly 0.95 to 1. Figure 64 shows the comparison at a liquid mass flow rate of 12 g/s. Similar behavior is seen at a liquid mass flow rate of 10 g/s as well. Throughout the entire gas Reynolds number range, there is very little change in the ratio of mixer to empty pipe static pressure. Figure 65 shows the static pressure comparison at a liquid mass flow rate of 15 g/s. Throughout the entire range of gas Reynolds number there is an increase in the static pressure ratio. This is different to what has been seen in the other liquid flow rate experiments and could be due to the flow regime or intermittent behavior that is occurring at the given gas and liquid mass flow rates. However, this could only be determined by more flow experiments related to flow visualization or void fraction measurements. Figure 66 shows the pressure comparison for a liquid mass flow rate of 18 g/s and is very similar to the behavior for a liquid mass flow rate of 21 g/s. Throughout the gas Reynolds number range, the pressure ratio decreases in the system. This could be due to after the 15 g/s experiment, the flow regime goes from an intermittent flow pattern to a more uniform flow pattern as the liquid phase starts to dominate in the system. Overall, the double plate style

static mixer has the largest pressure ratio at all flow rate set ups, followed by the helical style and then the triple plate style static mixer.

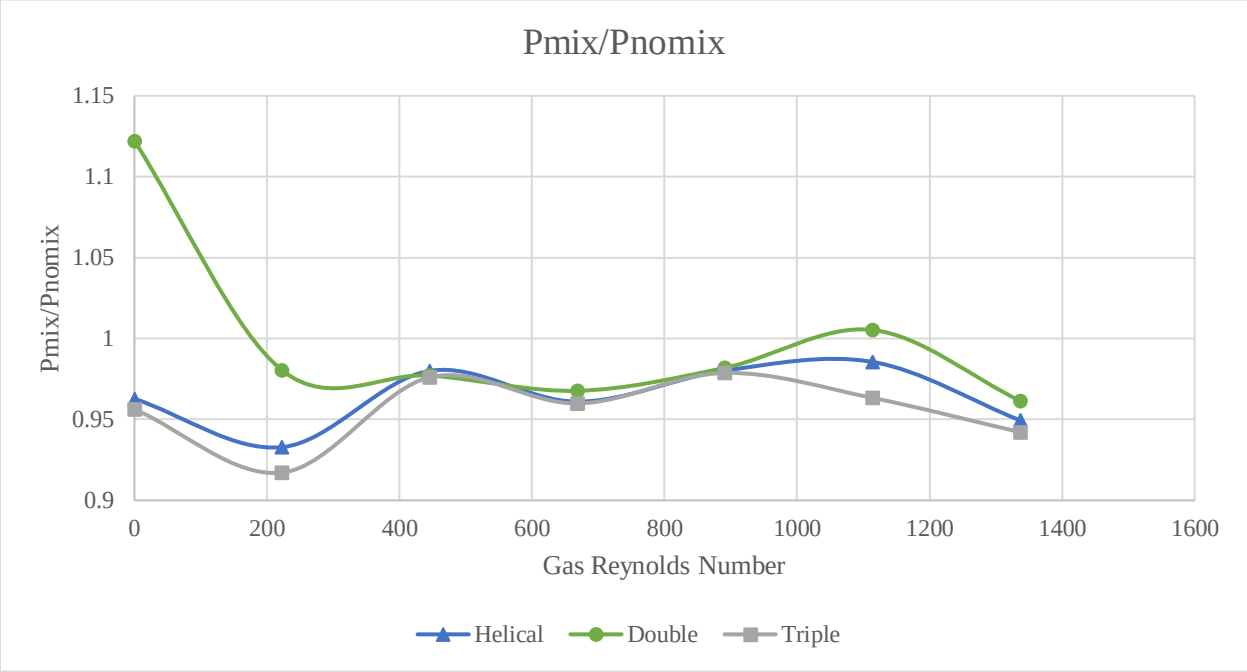

Figure 62 Static mixer pressure compared to pressure of empty pipe versus gas mass flow rate with a 4.75 g/s liquid mass flow rate

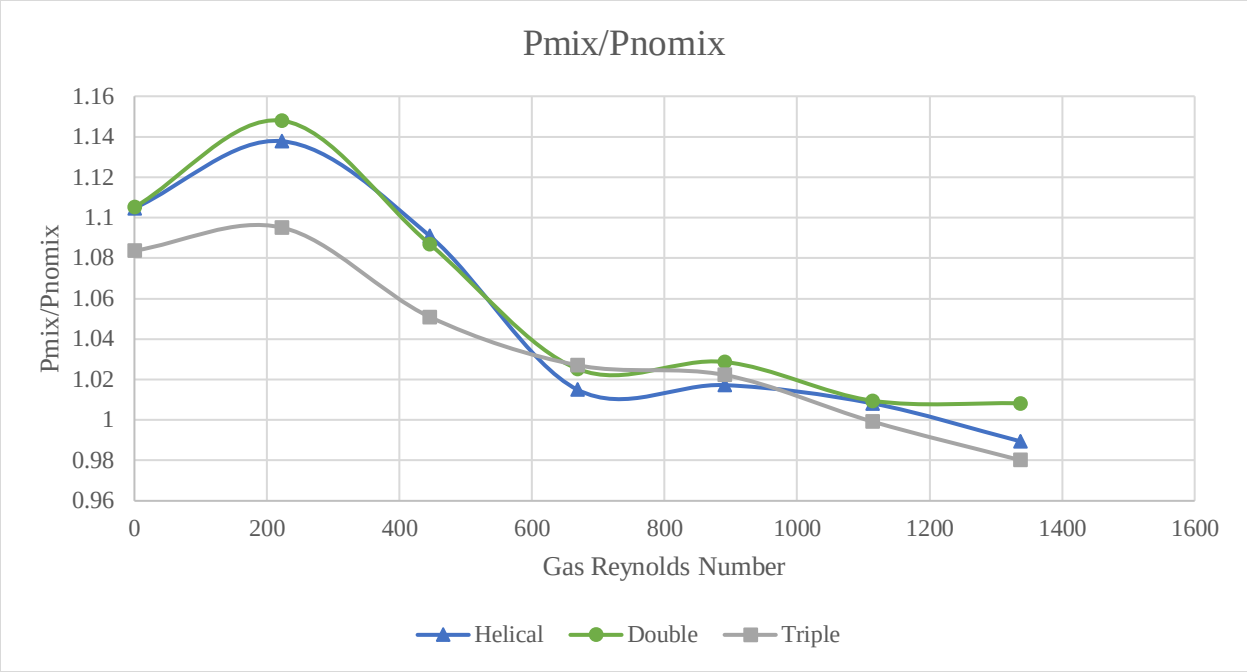

Figure 63 Static mixer pressure compared to pressure of empty pipe versus gas mass flow rate with a 7 g/s liquid mass flow rate

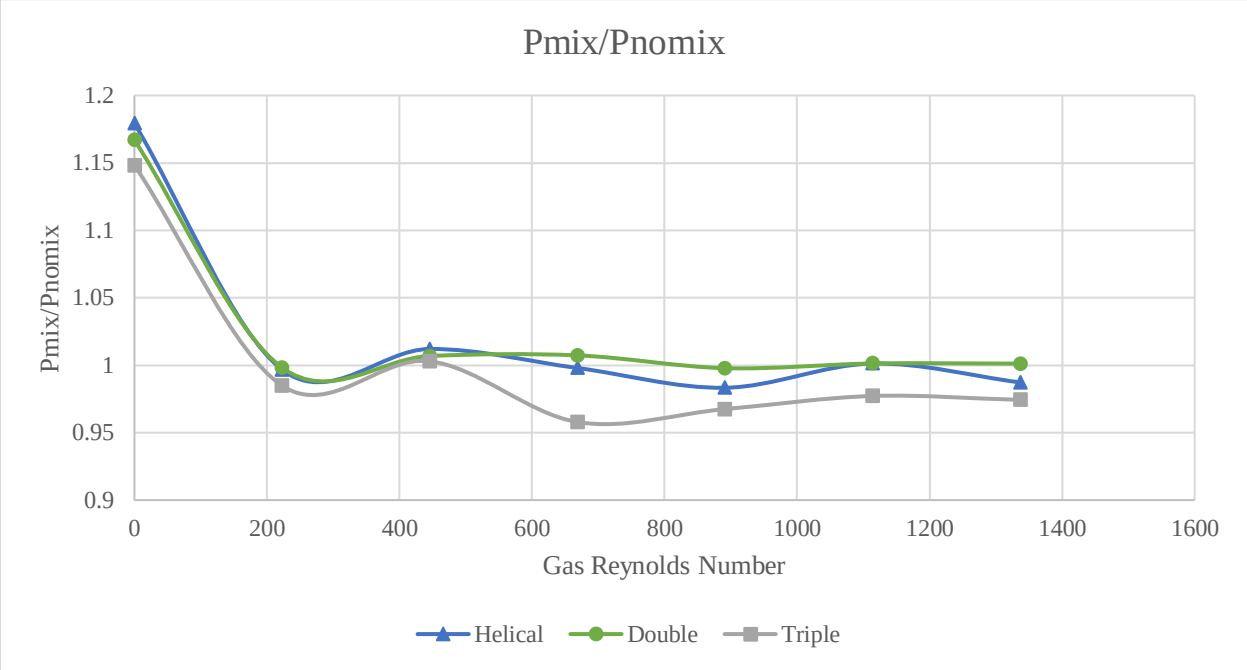

Figure 64 Static mixer pressure compared to pressure of empty pipe versus gas mass flow rate with a 12 g/s liquid mass flow rate

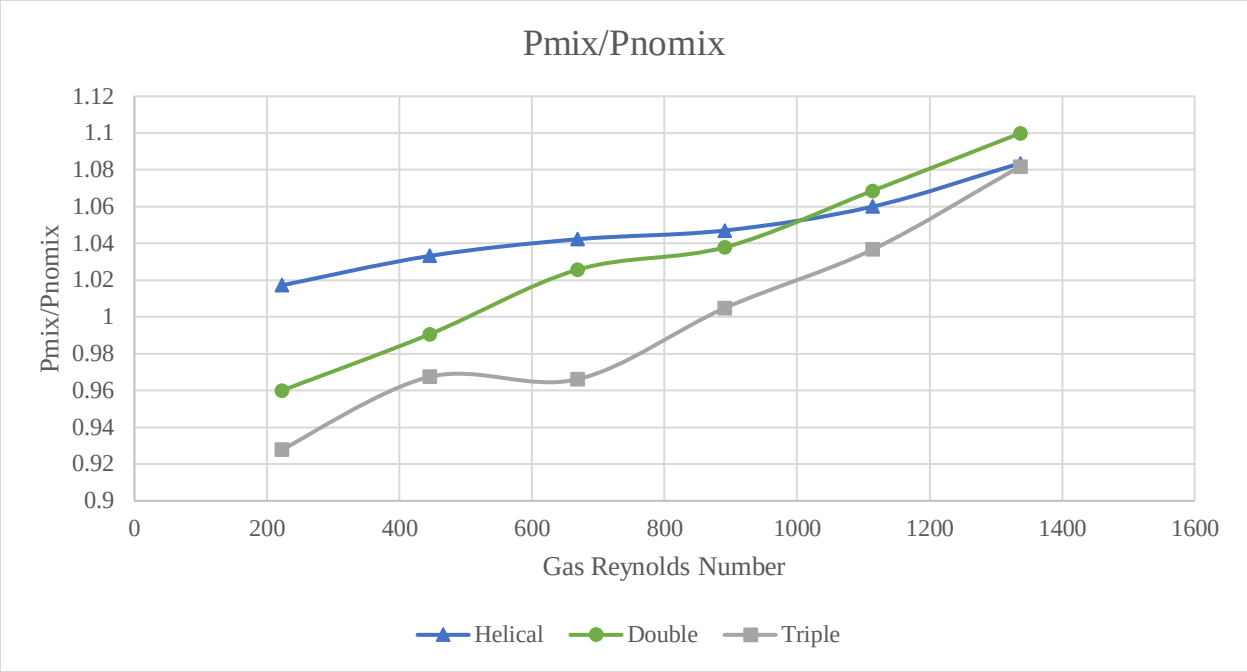

Figure 65 Static mixer pressure compared to pressure of empty pipe versus gas mass flow rate with a 15 g/s liquid mass flow rate

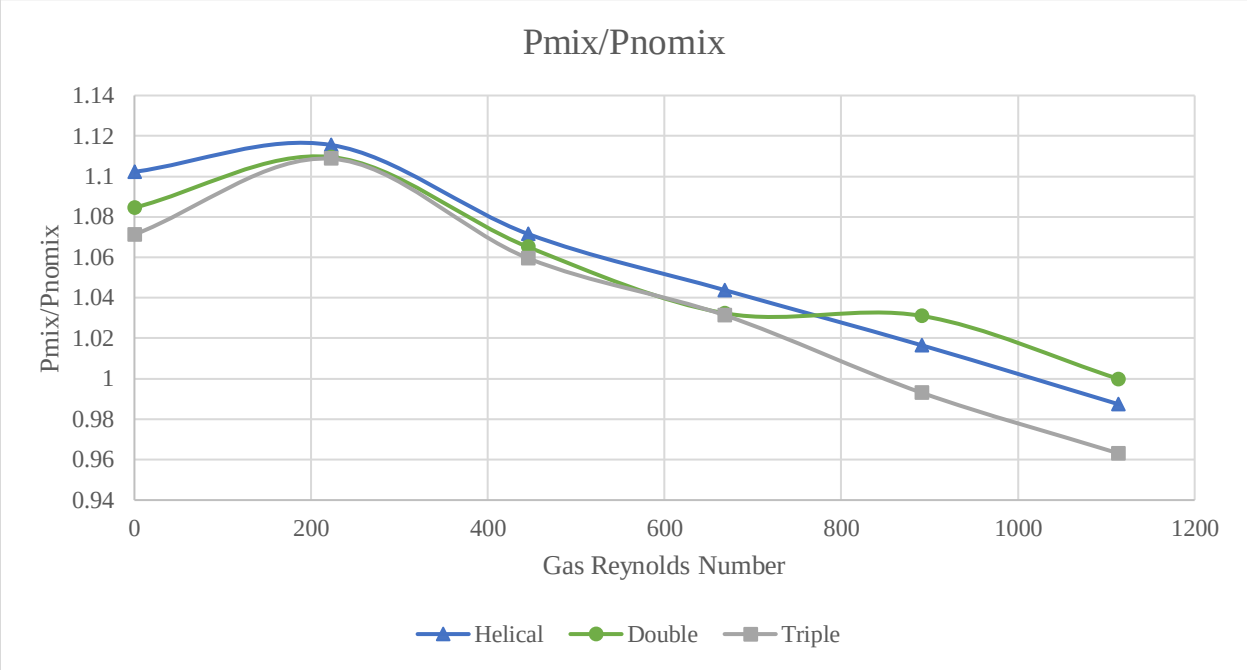

Figure 66 Static mixer pressure compared to pressure of empty pipe versus gas mass flow rate with a 18 g/s liquid mass flow rate

Figure 67 through Figure 70 show the differential pressure ratio over the static pressure transducer test section for experiments with a static mixer to that with an empty pipe. The differential pressure across the pressure transducer test section was averaged for all experiments. The ratio was then plotted versus the entire gas Reynolds number range. The knowledge of the downstream differential pressure ratio can help in knowing the pumping power needed across the pressure transducer test section. The pumping power can then be compared with and without a static mixer using the DP pressure ratio, to determine the need and usefulness of a static mixer in a system. It also shows the magnitude that the static pressure decreases over the pressure transducer test section which could aid in determining mixing performance and mixing length downstream of the static mixer, with further experiments. Another benefit to knowing the differential pressure is for determining the friction factor and for filling the knowledge gaps of CFD models and research literature.

Figure 67 shows the DP ratio at a liquid mass flow rate of 4.75 g/s. The DP ratio increases with an increase in gas Reynolds number by up to 30 percent at the max gas mass flow rate. Figure 68 shows the DP ratio at a liquid mass flow rate of 7g/s. The ratio comparison between the static mixer section and empty pipe tends to decrease with an increase in gas mass flow rate. At the maximum gas mass flow rate the ratios of all static mixers start to approach 1, which could indicate that the DP with a static mixer is like that with an empty pipe. The implications of this are that the pumping power is roughly the same with and without a mixer, so there would be a smaller cost of increasing mixing performance with a static mixer than at lower gas flow rates. Figure 69 shows the comparison at a liquid mass flow rate of 12 g/s, which also resembles the

behavior at 10 and 15 g/s. During these ranges of liquid and gas mass flow rate there is a very small difference in differential pressure when comparing static mixers to an empty pipe. Again, this could be beneficial in industry when mixing performance and cost friendly experiments are needed. Figure 70 shows the comparison of DP ratios at a liquid mass flow rate of 18 g/s, which shows similar behavior to that of 21 g/s. Over the range of gas mass flow rates, the DP ratio tends to drop, which could be due to the flow being dominated more by the liquid phase at the beginning and slowly dropping towards one as the gas phase is increased. Overall, the triple plate static mixer tends to have the lowest ratio when compared to that of an empty pipe, followed by the double plate and helical style over a range of gas mas flow rates. Throughout all the liquid mass flow rates besides the 4.75 g/s experiment, most of the increase in DP by using a static mixer is roughly 5 to 20% when compared to an empty pipe. The implications of this are that the use of these style of static mixers are to enhance mixing performance. Therefore, with a small increase in the differential pressure in these experiments, it might be cost effective to utilize static mixers over the use of an empty pipe.

Utilizing the static pressure and differential pressure comparison plots, it can be shown that in some cases at higher flow rates mixing could be inherently occuring in the empty pipe set up, without the need for a static mixer. This is assuming that static pressure is related to mixing efficiency, and this is shown when the static pressure ratio is close to one. Overall however, the static pressure ratio is generally larger than one, which could mean that mixing behavior due to the static mixers is better than when using an empty pipe. Trade offs must be made in industrial applications when comparing mixing performance (static pressure ratio) to cost effectiveness, or pumping power (differential pressure ratio).

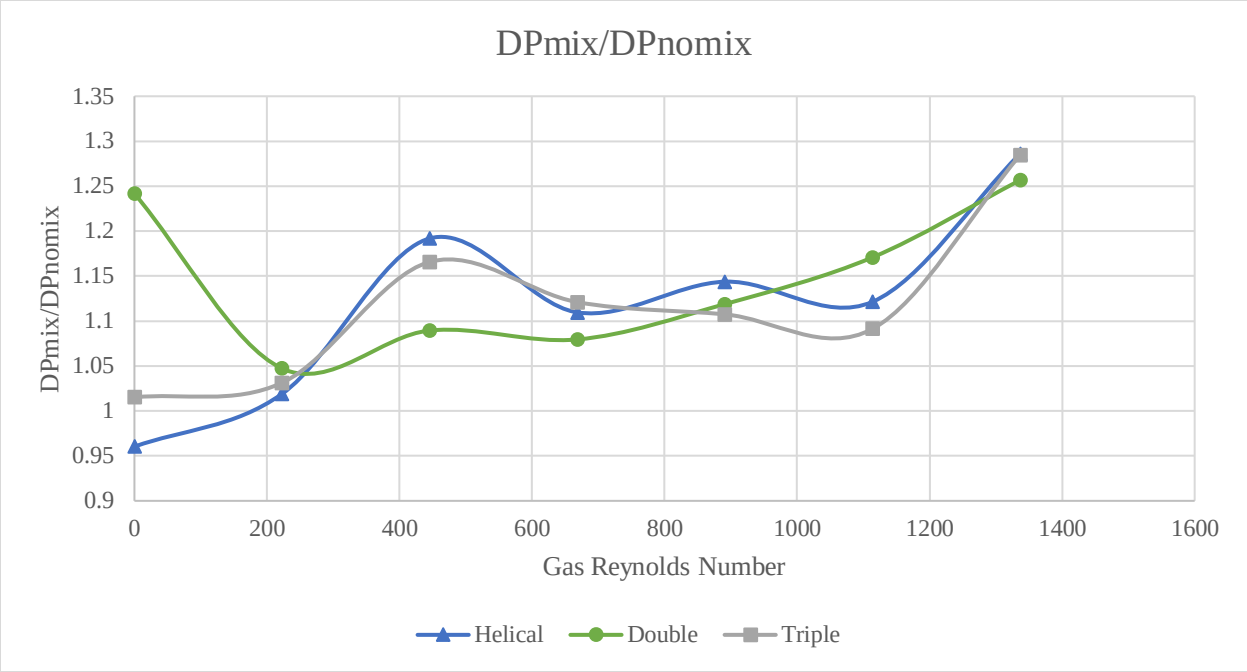

Figure 67 Differential pressure of transducer test section to pressure of empty pipe versus gas mass flow rate with a 4.75 g/s liquid mass flow rate

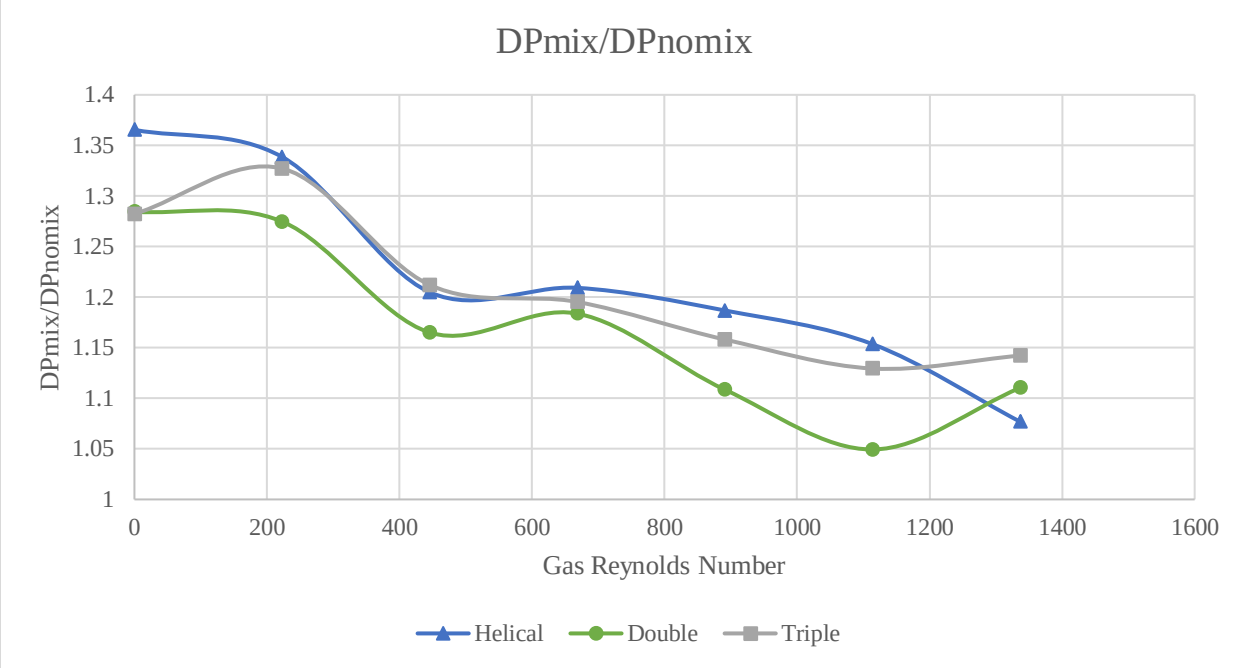

Figure 68 Differential pressure of transducer test section to pressure of empty pipe versus gas mass flow rate with a 7 g/s liquid mass flow rate

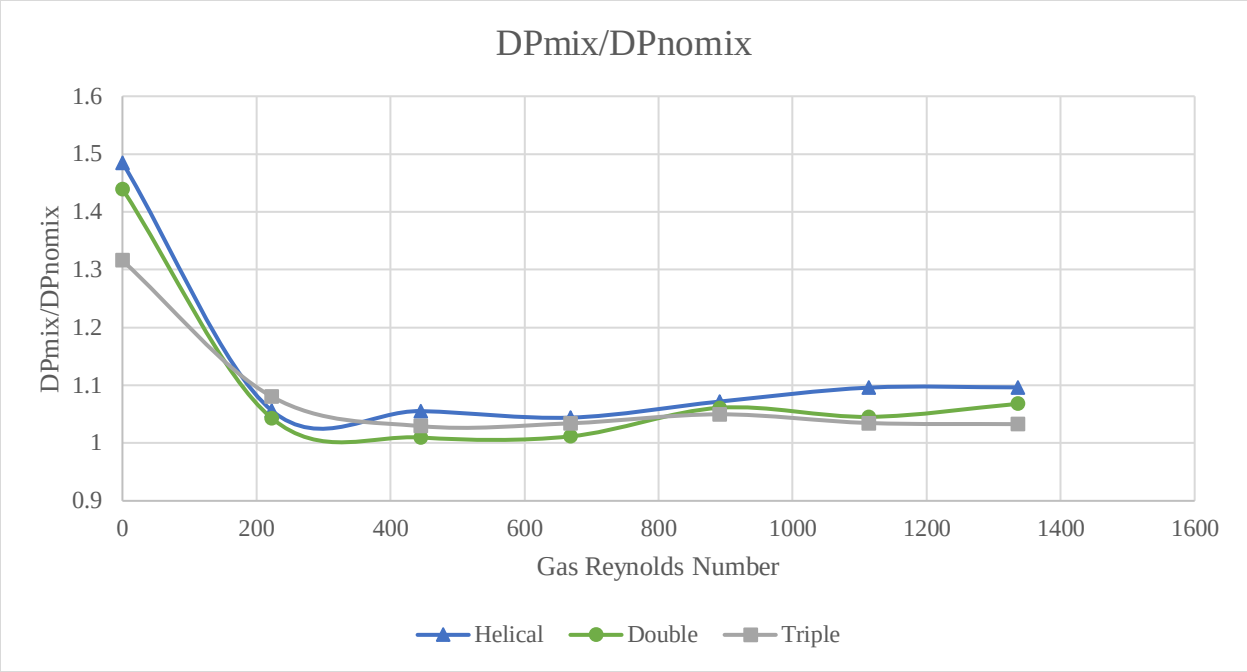

Figure 69 Differential pressure of transducer test section to pressure of empty pipe versus gas mass flow rate with a 12 g/s liquid mass flow rate

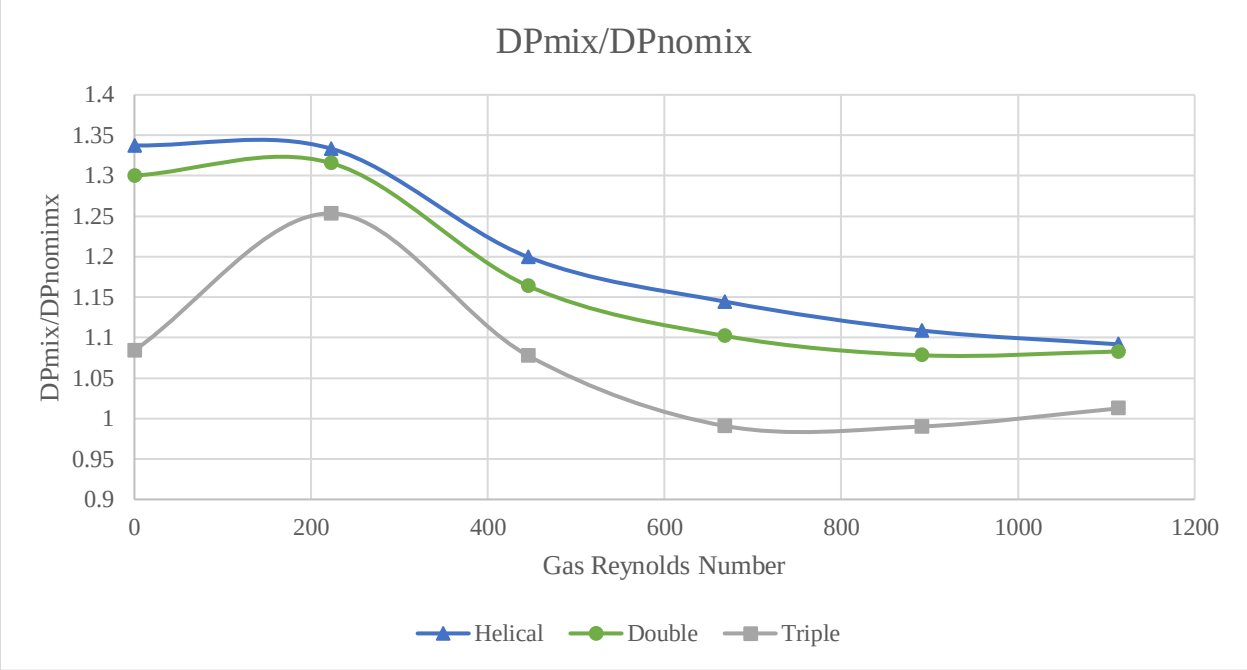

Figure 70 Differential pressure of transducer test section to pressure of empty pipe versus gas mass flow rate with an 18 g/s liquid mass flow rate

The differential pressure ratios were then investigated with their respective mixture Reynolds number. The importance of plotting mixture Reynolds number with all static mixers gives better comparison between the static mixers by having a characteristic flow rate for the respective mixers. The range of liquid Reynolds number (ReDl) was 328 to 1452, and the range of gas Reynolds number (ReDv) was 223 to 1337. Mass flow rates, diameter, and gas and liquid viscosities were then utilized to achieve the values for the mixture Reynolds number (ReDmix) based off the homogeneous flow model with a range of 328.4 to 2373.9. The homogeneous flow model was chosen because the liquid and gas mass flow rates are readily available and due to the flow regime primarily being intermittent flow through observation. The void fraction would need to be known to analyze the separate mass flow rates in the separated flow model. The Reynolds number mixtures utilized in the experiments consisted of laminar and turbulent flow, as turbulence in static mixers has been shown to occur at Reynolds numbers of around 1000 in many single-phase flow applications [28, 29]. Overall, the general trend is that as the ReDmix is increased the DP ratio tends to decrease. This could be due to more inherent mixing in the empty pipe as the flow rates of the liquid and gas are increased, causing the static mixer to empty pipe ratio to drop. At a ReDmix of around 800 is the largest DP ratio, or the largest increase in differential pressure with the use of a mixer, and the largest ratio is the helical style followed by the double and triple plate static mixers. At the maximum ReDmix of around 2400 is one of the smallest overall DP ratios for all static mixers. The helical style remains as the highest DP ratio, while the double and triple plate static mixers follow. The DP ratios at this ReDmix fall between 1 and 1.1, which indicated relatively similar behavior between the static mixers and the empty pipe.

Figure 71 shows the static mixer test sections after the flow experiments were conducted. The test sections are arranged by empty pipe, helical, double plate, and triple plate style from top to bottom. The empty pipe has little to no discoloration to it while the double plate has slight discoloration. The helical and triple plate style static mixers have a lot of discoloration. The heavy discoloration in those two static mixers could be due to their volume to length ratio being the largest. This volume to length ratio could be considered as the overall cross-sectional area of the static mixers. As the cross-sectional area is increased, it is allowing for the Hydromx, which has the reddish color, to stay in the test section longer, thus allowing for more discoloration over time. More studies could be done to confirm this behavior such as residence time experiments inside the static mixer test section.

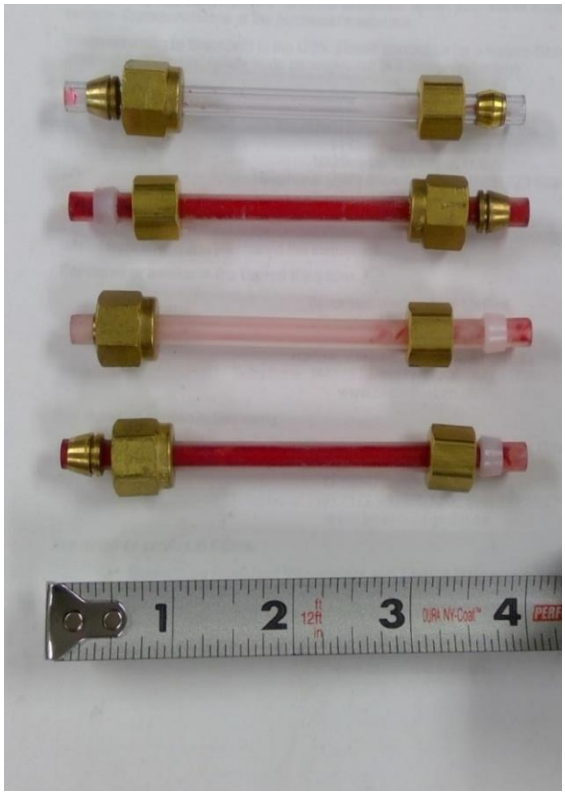

Figure 71 Static mixer test section tint after experimental tests arranged from top to bottom: empty pipe, helical, double plate, triple plate

Table 4 shows the percentage uncertainty for all measured parameters from the instruments. It also shows the uncertainties for the calculated values in the experiments such as density and the different Reynolds numbers. As shown, the percentage uncertainty values are relatively low, which represents good results on the calculated data.

Table 4 Percentage uncertainties of various parameters

Parameter	**Uncertainty (%)**
Static Pressure (P)	± 0.25% of Full Scale
Differential Pressure (DP)	± 0.65%
Density	± 5.00%
ReDmix	± 2.06%
ReDl	± 1.00%
ReDV	± 4.90%
ṁl	± .05%
ṁv	± (0.8% of Reading + 0.2% of Full Scale)
Temperature	± 0.4%
Diameter	± 0.08%
Viscosity	± 1%
Volume	± 5%

CHAPTER 5

CONCLUSIONS AND RECOMMENDATIONS

5.1 Conclusion

The use of static mixers in industrial and research applications have been increasing throughout the recent years. Static mixers are utilized due to their enhanced mixing performance and their reduction of maintenance cost when compared to dynamic mixers. Determining the pressure drop effects, static pressure effects, and the flow regime are used to find certain parameters that arise when using static mixers have been studied in the past. These parameters, along with the knowledge of the working fluid properties lead to a better understanding of the two-phase flow system that is being utilized.

Hydromx fluid properties such as viscosity and density were studied in detail. The ability to accurately predict density, viscosity, and the viscous behavior of the fluid is important when determining many of the fluid flow parameters such as liquid and mixture Reynolds number. Density was determined by measuring the volume and mass of the fluid at room temperature and was found to be 1.07 g/cm^3 with an uncertainty of ± 5.00%. Viscosity was measured using a Brookfield Rheometer to determine its viscous behavior through shear rate experiments as well as its viscosity at a variety of temperatures. The shear rate viscosity tests yielded positive results when trying to determine Newtonian like behavior. The viscosity for a variety of shear rate ranges at different temperatures was found to have a linear fit when plotting the shear stress on

the fluid versus the shear rate of the rheometer spindle. 100 percent Hydromx, 50:50 mixture of Hydromx and water, and calibration fluid was measured to determine the accuracy of the rheometer and the fluid properties of each of the fluids. This linearity confirms that the fluid is Newtonian, and the slope of the linear fit line represented the viscosity of the fluid. In most of the flow experiments conducted in the research, the temperature of the 50:50 Hydromx and water working fluid ranged from eight to twelve degrees Celsius, thus a viscosity average at ten degrees Celsius (5.8 cP) was used for all fluid flow property calculations with an uncertainty of ± 1% . The Newtonian behavior led for an easier time of calculating fluid properties and the Reynolds number behavior, because viscosity change with respect to flow rate didn't need to be considered.

Single phase and two-phase flow was studied from laminar to turbulent flow rates, ranging from a Reynolds liquid number of 328 to 1452 ± 1.00% and a Reynolds mixture number of 328.4 to 2373.9 ± 2.06%. Previous studies have shown that turbulence can occur after a static mixer at Reynolds numbers of up to 1000. This broad range of flow rates allowed for the inspection of what occurs downstream of a static mixer. During the single-phase flow experiments differential pressure across the entire test section including the static mixer and pressure transducer section showed that there was a large discrepancy in DP when using a static mixer versus an empty pipe, thus validating the assumption that there is an increase of power needed when using a static mixer. The other finding was that the static mixers behave similar in the lower flow rates but tend to change their DP behavior when the flow rate is increased with the Triple Plate style having the highest. The static pressure profiles at various liquid mass flow rates were then analyzed. From the analysis, the empty pipe had an overall lower static pressure when compared

to the static mixer, which could provide insight to how the mixing behavior of static mixers affects static pressure downstream. However, at lower flow rates the static mixers behaved very similar, and as the liquid mass flow rate was increased, the static mixer static profile began to deviate from one another, with similar behavior but different overall average pressures at each of the pressure transducers, with the helical style having the highest average static pressure, followed by the double plate and triple plate style static mixers. This could potentially mean that the helical style static mixer is better suited for mixing at higher flow rates compared to the other models. More experiments regarding the pressure profile and average static pressure downstream of the static mixer could help give insight in to whether the mixing behavior of the static mixer is related to the static pressure profile and average static pressure, along with other methods.

The two-phase flow through a static mixer investigation yielded interesting results to help solidify the outcomes of using a static mixer, and help filling some of the gaps left in previous studies and current research pertaining to pumping power, and CFD analysis. The DP measurements with varying liquid and gas flow rates over the entire system showed similar behavior as the single-phase flow experiments. The difference was that the two-phase flow behavior exhibited higher overall pressure drop when compared to single-phase flow, which is expected. The same trend was also seen as the triple plate style mixer had the highest differential pressure across the system, followed by the double plate and then the helical style mixer. This could be due in part to the volume per length parameter, which could be like a cross-sectional area measurement, as well as other influences in geometry. Differential pressure correlations have been created in previous studies on similar geometric style static mixers but are limited in creating a broad way of predicting the behavior of many sizes and shapes of mixers. This also is

the problem for the current study, as more measurements for a range of flow rates, as well as size of the current geometries need to be expanded to allow for a broader correlation of DP behavior predictions.

The static pressure profile and differential pressure across a length downstream of static mixers has been studied minimally in current literature and the effects of using a static mixer over just an empty pipe. These parameters can help with the better understanding of how fluid moves downstream of static mixers, how static pressure can be possibly used to point to how well a static mixer performs, power consumption, friction factor, and its usefulness in CFD analysis validation. Overall, the two-phase flow static pressure profile was different than the single-phase model. In most cases, the average static pressure was similar in all the static mixers, with the triple plate mixer always being the lowest. As the liquid mass flow rate was increased there was an increase in overall pressure, as well as a large increase in the empty pipe pressure profile. At the higher flow rates, the empty pipe displayed similar pressure profile behavior to that of the static mixers, which could be in part due to the inherent mixing of the phases. When comparing the overall average static pressure in the tube, care must be done in integrating over the entire test section. After the average static pressure was determined, it could be compared to that of the empty pipe to see how static mixers play a role in the average pressure. At relatively low ReDmix values the average static pressure contribution by the static mixer is higher than that with the empty pipe from a range of 10 to 20%, depending on the mixer and gradually had less of a contribution at the flow rate limits of this experiments by a range of 0 to 10%.

Differential pressure across the static pressure transducer test section was investigated to compare the effects of using a static mixer over an empty pipe. The DP ratio was dependent on

both the gas and liquid mass flow rates. Investigating the DP as a function of ReDmix showed that at lower flow rates the DP ratio could be as high as a 30% increase with the use of a static mixer. However, as the ReDmix was increased, the DP ratio dropped to around 5 to 20% at the maximum mixture Reynolds number. This has the implications that the static mixers chosen could potentially perform better at higher Reynolds number flows when looking strictly at the differential pressure increase that arises from using a static mixer.

5.2 Recommendations

One major component that limited the amount of data that could be obtained was due to the lack of liquid and gas flow rate that could enter the system. With a larger liquid pump, liquid flow rate would be able to enter the system at a higher value, which would then allow for a larger range of data to analyze. This could help fill in more gaps about what happens at higher liquid flow rates to aid in generating correlations for differential pressure, or the pressure profile downstream of the static mixer. Along with a larger pump, the static pressure transducers in this case were the largest limiting factor into how high the flow rates could go. To alleviate this, new pressure transducers with a higher pressure capacity should be utilized.

Hydromx fluid mixed with water is utilized as a heat transfer liquid. Along with the DP and pressure effects of mixing the liquid with an inert gas, heat transfer properties could be investigated with the addition of an inert gas. These experiments could show the mixing performance of the static mixer and its ability to possibly enhance heat transfer properties of the fluid.

Another aspect that could be investigated using the same experimental set up is the pressure fluctuations of each individual pressure transducer. The pressure fluctuations could indicate how

much mixing is occurring based on the oscillations of pressure readings as flow passes through the individual static pressure transducer test sections. As the flow moves downstream, it would be interesting to note if the fluctuations and their amplitudes increased or decreased, which could assist in determining mixing performance. Another aspect that understanding static pressure fluctuations downstream of the static mixer could help to better understand what happens in slug flow. Slug flow pressure fluctuation data could enhance modeling techniques in CFD models to better estimate what happens to the inside of pipes with regards to erosion when slugging is occurring. To ensure accurate readings without any aliasing, a data acquisition unit with higher sampling rate needs to be used. The current Agilent data acquisition unit, failed to capture the fluctuation cycles, and was therefore unable to be investigated.

In the future, to determine correlations for a broad range of geometries and sizes of static mixers, more data needs to be analyzed based on a larger range of flow rates as well as the size and surface finish of the static mixers themselves. Increasing the systems diameter could be tedious but would give insight to what happens with larger diameter systems and the effects from static mixers. The surface finish of the static mixers themselves could be enhanced from the 50-micron layer thickness chosen in this research to a 25-micron layer thickness using the Form 2 3D printer. The smaller layer thickness, and enhanced surface finish techniques could provide a smoother surface inside the static mixer test section. This could eliminate any effects due to surface roughness on the flow passing by the stating mixer.

A large component to why static mixers are utilized are for their mixing performance to enhance heat transfer properties, polymerization, and dispersion applications. To determine the mixing performance of individual static mixers, void fraction measurements and flow visualization

experiments need to be conducted. These experiments will help determine how well the mixing is performing by using the void fraction measurements, as well as what flow regime is exiting the static mixer utilizing a form of flow visualization that has been previously conducted. Knowing these parameters could help in determining a correlation for each of the static mixers and could possibly be extended to determine a correlation for a broad range of static mixers, sizes, and flow rates. The important outcome of knowing these factors is the elimination of information gaps in currently literature, as well as the enhancement of CFD models and to allow for future understanding of two-phase flow static mixer behavior.

BIBLIOGRAPHY

[1] M. E. Ewing, J. J. Weinandy and R. N. Christensen, Observations of Two-Phase Flow Patterns in a Horizontal Circular Channel, Heat Transfer Engineering, 1999, pp. 9-14.

[2] Y. Taitel and A. E. Dukler, "A Model for Predicting Flow Regime Transitions in Horizontal and Near Horizontal Gas-Liquid Flow," *AIChE,* vol. 22, no. 1, pp. 47-55, 1976.

[3] G. Breber, J. W. Palen and J. Taborek, " Prediction of Horizontal Tubeside Condensation of Pure Components Using Flow Regime Criteria," *Heat Transfer,* vol. 102, pp. 471-476, 1980.

[4] A. B. Kurtulus, N. Eskin and E. Deniz, "Experimental Study of Two-Phase Flow in a Horizontal Circular Channel: Influence of Gas Injection on the Bubble Diameters," *EPJ Web of Conferences,* vol. 67, 2014.

[5] A. Jaworek and A. Krupa, "Gas/liquid Ratio Measurements by RF Resonance Capacitance Sensor," *Sensors and Actuators,* pp. 133-139, 2004.

[6] A. Jaworek and A. Krupa, "Phase-shift Detection for Capacitance Sensor Measuring Void Fraction in Two-phase Flow," *Sensors and Actuators,* pp. 78-86, 2010.

[7] A. Jaworek, A. Krupa and M. Trela, "Capacitance Sensor for Void Fraction Measurement in Water/Steam flows," *Flow Measurement and Instrumentation,* vol. 15, pp. 317-324, 2004.

[8] M. S. Abouelwafa and E. J. Kendall, "The Use of Capacitance Sensors for Phase Percentage Determination in Multiphase Pipelines," *IEEE Instrumentation Measurement,* vol. 29, no. 1, pp. 24-27, 1980.

[9] S. M. Huang, A. L. Stott, R. G. Green and M. S. Beck, "A New Capacitance Transducer for Industrial Applications," *J. Phys. E: Sci. Instrum.*, vol. 21, pp. 251-256, 1988.

[10] H. C. Yang and S. K. Park, "Pressure Drop in Motionless Mixers," *KSME International Journal,* vol. 18, no. 3, pp. 526-532, 2004.

[11] A. Cybulski and K. Werner, "Static Mixers-Criteria for Applications and Selection," *International Chemical Engineering,* vol. 26, pp. 171-180, 1986.

[12] H. Kalbitz, "Effect of Static Mixer on the Flow, Heat Transfer and Pressure Drop in Tube Heat Exchanger," Ph.D Thesis of University of Braunschweig, Braunschweig, Germany, 1990.

[13] N. F. Shah and D. D. Kale, "Pressure Drop for Laminar Flow of Non-newtonian Fluids in Static Mixers," *Chemical Engineering Science,* vol. 46, pp. 2159-2161, 1991.

[14] H. Z. Li, C. H. Fasol and L. Choplin, "Hydrodynamics and Heat Transfer of Rheologicall Complex Fluids in a Sulzer SMX Static Mixer," *Chemical Engineering Science,* vol. 51, no. 10, pp. 1947-1955, 1996.

[15] K. Pehlivan, I. Hassan and M. Vaillancourt, "Experimental study on two-phase flow and pressure drop in millimeter-size channels," *Applied Thermal Engineering,* vol. 26, pp. 1506-1514, 2006.

[16] L. Friedel, "Improved Friction Pressure Drop Correlations for Horizontal and Vertical Two-phase Pipe Flow," European Two-phase Group Meeting, Ispra, Italy, 1979.

[17] D. Chisholm, "A Theoretical Basis for the Lockhart Martinello Correlation for Two-phase Flow," *International Journal Heat Mass Transfer,* vol. 10, pp. 1767-1778, 1967.

[18] A. Kawahara, P. M.-Y. Chung and M. Kawaji, "Investigation of Two-phase Flow Pattern, Void Fraction, and Pressure Drop in a Microchannel," *International Journal of Multiphase Flow,* vol. 28, pp. 1411-1435, 2002.

[19] K. A. Triplett, S. M. Ghiaasiaan, S. I. Abdel-Khalik and D. L. Sadowski, "Gas-liquid Two-phase Flow in Micro-channels part I: Two-pahse Flow Patterns," *International Journal Multiphase Flow,* vol. 25, pp. 377-394, 1999.

[20] C. Damianides and J. W. Westwater, "Two-phase Patterns in a Compact Heat Exhanger and in Small Tubes," Second UK National Conference on Heat Transfer, 1988.

[21] N. P. Ekberg, "Experimental Study on Two-phase Flow Regime Maps and Pressure Drop in Micro-channels," Georgia Tech, 1997.

[22] K. Pehlivan, "Experimental Study on Two-phase Flow Regimes and Pressure Drop in Mini- and Micro-channels," Concordia University, Canada, 2003.

[23] A. Heyouni, M. Roustan and Z. Do-Quang, "Hydrodynamics and Mass Transfer in Gas-liquid Flow Through Static Mixers," *Chemical Engineering Science,* vol. 57, pp. 3325-3333, 2002.

[24] M. Mustakis, F. A. Streiff and G. Schneider, "Advances in Static Mixing Technology," *Chemical Engineering Progress,* vol. 82, no. 7, pp. 42-48, 1986.

[25] K. J. Myers, A. Baker and D. Ryan, "Avoid Agitation by Selecting Static Mixers," *Chemical Engineering Progress,* pp. 28-38, 1997.

[26] J. R. Baker, "Motionless Mixers Stir Up New Uses," *Chemical Engineering Progress,* vol. 87, no. 6, pp. 32-38, 1991.

[27] M. Stec and P. M. Synowiec, "Study of Fluid Dynamic Conditions in the Selected Static Mixers Part 1 - Research of Pressure Drop," *The Canadian Journal of Chemical Engineering,* vol. 95, pp. 2156-2167, 2017.

[28] *Koflo Static In-Line Mixers. Tomorrow's Technololgy Today,* Koflo, 2016.

[29] R. K. Thakur, C. Vial, K. D. Nigam, E. B. Nauman and G. Djelveh, "Static Mixers in the Process Industries- A Review," *Chem. Eng. Res. Des.,* vol. 81, pp. 787-826, 2003.

[30] T. Bayer, K. Himmler and V. Hessel, "Don't be Baffled by Static Mixers," *Chemical Engineering,* 2003.

[31] M. Stec and P. M. Synowiec, "Study of Fluid Dynamic Conditions in the Selected Static Mixers Part 2 - Determination of the Residence Time Distribution," *The Canadian Journal of Chemical Engineering,* vol. 95, pp. 2410-2422, 2017.

[32] S. Fogler, Elements of Chemical Reaction Engineering, Pearson Education International, 2008, pp. 867-897.

[33] K. A. Hweij and F. Azizi, "Hydrodynamics and Residence Time Distribution of Liquid Flow in Tubular Reactors Equipped with Scree-type Static Mixers," *Chemical Engineering Journal,* 2015.

[34] S. Liu, A. N. Hrymak and P. E. Wood, "Design Modifications to SMX Static Mixer for Improving Mixing," *AIChE Journal,* vol. 52, no. 1, pp. 150-157, 2006.

[35] N. V. Rama Rao, M. H. Baird, A. N. Hrymak and P. E. Wood, "Dispersion of high-viscosity liquid-liquid systems by flow through SMX static mixer elements," *Chemican Engineering Science,* vol. 62, pp. 6885-6896, 2007.

[36] J. M. Zalc, E. S. Szalai and F. J. Muzzio, "Mixing Dynamics in the SMX Static Mixer as a Function of Injection Location and Flow Ratio," *Polym Eng Sci,* vol. 43, pp. 875-890, 2003.

[37] S. Hirschberg, R. Koubek, F. Moser and J. Schock, "An improvement of the Sulzer SMX static mixer significantly reducing the pressure drop," *Chemical Engineering Research and Design*, vol. 87, pp. 524-532, 2009.

[38] S. Hirschberg, P. Mathys and A. Rutti, "Validation of CFD simulations with LIF data for the Sulzer mixers SMX and sMR," in *Proceedings of the 12th European Conference on Mixing*, Bologna, 2006.

[39] M. K. Singh, P. D. Anderson and H. E. Meijer, "Understanding and Optimizing the SMX Static Mixer," *Macromolecular Rapid Communications,* vol. 30, pp. 362-376, 2009.

[40] "www.sulzerchemtech.com," Sulzer, 2008. [Online].

[41] A. Paglianti and G. Montante, "A mechanistic model for pressure drops in corrugated plates static mixers," *Chemical Engineering Science,* vol. 97, pp. 376-384, 2013.

[42] F. A. Streiff, "Adapted motionless mixer design," in *Third European Conference on Mixing*, York, 1979.

[43] K. Hartung and H. J. Hiby, "Examination of the transverse and longitudinal mixture in the circulatory reactor with the help of discoloration methods," *Chem. Eng. Tech.*, vol. 44, pp. 1051-1056, 1972.

[44] M. H. Pahl and E. Muschelknautz, "Static mixers and their applications," *Int. Chem. Eng.*, vol. 22, no. 2, pp. 197-205, 1982.

[45] K. S. Pak and M. T. Nasser, "Experimental study on the rheological properties of polymer solutions and solid suspensions," *International Journal of Current Engineering and Technology,* vol. 5, no. 2, 2015.

[46] G. Gray and H. Darley, "Composition and properties of oil well drilling fluids," Gulf Publishing Co, Houston, 1981.

[47] Kirk-Othemer, Encyclopedia of Chemical Technology, John Wiley and Sons, 1998.

[48] "3-series gear pumps," Liquiflo Chemical Processing Pumps, [Online]. Available: www.liquiflo.com/v2/gears/3/35f.htm.

[49] Emerson, "Micromotion Technical Overview and Specification Summary," January 2018. [Online]. Available: www.emerson.com/documents/automation/technical-overview-specification-summary-en-66168.pdf.

[50] Emerson, "MicroMotion Elite Coriolis Flow and Density Meters," January 2018. [Online]. Available: www.emerson.com/documents/automation/product-data-sheet-elite-series-coriolis-flow-density-meters-en-66748.pdf.

[51] Omega, "Thermocouple Tolerances," [Online]. Available: https://www.omega.com/toc_asp/frameset.html?book=Temperature&file=tc_colorcodes. [Accessed 2018].

[52] Honeywell, "Heavy Duty Pressure Transducers PX2 Series," Honeywell, 2017.

[53] FormLabs, "The Ultimate Guide to Stereolithography (SLA) 3D Printing," 2018. [Online]. Available: https://formlabs.com/blog/ultimate-guide-to-stereolithography-sla-3d-printing/. [Accessed April 2018].

[54] Chemineer, "Kenics KM Static Mixer," [Online]. Available: https://www.chemineer.com/products/kenics/km-mixers.html. [Accessed 2018].

[55] A. Brookfield, More solutions to sticky problems, 2017.

[56] Hydromx, "Game Changing Technology," Hydromx, 2015.